Colorectal Cancer Small Extracellular Vesicles Induce Matrix Metalloproteinase Expression, an Invasion-Promoting Phenotype, and CD147-Dependent MAPK/AP-1 Activation in Macrophages

By

Isaac Menghisteab

A thesis submitted in partial fulfillment of the requirements for the degree of

Master of Science

In

Cancer Science

Department of Oncology

University of Alberta

ABSTRACT

Exosomes and small microvesicles are types of small extracellular vesicle (sEVs) secreted by cancerous and normal cells. sEVs are filled with cargo from cancer cells that may affect both nearby and distant tissues. sEVs from colorectal cancers that enter blood vessels draining the intestine will traffic to the liver due to the normal blood flow path through the portal vein. Exosomes from colorectal cancers may induce changes in liver tissues by mechanisms such as the digestion of extracellular matrix (ECM) proteins. This creates sites known as premetastatic niches in the liver that are favorable to metastasis. Because Kupffer cells, which are tissue resident liver macrophages, and recruited inflammatory macrophages may be affected by colorectal cancer sEVs, we hypothesized that liver macrophages are conditioned by colorectal cancers sEVs to degrade the liver ECM through release of matrix metalloproteinases (MMP)s. We predict such ECM degradation by Kupffer cells may be one mechanism by which colorectal cancer sEVs help establish a premetastatic niche in the liver. Using in vitro and ex vivo models, we have found that sEVs from colon cancer cell lines directly induce invasion-promoting behaviours in liver macrophages that involve upregulating MMP production in a way that facilitates colorectal cancer cell migration,. These two consequences of sEV stimulation of macrophages occurs simultaneously with MAPK/AP-1 activation and is regulated in part by CD147 proteins on the colon cancer cell sEVs. These results confirm our hypothesis and support a role of colorectal cancer sEVs in preparing a liver pre-metastatic niche through conditioning liver macrophages.

PREFACE

This thesis is an original work by Isaac Teclemariam Menghisteab, and no part of this thesis has been previously published. The research project, of which this thesis is a part, receive research ethics approval from the Cross Cancer Institute Animal Care Committee, Project Title “Impact of genomic instability in colorectal cancer and the immune system”, Protocol No. “AC15219” (May 31, 2015), and Protocol No. “AC19248” (May 31, 2019).

ACKNOWLEDGEMENTS

I owe a great deal to Dr. Kristi Baker, my primary research supervisor, and fellow members of her lab. Courtney Mowat as a senior graduate student has helped me through many technical challenges. Allison McNamara, another senior graduate student provided me with expertise on extracellular vesicles as I started this project. The undergraduate students I have worked with, Hamda Memon and Yulin Xi have contributed significantly to the work I present in this thesis, I am proud I had the opportunity to work with them. Finally, Kristi has for years, graciously and generously provided me with mentorship and guidance, without which I would not have reached this point in my research career, and I am extraordinarily grateful for the good fortune I had to study in her laboratory.

Without the services of Jack Moore at the Alberta Proteomics and Mass Spectrometry Facility none of the essential proteomics work in this thesis could have been done. Priscilla Gao and Geraldine Baron of the Cross Cancer Institute Imaging Facility were essential for the transmission electron microscopy and invasion assay experiments respectively. Dan McGinn, Cheryl Santos, Daming Li provided valuable aid with the management of animals in the Cross Cancer Institute also. I must also thank Darryl Glubrecht for training me in the processes of tissue sectioning and H&E staining of tissues.

A large part of my funding was provided by the Antoine Noujaim Entrance Scholarship. The remainder of my funding has come through the NSERC Discovery Grant and CIHR

Project Grant funding of Dr. Kristi Baker, my supervisor. It has been a privilege to study and be provided with the necessary funds by the aforementioned sources, I am deeply grateful for the funds that supported this research project.

I must also thank my supervisory committee members, past and present, for their advice and mentorship. The supervision of Dr. John Lewis, Dr. Manijeh Pasdar, and Dr. Robert Ingham have been invaluable. Their comments have significantly impacted the direction of my research, I am indebted to them for their guidance of this thesis.

TABLE OF CONTENTS

LIST OF TABLES

Table 10 – MC38 Δ*Rad51* cell sEV LC-MS/MS Round 2: Identified Proteins and Peptides List

LIST OF FIGURES

ABBREVIATIONS

AP-1 – activator protein 1

BMDC – bone marrow derived dendritic cells

BMDM – bone marrow derived macrophage

CIMP – CpG island methylator phenotype

CIN – chromosomal instable

CRC – colorectal cancer

ECM – extracellular matrix

ILV – intraluminal vesicle

MAPK – mitogen activated protein kinase

MMP – matrix metalloproteinase

MMR – Mismatch repair

MSI – microsatellite instable

MVE – multivesicular endosome

NTA – nanoparticle tracking analysis

PMN – pre-metastatic niche

sEV – small extracellular vesicle

TEM – transmission electron microscopy

Δ*Mlh1* – *Mlh1*-knockout cells, generated by CRISPR/Cas9 in MC38 cells

Δ*Polε* – *Polε*-knockout cells, generated by CRISPR/Cas9 in MC38 cells

Δ*Rad51* – *Rad51*-knockout cells, generated by CRISPR/Cas9 in MC38 cells

CHAPTER 1: INTRODUCTION

COLORECTAL CANCER

Colorectal Cancer Incidence and Mortality

Colorectal cancer (CRC) is the second most commonly diagnosed cancer in Canada. Approximately 13% of cancers diagnosed in Canada are colorectal. CRC is also the 2nd leading cause of cancer death with a 5-year net survival of 62%. Early detection of CRC (Stage I) affords patients an estimated 87-92% 5-year relative survival while Stage IV diagnoses are grim with estimates of 11-12% five-year survival[1].

The Development and Subtypes of Colorectal Cancer

The majority of CRC will develop sporadically although rare heritable CRC syndromes do exist. These include Hereditary Non-Polyposis Coli[2] (HNPCC) which is also called Lynch Syndrome and is caused by inherited mutation in mismatch-repair genes (typically *hMLH1* in CRC[3]), and Familial Adenomatous Polyposis (FAP) which is caused by inherited mutations in the *APC* gene[3]. Sporadic CRC is the majority of CRC that is diagnosed, and sporadic CRC can be subcategorized according to the type of genetic instability it exhibits. Typically, 85% of sporadic CRC will exhibit chromosomal instability (CIN) characterized by irregular copy-number and aneuploidy and 15% of CRC will exhibit microsatellite instability (MSI) in which mismatch-repair mechanisms are defective leading to expansion and deletion of microsatellite DNA. While the 85% CIN, 15% MSI CRC split is often quoted, Hveem et al.[4] report some variation and identification of CRC which is not either CIN or MSI. Inverse correlation of CIN and MSI

genetic instability in sporadic CRC show that these phenotypes are mutually exclusive genetic instability pathways and suggests that there is negative-selection for the dual MSI/CIN phenotype[5,6]. In addition to subtyping of CRC by genetic instability type, colorectal cancer can be organized into four consensus molecular subtypes[7,8] (CMS: 1-4). Further supporting the mutual exclusivity of CIN or MSI genetic instability, CMS1 CRC alone exhibits MSI while CMS2-4 are either CIN or neither.

Prognostic Relevance of Microsatellite Instable Colorectal Cancer Status

Up to and including Stage II CRC, MSI is a favorable prognostic marker and CIN (aneuploidy can be measured as a proxy for CIN) is unfavorable[4,9,10]. The reasons for this difference in prognosis are not fully known. Two relevant observations which may explain the difference in prognosis between MSI and CIN CRC are that MSI CRCs have a higher level of tumor infiltrating lymphocytes (TILs), and MSI CRCs are expected to have a higher mutational load resulting in immunogenic neo-antigens[11]. CIN CRCs have a low rate of TILs and contain many fewer mutations.

Pathobiology of Colorectal Cancer Genetic Instability Subtypes

CIN CRC develops following a series of mutation acquisitions beginning with mutation in *APC*[12] and accumulating mutations or dysregulation in the *WNT, MAPK, PI3K, TGFβ*, and *TP53* pathways[13]. MSI CRC develops dysregulation in similar pathways as CIN CRC but via a mechanism initiated by mutation or silencing of DNA mismatch-repair (MMR) genes and subsequently perpetuated by genetic instability[14]. Additionally MSI CRC is associated with the CpG-island methylator phenotype (CIMP) which has a

higher frequency of concurrence with MSI status although CIMP can also occur in CIN CRC[15,16].

In addition to MSI CRC having a better prognosis than CIN CRC, MSI CRC tend to have fewer metastases[17]. It has been speculated that MSI CRC leads to a better overall prognosis and lower rates of metastasis because they generate abundant neo-antigens which potentiate an immune response against the tumor[18]. Furthermore, there is evidence to suggest that neo-antigens may be disseminated throughout the body via vesicles called exosomes[19]. Neo-antigens are the products of novel protein coding sequences to which adaptive immune cells may react. In contrast, CIN CRCs are not expected to generate many neo-antigens as CIN is characterized by translocations, amplifications, or deletions of large chromosomal segments. In addition to other immune-evasive strategies, such as inducing suppressive *TGFβ* signalling[20,21], this lack of neo-antigens would allow CIN CRCs to avoid the type of immune detection that characterizes MSI CRCs and may explain a substantial component of the prognostic differences between these two CRC subtypes. While also important in many other respects, exosomes and other extracellular vesicles may traffic CRC neo-antigens to antigen presenting cells resulting in anti-tumour immunity. Despite the pro-tumorigenic effects that exosomes and other extracellular vesicles have been shown to mediate[22], their circulation also engenders risk of immune detection to the tumor.

EXOSOMES

Definition of Exosomes

Small extracellular vesicles (sEVs) are the subset of extracellular vesicles (EVs) released by cells that are between 30-150 nm in diameter. Exosomes are between 50-200 nm in diameter, however microvesicles, another class of extracellular vesicles, range from 10 nm – 10 μm in diameter, overlapping with exosomes (Fig.1). The International Society for Extracellular Vesicles (ISEV), has proposed standardized nomenclature and standardized methods for EV characterization and reporting of EV research in the MISEV 2018 guidelines[23]. Good scientific practice according to MISEV 2018 recommends that exosome researchers identify their exosome enriched research materials as sEVs until the field can agree upon a set of markers that clearly identify exosomes.

Exosome Biogenesis

Exosome research dates back into the 1980s. Johnstone et al.[24], Pan et al.[25], and Harding et al.[26], were among the first to identify what we now call exosomes. Viewing the phenomenon of exosome release as the reverse of endocytosis, Johnstone et al. dubbed the vesicles they observed ‘exosomes’. Pan et al. used electron microscopy and labelling of the transferrin protein (TFR) with gold labelled antibodies to observe the formation of TFR expressing vesicles within multivesicular endosomes (MVEs), and the release of those vesicles into the extracellular space as a result of MVE fusion with the plasma membrane.

Johnstone et al. were able to show by Coomassie staining that the protein content of exosomes differs from that of cytosolic protein, establishing that exosomes are not the product of simple plasma membrane shedding and that exosomes are somehow selectively loaded with protein cargos. Additionally, Johnstone et al. demonstrated that the proteins in exosomes maintained their catalytic functions and ligand binding ability. Overall, this early work in the field of exosomes established some of the foundations of the field. Johnstone et al. also uncovered a yet unresolved question in the field of exosomes by identifying at least two distinct populations of extracellular vesicles from reticulocytes. Those which expressed the transferrin receptor (TFR) and those which contained lysosomal proteins. While much progress has been made in identifying heterogeneity within exosomes, and exosome heterogeneity appears to be more complex than the simple presence or absence of a single protein such as TFR, it remains unclear how many distinct populations of exosomes exist and how they might arise.

Composition and Protein Loading

Johnstone et al.'s discovery that exosomes are selectively loaded with protein cargoes revealed that exosomes are not merely vesicles reflecting the composition of a cell's cytoplasm. The field of exosome research has recently started to uncover how exosomes and microvesicles are formed and loaded with cargo through several interconnected mechanisms.

The best known pathway by which exosomes can be formed is the endosomal sorting complexes required for transport (ESCRT)-dependent pathway (Fig.2), although some

potentially ESCRT-independent biogenesis pathways may exist[31]. The formation of intraluminal vesicles (ILVs) requires two general and overlapping steps: the loading of cargo into ILVs as they are formed, and the budding and scission of ILVs into the MVE. Purified microvesicles are enriched in different proteins relative to sEVs, including mitochondrial and ribosomal proteins[32]. The mechanisms by which microvesicles are loaded with cargo are not clear since they are shed seemingly non-specifically from the plasma membrane[33,34]. The formation of microvesicles is described as an imprecise "blebbing" process compared to the sorting of proteins into ILVs. Indeed, microvesicles may contain endoplasmic reticulum proteins and mitochondrial proteins while exosomes typically do not[32]. Unfortunately, much is unknown concerning the mechanisms of cargo loading into microvesicles, especially whether microvesicles stochastically incorporate any nearby cytoplasmic material, or if most cargo are selectively sorted into microvesicles. In the ESCRT exosome biogenesis pathway ESCRT proteins are recruited to the multivesicular endosome membrane in a series of protein complexes numbering ESCRT-0 to ESCRT-III. After formation of ILVs, only the MVEs which fuse with the plasma membrane and release ILVs produce extracellular ILVs (exosomes), other MVEs, which are synonymous with late endosomes, will fuse with lysosomes and have their contents degraded[35]. In the ESCRT-dependent pathway, ESCRT-0 is initially recruited to the MVE membrane by ubiquitinated proteins, and initiates the recruitment of other downstream ESCRT complexes[36]. Ubiquitination appears to be the main signal for protein loading into ILVs[37,38] through the ESCRT exosome biogenesis machinery. The ESCRT-0 and ESCRT-I complexes sort ubiquitinated proteins into ILVs during MVE formation[39,40]. ESCRT-I then recruits ESCRT-II which continues sorting proteins into

ILVs[41]. ESCRT-II then recruits ESCRT-III which is required both for the invagination of MVE to create ILVs[42] and for sorting of cargos[43]. Finally, ESCRT-III, Vesicular Protein Sorting 4- ATPase (VPS4), and Vesicle Trafficking 1 (VTA1) accomplish the scission of MVE membrane invaginations to form ILVs[44,45]. Potentially ESCRT-independent biogenesis of exosomes may occur through syndecan proteins (SDCs) and syntenins, which are required for the normal sorting of cargo into ILVs[46], however this biogenesis process may still require ESCRT proteins and may not be truly ESCRT-independent[28].

Once intraluminal vesicles (ILVs) are formed inside of the MVE, the MVE may localize to the plasma membrane and fuse with the plasma membrane in order to release exosomes into the extracellular space. The proteins RAB27A/B are required for the translocation of MVEs to the plasma membrane and also for the subsequent fusion of MVEs with the plasma membrane[27] (Fig.3). Other RABs, such as RAB5 and RAB7[28], RAB11[29], and RAB35[30] may also be involved in MVE trafficking and exosome secretion.

Exosomes in Cancer

In addition to protein cargo, exosomes are able to transport potentially functional nucleic acids such as mRNA[47] and miRNAs[48,49]. Numerous studies have associated miRNA cargoes of exosomes with cancer progression[50–52]. Likewise, the presence or absence of “exosome biomarkers” is a growing field of diagnostic and prognostic applications. For instance, Tian et al.[53] reported on the utility of CD147 expressing extracellular vesicles in colorectal cancer patient serum as a predictive tool. Tian et al. found significantly higher CD147 in colorectal cancer patient sEVs from the plasma, which also was reduced after tumor resection. Exosomes and other extracellular vesicles are

increasingly being appreciated as vehicles by which cancers can influence their environments, and even distant organs.

CD147+ sEVs

The transmembrane protein CD147 is a multifunctional, highly glycosylated protein[54] involved in mono-carboxylate transport through interaction with monocarboxylate transporter 1 (MCT1) and monocarboxylate transporter 4 (MCT4)[55], cell signalling through binding of cyclophilin-A[56], activation of MMPs and expression of MMPs. CD147 potentially signals through homophilic interactions with secreted or cellular CD147[57], and likely through the MAPK pathway as Lim et al. demonstrated that purified CD147 induced MMP-1 transcription through MAPK protein p38[58]. CD147 engages in *cis* interactions with other membrane proteins probably due to an unstable glutamic acid residue in the single transmembrane domain of CD147[59]. The polar glutamic acid residue is shielded from the hydrophobic membrane lipid tails when CD147 oligomerizes. As such CD147 is frequently bound to CD44[60] and MCTs in the membrane and is unlikely to exist alone. CD147 has several names including tissue collagenase stimulating factor (TCSF), extracellular matrix metalloproteinase inducer (EMMPRIN), and Basigin-2 (BSG), as well as some others. CD147 is found on exosomes quite often, it is currently the 85th most commonly identified exosome protein in the ExoCarta database, a compendium of proteins and nucleic acids identified in exosomes by exosome researchers (http://exocarta.org/)[148–151]. As is the case for many other proteins it is not clear whether CD147 is selectively sorted onto exosomes either alone or as a passenger with one of its many *cis* interacting proteins. Some research groups have shown that tumor vesicles expressing CD147 are critical for MMP

production. Milia-Argieiti et al. showed that malignant human testicular germ cell sEVs induced MMP-2 expression in fibroblasts through CD147[61], similarly Colangelo et al. have published similar results showing sEVs enriched for CD147 due to irradiation enhanced astrocyte production of MMP2 and active-MMP9[62]. sEVs expressing CD147 may play a critical role in cancers modifying their environment and other organs, especially as this may speed up the process of metastasis.

MACROPHAGE BIOLOGY

Origins of tissue-resident macrophages

Macrophages are large mononuclear and phagocytic cells, typically identified by surface expression of CD97 (recognized by the antibody 'F4/80'), and usually deriving from monocytes from the yolk-sac, fetal liver or the bone marrow. Macrophages are either inflammatory or tissue-resident[63]. Circulating monocytes are recruited to sites of inflammation where they differentiate into inflammatory macrophages. Tissue-resident macrophages constitute a number of specialized macrophage types that have adapted to their unique tissue environment. With few exceptions, tissue-resident macrophages differentiate from circulating monocytes under homeostatic conditions[63]. Tissue-resident macrophage populations in adults derive mainly from fetal yolk-sac or fetal-liver monocytes or precursor cells, and are self-renewing[63–65]. However, in certain tissues, adult bone-marrow monocytes are also a source of tissue resident macrophages[64,65]. The liver is an example of an organ in which the tissue-resident macrophages derive from yolk-sac progenitor cells[64,65]. Kupffer cells, which are the tissue-resident

macrophages of the liver, represent a population of self-renewing tissue-resident macrophages derived from yolk-sac monocytes[65].

General functions of tissue-resident macrophages

Tissue resident macrophages have three general functions: (1) sampling and filtration of blood, (2) immune defense of the tissue, and (3) antigen processing and presentation to adaptive immune cells[63]. Sampling and filtration of blood by macrophages may be achieved by pinocytosis, phagocytosis of opsonized material, or receptor mediated uptake. Engulfment of circulating material by macrophages allows macrophage to collect certain materials from circulation. For example, Alveolar macrophages in the lung play a critical role in clearing inhaled particulates from the lung[63]. Liver Kupffer cells and renal Mesangial cells also play important roles in regulating the contents of blood in the portal circulation or glomerular blood respectively[63]. Macrophages express Fc Receptors (FcRs), Complement Receptors (CRs), Pattern Recognition Receptors (PRRs), apolipoprotein receptors, and other types of receptors which mediate the uptake of substances in the blood[63].

Macrophages defend the tissues in which they reside through the recognition and phagocytosis of pathogens. This in turn leads them to prime first innate and then subsequent adaptive immune responses. For instance, the phagocytosis of pathogens by Microglial cells in the central nervous system (CNS) is critical to defense of the CNS against pathogens[63]. Macrophages can detect pathogens through pattern recognition receptors (PRRs) which are a class of receptors recognizing signs of bacterial or viral presence in the tissue. PRRs, opsonin receptors (Fc-receptors and complement

receptors), and lectins all mediate the phagocytosis of pathogens by macrophages[63]. When tissue resident macrophages recognize a pathogen, they can then release inflammatory molecules such as reactive oxygen species (ROSs) to combat invading pathogens[66], as well as inflammatory cytokines and chemokines which recruit immune cells to the site of inflammation[63]. While tissue-resident macrophages can mount a defense against invading pathogens, activated tissue-resident macrophages will ultimately recruit monocytes and adaptive immune cells from the circulation through the release of cytokines[63]. Upon arrival of the latter cell types into the tissue, resident macrophages directly promote their activation via antigen presentation. Macrophages are considered “professional” antigen-presenting cells (APCs) since they route phagocytosed pathogens to the lysosome for degradation via mechanisms that generate antigens for loading onto MHC class II molecules. These complexes are then recognized by naïve T cells, resulting in activation of T-cell mediated immunity[67]

Inflammation results in the activation of tissue-resident macrophages which then participate in the recruitment of inflammatory macrophages and other immune cells[63]. Inflammatory environments, comprising the set of cytokines and immune processes that may occur in a specific location, can be divided into two classes: the Th1 or Th2 immune environments[63]. Th1 immune environments correspond with pro-inflammatory polarization of macrophages to the M1 phenotype, also called classically activated macrophages, which release proinflammatory cytokines. In contrast, Th2 immune environments correspond with M2 macrophages, also called alternatively activated macrophages, which suppress immunity through ARG1 secretion and release of anti-inflammatory IL-10 and TGF-β[63]. In the context of cancer, the phenotype of

macrophages is more complex than polarization towards one of two extremes[68] and it is not necessarily the case that all macrophages in a given tumor site will exhibit identical phenotypes. However, mapping macrophage states and immune environments to the M1/M2 and Th1/Th2 spectra provide useful reference points to explain how these cells orchestrate immune responses in the tumor microenvironment.

TUMOR ASSOCIATED MACROPHAGES

Macrophages in tumor initiation and progression

Macrophages contribute to cancer initiation through their role in inflammation. Tumor associated macrophages can participate in inflammation through the release of IL-6, TNF-α, and IFN-γ[69,70]. Tissue-resident macrophages may initiate a local inflammatory state, recruiting inflammatory macrophages from the circulation that further contribute to inflammation in the pre-cancerous tissue. Indeed, chronic inflammation such as in Crohn's disease[71] is associated with an increased risk of colorectal cancer and uncontrolled inflammation by macrophages is associated with increased risk of developing cancers in animal models[72]. Macrophages also directly contribute to tumorigenesis by producing mutagenic oxygen radicals[73,74] that can mutate cancer driver genes or cytokines and growth factors which can fuel cancer growth[70].

TAMs contribute to cancer progression

Tumor associated macrophages (TAMs) are inflammatory macrophages that contribute to cancer progression through cytokine production, recruitment of immune cells, induction of immune-suppression, promotion of angiogenesis, and promotion of

metastasis. As attested to by their Ly6C+ phenotype, TAMs are typically bone-marrow derived monocytes recruited from the circulation by inflammation[75].

The tumor microenvironment may initially be a Th1-type environment, which is highly inflammatory and associated with an M1 macrophage phenotype. Eventually, Il-4 and CSF from CD4 T cells and tumor cells[76–78] result in M2 polarization of TAMs as the tumor progresses. M2 TAMs and M2 macrophages in general are less inflammatory than M1 macrophages and are considered pro-tumorigenic for their immunosuppressive, pro-angiogenic, and pro-metastatic functions. Specifically, M2 macrophages may express and secrete decoy receptors such as the PD-1 ligand and non-classical MHCI molecules HLA-E and HLA-G. These inhibit CD8 T cell function and NK cell function, respectively[79,80]. The cytokines CCL20 and CCL5 produced by M2 macrophages can recruit[81–84] or induce[85] regulatory CD4 T cells. Additionally, M2 macrophages can suppress immunity globally through IL-10, TGF-β, and ARGINASE-1 secretion[86–89].

TAMs also play an important role in angiogenesis. M2 macrophages release the angiogenic protein VEGF under certain conditions[90]. Macrophages also produce VEGF directly as a consequence of stimulation by CSF[91]. Furthermore, Wnt7b from TAMs appears to cause VEGF expression in endothelial[92]. TAMs participate in a feedback loop with tumor cells leading to intravasation, which is the process of tumor cells entering circulation that is also necessary for metastasis. TAMs appear to release EGF in response to CSF from tumor cells. EGF from TAMs in turn promotes cancer cell CSF production, establishing a paracrine loop that has been shown to be required for

migration in a mammary tumor model[93,94]. This paracrine loop occurs in the context of IL-4 release from regulatory CD4 T cells, which supports M2 polarization of macrophages, and TGF-β secretion by TAMs, which promotes epithelial to mesenchymal transition in tumor cells[95,96]. Overall, this loop supports the migration of tumors into blood vessels and supports their wider dissemination to metastatic sites[97]. TAMs also produce ECM degrading proteases which may support the co-migration of tumor cells and macrophages[75,98].

Metastasis and Metastasis associated macrophages (MAMs)

Macrophages that are both resident in and recruited into metastatic sites aid cancer cells in forming secondary cancers through (1) encouraging tumor cell extravasation and (2) inhibiting anti-tumor immunity at the metastatic site (Fig.4). The mechanisms by which metastasis associated macrophages (MAMs) inhibit anti-tumor immunity are the same as the ways in which TAMs generally inhibit anti-tumor immunity. However, the role of metastasis associated macrophages is unique in that these macrophages also promote arrest of circulating tumor cells in the vasculature at metastatic sites and aid in their extravasation and outgrowth into metastases. Qian et al.(2009 and 2011), found that preventing the recruitment of macrophages to arrested circulating tumor cells in the vasculature prevented their extravasation[99,100]. They observed that when macrophage recruitment is inhibited, metastases that do form are infiltrated by dendritic cells and cytotoxic CD8 T cells, suggesting that MAMs establish an immunosuppressive immune environment that promotes growth of newly-established metastases[101].

THE LIVER PREMETASTATIC NICHE

Colorectal cancers metastasize mainly to the liver, with a large amount of metastases in the lungs also[102]. The process of metastasis has long been thought to include complex interactions between the metastasizing cancer cell and its environment, beyond mere circulation and random distribution. Observations of some selectivity in the site of metastasis were explained by two hypotheses: Paget's seed and soil hypothesis, where the properties of the "seed", the circulating cancer cells (CTCs), are essential, and Ewing's hypothesis that mechanics of blood flow and vascular structure determine the site of metastasis. In the case of colorectal cancer, preferential metastasis to the liver is usually attributed to circulating tumor cells traveling through the portal vein that leaves the colon and directly enters the liver. The past two decades have uncovered the existence of a pre-metastatic niche (PMN) that aids in establishing metastases[103]. The PMN forms before metastases through the influence of cancer secreted factors and extracellular vesicles and involves changes in cellular composition, extracellular matrix structure, and vascular structure. These changes in the pre-metastatic site are thought to increase the likelihood of successful metastasis formation.

Tumor Extracellular Vesicles in Pre-Metastatic Niche Formation

In 2015 Hoshino et al.[104] and Costa-Silva et al.[105], published evidence that a pre-metastatic niche can be formed by extracellular vesicles from cancer cells. While Costa-Silva et al. demonstrated that pancreatic cancer cell line exosomes induce liver metastasis in a TGF-beta-dependent manner, Hoshino et al. explored the role of integrins in directing exosomes to future site of metastasis and uncovered integrin

alpha/beta combinations in mice which direct exosomes to one tissue or another. Hoshino et al. also discovered that Kupffer cells in the mouse liver were the main recipient of exosomes applied intravenously. Other extracellular vesicles such as apoptosomes and microvesicles may also play important roles in PMN formation. Some mechanisms by which extracellular vesicles might induce a PMN are known, such as through macrophage migration inhibitory factor (MIF), and activation of S100 genes[104,105]. It is likely that many components of the extracellular cargo including nucleic acids, such as miRNAs, and proteins, both within the extracellular vesicle and incorporated in the vesicle membrane, can exert pro-metastatic effects at any conceivable site of metastasis before metastasis establishment. The early results in this field present proofs of principle however, there remains a need to collect clinical data from pre- and post- metastasis patients to better understand the mechanisms by which extracellular vesicles create PMNs.

MATRIX METALLOPROTEINASES (MMPS)

General

Matrix metalloproteinases (MMPs) are a family of zinc-dependent proteases that are collectively capable of digesting most components of the extracellular matrix. MMPs also process growth factors, cytokines, chemokines, cell-receptors, and other MMPs[106,107]. The basic structure of MMPs consists of a pro-domain and a Zn^{2+}-binding catalytic domain, and MMPs may also possess furin domains, fibronectin II-like domains, and hemopexin domains. MMPs possessing C-terminal or N-terminal transmembrane domains are categorized as membrane-tethered MMPs (MT-

MMPs)[108]s, whereas all other MMPs are eventually secreted into the extracellular space. MMPs are potent contributors to PMN formation. The modification of the extracellular matrix in the PMN liberates growth factors into the microenvironment and is part of vascular remodelling promoting metastasis establishment[109], further, MMPs release degradation products that promote carcinogenesis[110].

ECM Degradation

The most widely recognized function of MMPs is the degradation of ECM proteins. Each MMP has a unique affinity for certain ECM proteins, usually with a single favored substrate. MMP substrates include collagens, gelatin, elastin, laminin, and several other ECM proteins[111]. MMPs expression in cancers is associated with poor prognosis[112–114]. The ability of MMPs to degrade ECM proteins suggests a role for MMPs in the invasion and metastasis of cancers, as invasion requires invasion through the tissue ECM, and metastasis requires degradation of the collagen basement membrane in order for cancer cells to intravasate. Degradation of the ECM by MMPs contributes to several aspects of PMN formation. MMPs are able to induce angiogenesis through the release of VEGF from the ECM[115]. MMPs also cleave several chemokines [116–118], which are activated or inactivated due to MMP processing and may cause the recruitment of immune cells. ECM degradation as a direct consequence of MMP proteolytic activity also creates space for invading cells. In summary, MMPs can contribute to angiogenesis, cell recruitment through chemokine activation, and ECM degradation, all of which are important components of PMN formation.

MMP12

We investigated MMP12 in particular due to some preliminary data suggesting it was regulated by sEVs (data not shown). MMP12 is an elastase enzyme that preferentially degrades elastin in the extracellular matrix. Elastin is not a component of the basement membrane, and thus MMP12 will play a limited role in extravasation and intravasation. As is the case for other MMPs, MMP12 activity releases degradation fragments known as “matrikines”[110]. Matrikines are the fragments of ECM components which often have unique biological properties. Elastin degradation products are able to induce pro-tumorigenic processes including angiogenesis in rats[119], and proliferation in human astrocytoma cells[120]. Notably, elastin degradation products can induce MMP-1 and MMP-3 expression in human fibroblasts[121,122], both of which are associated with poor cancer prognosis. The role of MMP-12 in cancer is not well-studied, although considering that MMP-12 activity can drive MMP-1 and MMP-3 expression through matrikine release it may be a significant contributor to cancer progression. The transcription of MMP12 is regulated by AP-1[123] as well as some other transcription factors such as TCF-4, PEA-3 and TRF[124]. The promoters of several other MMP genes contain AP-1 binding sites[125], suggesting that the AP-1 transcription factor is critically important in regulating MMP expression and downstream events.

MAPK/AP-1 Signalling

The MAPK/AP-1 Proteins

The MAPK signalling cascade involves a number of kinase kinases beginning with MAPKKKKs (MAP4Ks) and culminating in the phosphorylation of MAPKs which then

carry out transcription or phosphorylation of transcription factors and other proteins. The stimuli which induce MAPK pathway activation are numerous and diverse. Growth factors[126], phorbol esters[127], heat shock[128], DNA damage[129], osmotic shock[130], and hypoxia[131] are able to activate one or more branches of the MAPK pathway Downstream of MAPK signalling through either ERK, JNK, or p38 is the AP-1 transcription factor family[132]. The AP-1 transcription factor complex is the combination of dimers made of JUN, FOS/FRA, ATF, and MAF proteins capable of binding to the AP-1 DNA binding sites known as the TPA response element (TRE) and cyclic-AMP response element (CRE) in gene promoter regions[133]. AP-1 proteins also belong to the basic leucine zipper protein (bZIP) family. Notably, some AP-1 transcription factors are both transcribed and post-translationally modified by MAPK pathway activation.

All the JUN proteins are able to bind the consensus AP-1 site (TGACTCA) and this DNA requires the C-terminal homologous region of JUN proteins. The other heterogeneous domains of JUN proteins are likely responsible for the difference in function between JUNs[134]. When AP-1 is activated through the JNK-MAPK pathway, JNK phosphorylates c-JUN, enhancing its transcriptional activity[135]. Activated c-JUN may then form an AP-1 homodimer or heterodimer and bind DNA to perform it's transcriptional function[136–138]. The result of AP-1 protein phosphorylation is dependent on the phosphorylation site, seemingly on a domain by domain basis. Phosphorylation of the basic DNA binding region appears to inhibit JUN activity[139], presumably by causing repulsive electrostatic interactions between added phosphates and the phosphate backbone of DNA strands. Based on this finding, the phosphorylation of JUN proteins and other AP-1 proteins in the DNA binding domain is probably inhibitory. The Fos proteins all dimerize with Jun to

form AP-1 heterodimers and unlike Jun proteins do not form homodimers. Interestingly, the AP-1 dimers formed between Jun and Fos bind AP-1 sites with greater affinity than Jun homodimers[136] suggesting that the Jun/Fos dimer is among the most potent AP-1 dimer configurations.

HYPOTHESIS

We hypothesized that CRC sEVs regulate formation of the pre-metastatic niche through activation of MMP expression and secretion by liver macrophages. Mechanistically, we hypothesized that CD147+ CRC sEVs form the pre-metastatic niche by inducing MAPK/AP-1 pathway activation in macrophages which leads to MMP expression. The following research aims summarize our strategy to test our hypothesis. AIM 1: To discover the impact of genetic instability subtypes on colorectal cancer cell sEV composition. AIM 2: To test the role of colorectal cancer sEVs in enhancing macrophage MMP release, macrophage invasion-promoting behaviour, and MAPK/AP-1 pathway activation. AIM 3: To test the necessity of CD147 positive (CD147+) sEVs in sEV induced macrophage phenotypes. The results of these studies will contribute to a growing body of knowledge concerning the composition and function of sEVs in cancer and in cancer metastasis, and also elaborate upon the role of CD147+ sEVs in pro-metastatic sEV functions (Fig.5)

FIGURES

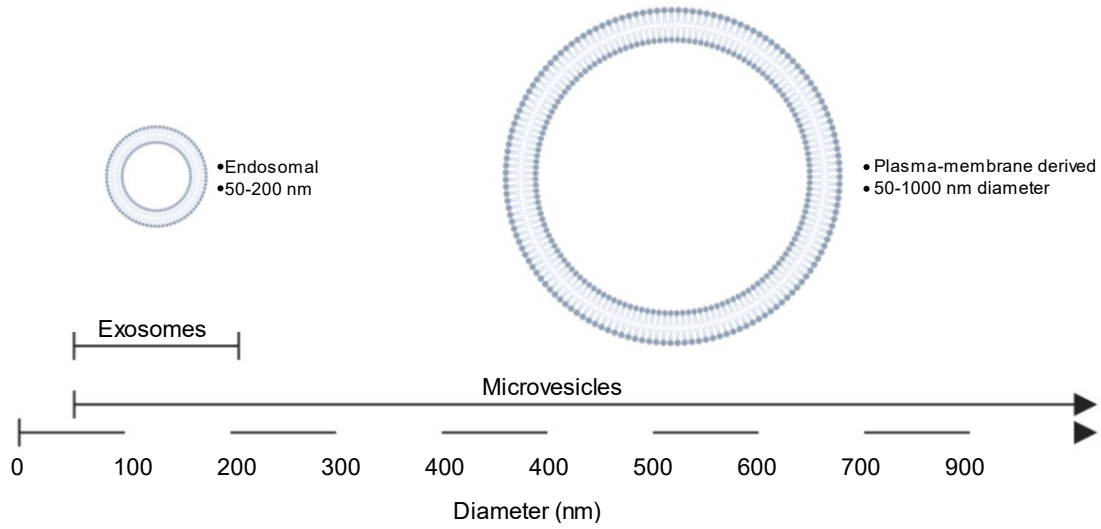

Figure 1 - Simple categorization of extracellular vesicles.

Exosomes (left) are small extracellular vesicles with diameters between 50-200 nm (sometimes said to be smaller), and that originate in the endosomes. Microvesicles (right) are larger extracellular vesicles which originate in the plasma membrane.

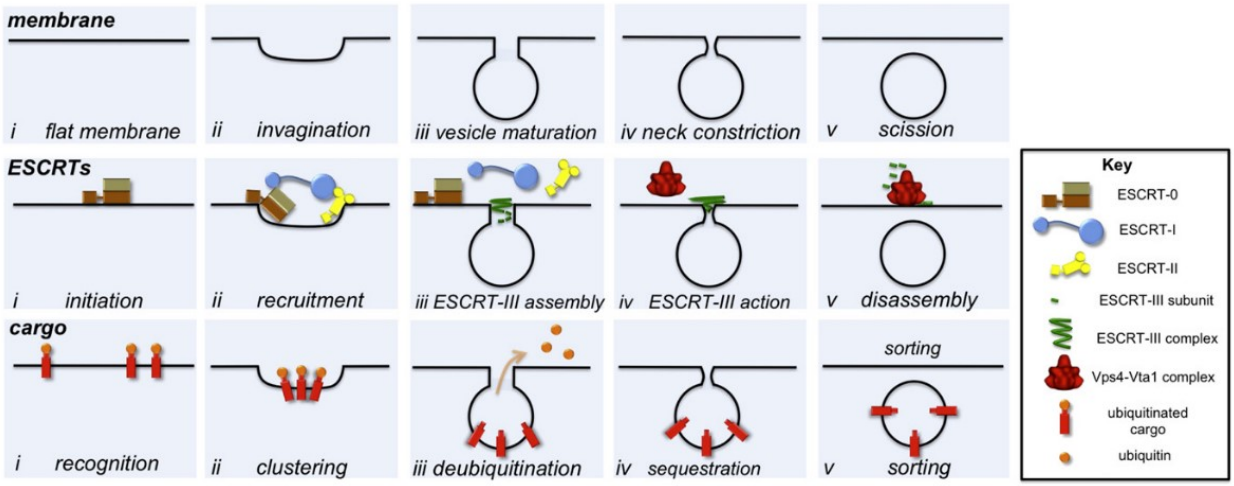

Figure 2 - The ESCRT-dependent ILV and Exosome Biogenesis Pathway

Three processes occur simultaneously during ESCRT-dependent ILV formation: (1) inward budding of the endosomal membrane (top row), (2) recruitment of ESCRT complexes ESCRT-0 to ESCRT-III in series, and finally, recruitment of VPS4 and VTA-1, and (3) sorting of cargo into the ILV. The ESCRT complexes participate in both the inward budding of the endosomal membrane and the sorting of ubiquitinated proteins into the ILV. Ultimately, ILVs may be released into the plasma membrane and hence the ESCRT pathway is an exosome biogenesis pathway. Adapted from Henne, *Developmental Cell* (2011)[140].

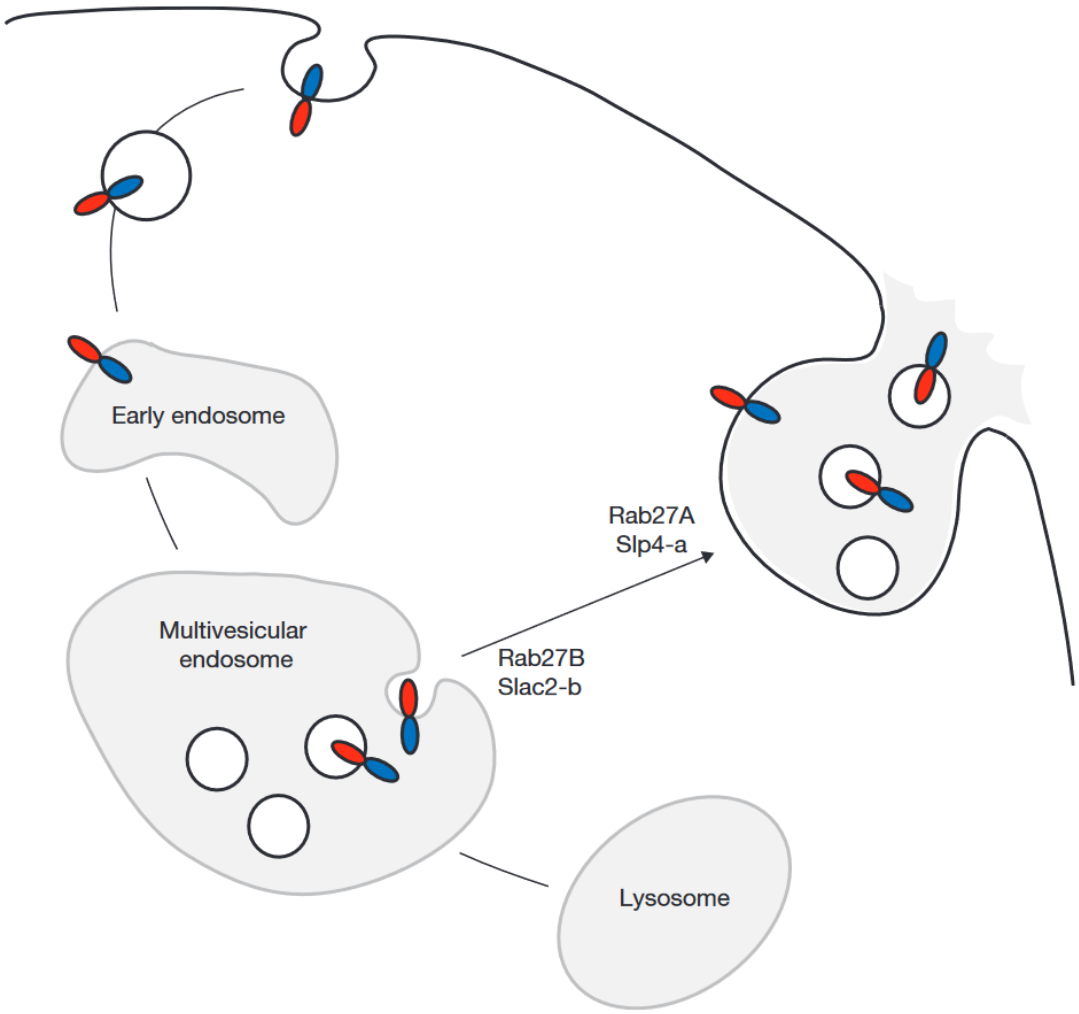

Figure 3 - Multivesicular Endosomes are trafficked to the plasma membrane by the proteins RAB27A and RAB27B.

Multivesicular endosomes are essentially late endosomes, in which the process of ILV formation has already occurred. Multivesicular endosomes may fuse with the lysosome resulting in degradation of the material they carry. Alternatively, the proteins RAB27A and RAB27B can facilitate fusion of the multivesicular endosome with the plasma membrane. RAB27B is required for the translocation of multivesicular endosomes to the

plasma membrane and RAB27A is required for fusion with the plasma membrane[27].

Adapted from Pfeffer, *Nature Cell Biology* (2010)[141].

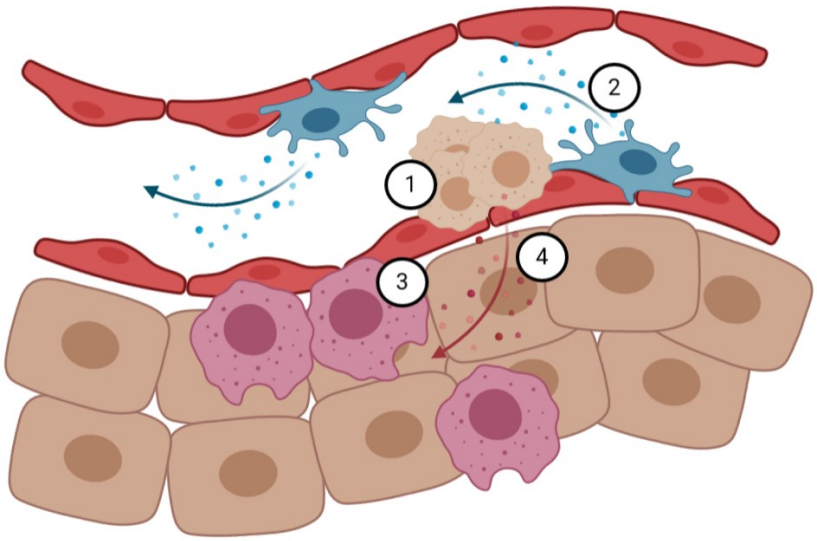

Figure 4 - Simplified role of macrophages in tumor metastasis

Circulating tumor cells (1) may arrest in the vasculature of an organ and cause inflammation. Tissue-resident macrophages, such as Kupffer cells in the liver (2), will then recruit inflammatory macrophages (3) that infiltrate the inflamed tissue, contribute to further inflammation, and may promote extravasation of the tumor cell. The interaction of tumor cells with tissue-resident and inflammatory macrophages (4) results in polarization of macrophages towards the immunosuppressive and potentially pro-angiogenic M2 phenotype via tumor cell release of CSF, and macrophage production of ARG1, IL-10, and TGF-β. Of course, it is possible the macrophage populations of a tissue are changed prior to the arrival of circulating tumor cells, as is the case in the premetastatic niche. Figure made with Biorender®.

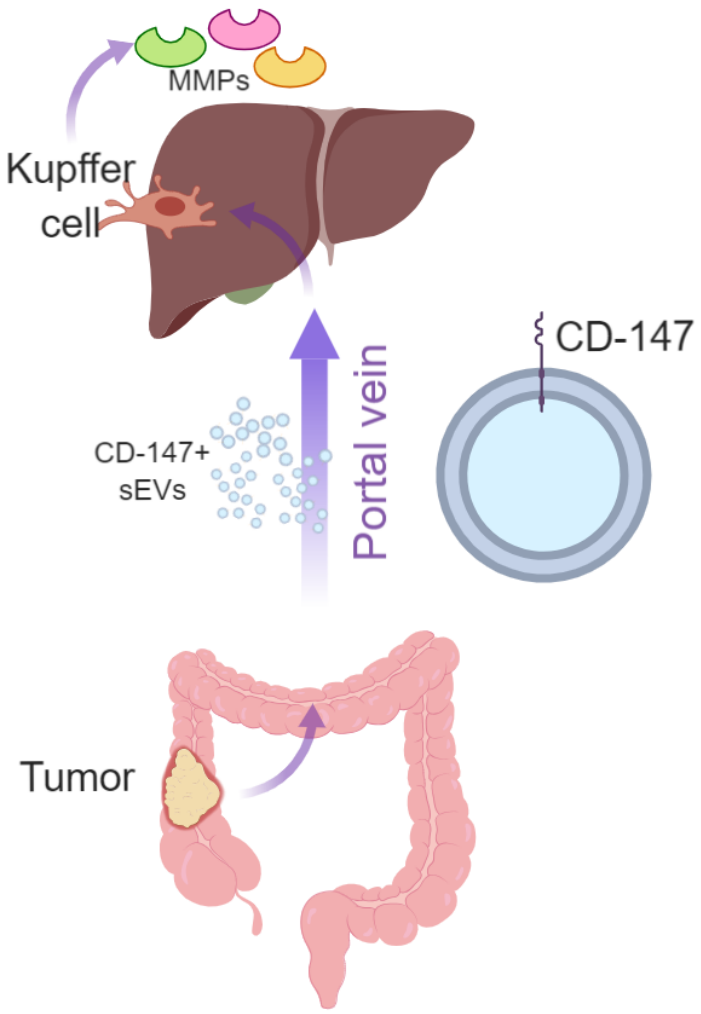

Figure 5 – Schematic of the hypothesis investigated in this thesis: CD147+ sEVs cause MMP-mediated PMN formation by Kupffer cells.

Colorectal cancers (bottom) may release CD147+ sEVs (center; arrow, bottom), which traverse the portal vein (center) and induce Kupffer cell MMP production (top; arrow, top) that facilitates establishment of liver metastases. Figure made with Biorender®.

CHAPTER 2: MATERIALS AND METHODS

CELL CULTURE

Cell Lines

All cell lines and primary cells were grown in 37 °C, 5% CO_2 incubators. We used the MC38 colorectal adenocarcinoma cell line[142], RAW264.7 cells, and the NIH-3T3 cell line. Knockout MC38 mouse colorectal cancer cells were generated by another graduate student in the lab, Courtney Mowat. MC38 cells (Kerafast) were transfected with the pSpCas9(BB)-2A-puro (px459) V2.0 plasmid (Addgene) either without a guide-RNA in the case of the empty vector plasmid, or containing guide-RNAs directed to the *Mlh1*, *Polε,* or *Rad51* gene (Table 2). Transfected cells were selected in puromycin-containing media (2 µg/mL) and successfully knocked out clones for each gene were identified via sequencing and Western blotting. Confirmed knockout cells were grown in high-glucose DMEM supplemented with 10% FBS, 1%Penicillin/Streptomycin, and 1%HEPES. High glucose DMEM is supplied by facilities of the Cross Cancer Institute.

In order to knock down CD147, MC38 Empty pSpCas9 Vector cells were subsequently transfected using Lipofectamine 2000 (ThermoFisher) with a pLKO.1-HygroR shRNA (Addgene) plasmid containing a CD147 targeting shRNA sequence (Table 2). Successfully knocked down cells were selected, verified for CD147 depletion using Western blotting, and maintained in hygromycin (250 µg/mL).

Mouse macrophage RAW264.7 cells from ATCC were generously provided by Dr. Matthew Macauley (University of Alberta). RAW264.7 cells were maintained in RPMI-

1640 (Gibco) supplemented with 10% FBS, 1% Penicillin/Streptomycin, and 1% HEPES. NIH-3T3 cells were generously provided by Dr. Rosaline Godbout (University of Alberta). The fibroblast NIH-3T3 cells were cultured in 10% FBS, 1% Penicillin/Streptomycin, 1% HEPES supplemented high-glucose DMEM.

Primary Cells

Bone-marrow derived macrophages (BMDM) and bone-marrow derived dendritic cells (BMDC) were made from C57BL/6 mice purchased from Charles River and bred and maintained in the Cross Cancer Institute facilities. In order to culture BMDM and BMDC, bone marrow cells were collected from the femur and tibia of mice . The femurs and tibias were resected from the mouse, de-fleshed using kimwipes, and then sterilized in 70% ethanol for 2 minutes. Femurs and tibias were then washed in phosphate buffered saline (PBS, Hyclone), and cut to remove the epiphyses. The bone marrow was flushed from the bone-shaft using PBS injected through a needle and syringe. Bone marrow cells were then mixed by pipetting using a 5 mL serological pipette, filtered using a 40 µm filter, and then the filtered cell suspension was pelleted at 1,500 rpm for 5 minutes (Allegra X-30R Centrifuge, SX4400 rotor, Beckman Coulter). After 1 wash with PBS, the bone-marrow cells were counted then plated in non-tissue culture treated petri dishes in high-glucose DMEM, with 10% FBS, 10 mM HEPES, 1% Penicillin/Streptomycin. For BMDM culture, 20 x 10^6 bone-marrow cells were plated with 20% M-CSF supernatant from L929 murine fibroblast cells. For BMDC culture, 5 x 10^6 bone-marrow cells were plated with 10% GM-CSF supernatant from B16-GMCSF melanocytes. BMDM and BMDC were supplied fresh media on day 3 after plating, then the BMDM and BMDC were harvested on Day 7 or Day 5 depending on cell confluence, frozen in media with

10% DMSO, and stored in liquid-nitrogen cryopreservation tanks in aliquots containing 5-10 x 10^6 cells.

Kupffer cells, the liver tissue resident macrophages, were purified from mice as described in Li et al.[143]. In order to collect Kupffer cells, C57BL/6 mice livers were perfused with warm PBS to flush blood. PBS was injected into the liver blood vessels through the portal vein and allowed to flush from the liver through a severed inferior vena cava. After perfusion, the liver was resected and placed in PBS on ice until further processing. Mouse livers were mechanically homogenized in 1.5 mL microfuge tubes using scissors, then enzymatically digested for 30 minutes at 37°C in 10 mL RPMI-1640 containing 0.1% Type IV collagenase (Sigma Aldrich C5138-5G) and 0.1 mg/mL DNase I (Mandel Scientific, EPI-E3101K). After enzymatic digestion, the liver homogenate was filtered through a 100 µm cell strainer and then undesired cell populations were removed through a series of centrifugations, all performed at 4°C. First, the liver homogenate was centrifuged at 300 g for 5 minutes and the supernatant was discarded. The cell sediment was then washed in RPMI-1640 and centrifuged once more at 300 g for 5 minutes. The cell sediment was washed in RPMI-1640 once more and centrifuged at 50g for 3 minutes, after which the supernatant was kept and transferred to a new tube. Finally, the supernatant was centrifuged at 300g for 5 minutes, and the cell sediment was resuspended in supplemented DMEM and plated as needed for downstream experiments. Two hours after plating, the non-adherent cells were washed away and the media is replaced. This adherent population of cells were the desired liver macrophages with potentially some other contaminating cells. In order to validate the identity of Kupffer cells purified from mice, the cells were stained with antibodies for

CD11B, CD11C, CD45, and F4/80 (Table 1) and analyzed on the CytoFLEX flow-cytometer (Beckman Coulter). FlowJo (BD Biosciences) was subsequently used for analysis of the Kupffer cell immunophenotype.

NANOPARTICLE TRACKING ANALYSIS (NTA)

sEVs were purified from the supernatant of MC38 cells using standard techniques as outlined by Thery et al. in 2006[144]. 2-5 x 10^6 cells were seeded in normal cell culture media in 10-20 T175 cell culture flasks (SARSTEDT, TC Flask T175, Standard) and permitted to grow for 1 day. On day 2, the cell culture media was replaced with sEV collection media, which contains sEV-depleted FBS (dFBS) (Fig.6Bs), rather than regular FBS. sEV collection media comprised of 10% dFBS, 1% Penicillin/Streptomycin, 1% HEPES in high-glucose DMEM (Hyclone). After applying sEV collection media the cells were incubated for ~48 hours in order for sEVs to be released into the sEV collection media. After 48 hours of incubation, the sEV collection media from all flasks was pooled and subjected to serial ultracentrifugation in order to pellet the sEVs. Undesired particles in the sEV collection media were first pelleted in series at 300g for 10 minutes (Allegra X-30R, Beckman Coulter), 2,000g for 20 minutes (Allegra X-30R) and ultracentrifugation at 10,000g for 30 minutes (Beckman Coulter, SW-30 Ti). sEVs were finally pelleted at 100,000g for 1 hour 10 minutes (Beckman Coulter, SW-30 Ti) after which the sEVs were pooled and washed in PBS then re-pelleted at 100,000g for 1 hour 10 minutes. The resultant pellet of sEVs was resuspended in 200 µL of PBS (HyClone) and stored in 10 µl aliquots at -80°C.

NTA of cell line sEVs – The NanoSight LM10 (Malvern Panalytical) was always used to measure the diameter and concentrations of sEVs purified from MC38 cells, as established by Dragovic et al.[145]. To determine sEV concentrations, an aliquot of purified sEVs was diluted to concentrations within the measurable range of the Nanostight LM10 (40-200 particles per frame). The concentration of each sEV sample was then measured 3-5 times for 30-60 seconds using the Nanosight LM10.

Depletion of sEVs in FBS for use in sEV Collection media

FBS was centrifuged at 100,000g for 20 hours in order to deplete sEVs and generate dFBS. The resulting supernatant was collected and used in MC38 cell line culture as part of the sEV collection media. FBS diluted 1:10 or more was applied to NTA measurement to determine sEV concentration.

Measurement of sEV Concentration in Ultracentrifuged Conditioned Media

MC38 Empty Vector cells, which we treated as a control, and the MC38 shCD147 cells were grown by first seeding 1 x 10^6 cells in a 10 cm petri-dish and allowing them to adhere overnight. The next day, fresh media was applied to each plate, and over 24 hours of incubation at 37°C,, conditioned media was generated. For some experiments requiring sEV depletion, conditioned media generated by MC38 control or MC38 shCD147 cells was divided in two and half was subjected to ultracentrifugation to deplete sEVs (100,000g, 1 hour). After ultracentrifugation, NTA was used as described previously to measure sEV concentrations of conditioned media.

GW4869 Toxicity Curves

To assess the amount of cell death caused by different concentrations of the neutral sphingomyelinase inhibitor GW4869 (Sigma-Aldrich), we used the cell death detector dye ZombieAqua (Biolegend). MC38 Empty Vector or MC38 Mlh1 CRISPR knockout (Δ*Mlh1*) cells were treated with 0.1-50 μM GW4869 for 24 hours, detached from the plate using 0.125% Trypsin, then stained with ZombieAqua after which flow cytometry (CytoFLEX, Beckman Coulter) was used to detect fluorescence due to ZombieAqua (BioLegend) uptake, which is indicative of cell death.

Protein Quantification and Western Blotting

sEV protein lysates were generated by mixing equal volumes of sEV aliquots and protein lysis buffer (50mM Tris-HCl, 150mM NaCl, 50mM sodium pyrophosphate, 1mM EDTA, 0.5% NP40, 1% Triton X-100, 1mM sodium orthovanadate, and 1:100 protease inhibitor (Sigma-Aldrich)). Whole cell lysates from were collected from cells in 6-well plates or 10 cm plates. The cells were placed on ice, washed once in ice-cold PBS, and then we applied 200-300 μL of protein lysis buffer to lyse the cells. The lysates were then collected using a cell scraper and rotated in a 4-degree cold room for 30 minutes. After 30 minutes of rotation, the cell lysates were centrifuged at 12,000g for 15 minutes, and only the supernatant was kept. sEV protein and cell lysate concentrations were measured through the Bicinchoninic acid (BCA) protein quantification assay. To measure protein concentration, standard curves of bovine serum albumin (2000 μg/mL – 0 μg/mL) were prepared in 96-well plates through serial 1:1 dilution with protein lysis buffer. Alongside the standard curve, 10 or 25 μL of protein samples of any kind were

plated in duplicate, and 200 µL of BCA solution was applied to equal volumes of standard curve solution and sample solutions in duplicate. The BCA reaction was incubated at 37°C for 30 minutes, cooled at room temperature for 10 minutes. After cooling of the BCA reaction, the absorbance at 562 nm was measured in order to measure protein concentration. The concentration of protein samples was measured by interpolating from the absorbance of protein solutions in the standard curve. Finally, protein lysates are diluted to 0.8X by the addition of denaturing loading buffer (10% SDS, 25% glycerol, 0.25 M Tris-HCL ph 6.8). Equal amounts of protein alongside protein size ladders (BLUElf and PiNK Plus, FroggaBio) were loaded in all western blots, and then electrophoresed through 10% SDS poly-acrylamide gels for 1-1.5 hours. Proteins in the SDS-PAGE gels were then transferred to 0.22 µm nitrocellulose membranes (GE Healthcare Life Sciences) for 1-1.5 hours in 1X transfer buffer (0.25M Tris, 1.91M glycine, and 20% methanol). Subsequently, the nitrocellulose membranes were washed briefly in 1X TBST (10 mM Tris-HCl pH 8.0, 150 nM NaCl, 0.1% Tween-20), and blocked in 5% powdered skim milk in TBST (Carnation milk powder) for 1 hour. Membranes were then washed for 3x5 minutes with 1X TBST before the membranes were incubated at 4°C overnight with primary antibodies (Table 1) diluted in 5% BSA (1X TBST, 0.02% sodium azide) to concentrations ranging from 1:500 to 1:2000, depending on the antibody. The primary antibody was then washed off the membranes by 3x5 minutes washes with 1X TBST, and then the appropriate HRP-conjugated secondary antibody was applied for 1 hour to membranes diluted 1:2000 in 5% powdered skim milk in TBST. Finally, membranes were washed 3x5 minutes in 1X TBST, then visualized by chemiluminescence using ECL™ Prime Western Blotting

Detection Reagent (GE Healthcare Amersham™) and films (Fuji RX) developed in a Kodak developer.

sEV Western Blots

5 µg of sEVs from the MC38 empty vector cell line were prepared as described above, electrophoresed on SDS-PAGE gels and then directly immunoblotted with each relevant primary antibody.

Short-Term Stimulation of Macrophages with sEVs, and Western Blotting of MAPK/AP-1 Proteins

For these experiments, RAW264.7 cells were first cultured until sub-confluence, washed with 1X PBS (HyClone), then detached from the plate using fresh supplemented RPMI-1640 and cell-scraper (FisherScientific). RAW264.7 cells were counted using a heamocytometer or the CytoSmart counter (CORNING) and then 1 x 10^6 cells were seeded into as many wells of 6-well plates as required. Then, the RAW264.7 cells were allowed to adhere and were left overnight, on the next day the RAW264.7 cells were stimulated with either 0 sEVs, 1 µg/mL of MC38 Empty Vector sEVs, or 1 µg/mL of shCD147 sEVs for the 15 minutes, 30 minutes, 1 hour, or 2 hours. After the stimulation with CRC sEVs, RAW264.7 cell lysates were collected as described above. Kupffer cell stimulations were similarly performed after the first day of culture.

Transmission Electron Microscopy

sEVs were fixed in 2% paraformaldehyde, 1% glutaraldehyde at a 1:1 ratio. 5-10 µL of sEVs were placed on a Glow discharge 400 mesh carbon film grid, allowed to adsorb

for 2 minutes, after which we removed excess liquid and rinsed the film 3 times with water. Finally, we stained the film with 0.5% uranyl acetate in water for 1 minute then allowed it to air-dry for up to 24 hours before imaging using transmission electron microscopy (TEM). TEM was conducted by staff of the Cross Cancer Institute Imaging Facility on the JEM-2100 microscope (JEOL Ltd.), and analyzed using the software DigitalMicrograph (GATAN Inc.).

sEV Mass Spectrometry

sEVs were purified twice per cell line on two separate occasions and from separate batches of cells to generate true biological replicates. The cell lines used for this were MC38 Empty Vector cells, MC38 Δ*Mlh1* cells, MC38 Δ*Pole* cells, and MC38 Δ*Rad51* cells. The duplicate MC38 cell line sEVs were collected 10 months apart. Each time, 10 micrograms of sEVs were loaded in SDS-PAGE gels, electrophoresed and visualized with Brilliant Blue R-250 Coomassie (FisherScientific), or Silver-Stain, then submitted to the Alberta Proteomics and Mass Spectrometry Facility (University of Alberta) for total protein LC-MS/MS identification from whole lanes of a gel. Only proteins identified in both biological replicates for each cell line were included in our final analyses to stringently select protein hits that were stably associated with the cell line mutations.

Mass spectrometry figures were generated using the free bioinformatics tool 'FunRich'[146]. sEV proteins identified by mass spectrometry were comprehensively analyzed using the free bioinformatics resource DAVID[147] gene ontology analysis function. DAVID (https://david.ncifcrf.gov) allows the analysis of a set of genes or proteins through gene ontology (GO) terms, and other methods. DAVID allowed us to

comprehensively analyze the numerous proteins identified in our mass spectrometry experiments by identifying functionally-enriched or feature-enriched groups of proteins in the data. Our data was also compared to that uploaded on to the online exosome content database ExoCarta in order to determine which of our hits were are also frequently identified in exosomal proteins by other researchers.

MEASUREMENT OF MMP PRODUCTION

To robustly measure the release of MMP by RAW264.7 cells, BMDM, BMDC, and NIH-3T3 cells, 1 x 10^6 cells were plated in 35mm well, 6-well plate (Fisherbrand) and incubated in a 37°C incubator overnight to allow cells to adhere. The next day, the cells were treated in duplicate with sEVs from 4 batches of separately purified sEVs from the MC38 Empty Vector cells. Concentrations of either 25 ng/mL or 125 ng/mL were used for stimulation and media alone was added to the untreated controls. 24 hours after the addition of each dose of sEVs, the cell culture supernatant was collected. Cell culture supernatant was stored at -80°C before the activity assays were performed. gMMP and MMP12 levels in the cell culture supernatant were measured using the respective activity assays.

The level of MMP production by cells was determined using functional MMP assay kits purchased from AnaSpec (AS-71158, AS-71157). Generic MMP activity (gMMP) and MMP12 activity can be measured by these kits. To conduct the assays, cell culture supernatants were allowed to thaw at room temperature. gMMP and MMP12 activity in the supernatant were measured exactly as instructed in the kit protocols for measuring activity in biological samples in the 384-well plate (CORNING, No.3708) end-point

format, except cell culture media was not centrifuged and we did not first artificially activate MMPs in the supernatant with 4-aminophenylmercuric acetate before measuring MMP activity.

Treatment of Macrophages with Conditioned Media and Analysis of MMP Production

Conditioned media from MC38 cells after ultracentrifugation was applied to RAW264.7 or Kupffer cells for 1 hour, after which the conditioned media was removed and the macrophage cells were permitted to secrete MMPs into the supernatant for 24 hours.

Conditioned media from MC38 cells was generated as described above. RAW264.7 cells were seeded in 35 mm, 6-well plates, at 1 x 10^6 cells per well allowed to adhere for 24 hours. Kupffer cells were collected from mouse livers and the cells from one liver were divided across all wells of a 6-well plate, resulting in sub-confluent cells. Kupffer cells in this experiment were treated the day after they were purified as described above. RAW264.7 or Kupffer macrophages were then treated with plain media or MC38-conditioned media from the same batch that had or had not been depleted of sEVs using the ultracentrifugation protocol described above. Macrophages were treated with conditioned media for 24 hours. The conditioned media was then washed off and fresh media was added. The macrophages were then permitted to grow for 24 hours before their supernatant was collected and assayed for generic MMP and MMP12 activity as described above.

Measuring Changes to the Cancer Cell Invasion Promoting Behaviour of RAW264.7 cells and Kupffer Cells After sEV-treatment

RAW264.7 or Kupffer cells were treated as described above with either CRC sEVs or conditioned media. The resulting cell culture supernatants were applied below transwells inserts (Sarstedt) with 5 um pores that had been coated with Matrigel (Corning) to provide an ECM surface. 250,000 MC38 cells were seeded in 0.5% FBS media in the top-chamber of the transwells. MC38 cells were allowed to invade for 24 hours after which invaded cells were stained using 0.5% Crystal Violet, imaged using the AxioSkop optical microscope (Zeiss), and then counted manually using the free ImageJ software (National Institutes of Health).

Labelling of sEVs with a Fluorescent Dye (CM-DiI)

sEVs from the MC38 Empty Vector cells were stained with CellTracker CM-DiI dye (ThermoFisher) at the recommended concentration for 20 minutes at 37°C. After incubation, the sEVs were eluted as 500 µL fractions through an IZON qEV 35nm size-exclusion chromatography column in order to remove the unbound dye. Following fractionation, the sEV fractions were sequentially run through the CytoFLEX flow cytometer to detect the elution fraction of fluorescently labelled sEVs. The CytoFLEX flow cytometer was set up to detect sEVs using the 405 nm laser and violet side scatter (V-SSC) detectors. ApogeeMix calibration beads (Apogee, #4192) to calibrate V-SSC gains prior to measurement of sEVs. CM-DiI fluorescence in sEVs was measured in the PE-channel.

INTRASPLENIC LIVER METASTASIS MODEL

Intrasplenic injection of MC38 cells to form metastases was conducted as described by Kuruppu et al.[152] (Fig.13C). We anaesthetized mice for injection of tumor cells to the spleen using isoflurane. Anaesthetized mice were placed on water-heated beds to avoid hypothermia. We prepared the incision site by shaving fur around the incision site and sterilized it using soap and water, and the betadine antiseptic solution. To access the spleen, we made a 1.5 cm incision through the skin and abdominal wall of the mice. The incisions begin on the center of the left flank of the mouse, about 1 cm below the mouse rib cage, running lengthwise down the mouse, towards the rear legs. The spleen was then pulled halfway out of the mouse and laid on saline solution soaked gauze to immobilize it. We used a 1 mL syringe connected to tubing ending in a 27 gauge needle tip to inject cells into the spleen. The needle tip was clamped onto the spleen to prevent backflow of cells. A pump (Pump 33, Harvard Apparatus) was used to slowly inject 100 µl of a 1,000 cell/µl suspension of MC38 Empty Vector cells over 1 minute. After injecting the cells, we waited for 5 minutes to avoid backflow, and then remove the needle and resected the spleen using a cauterizer. Following the injection and splenectomy, the abdominal wall of the mouse was sutured shut with 2 single stitches of biodegradable sutures, and the skin was closed using 2-3 staples. The mouse was then removed from anaesthesia, given buprenorphine (0.5 mg/kg) for pain-relief, and once awake, put back in a cage. 2-3 weeks post-injection, mouse livers were collected, fixed in 10% formalin and embedded in paraffin. Sections were cut with a microtome and then stained with Haemotoxylin and Eosin to visualize liver cells and metastasis formation.

Statistical Analyses

Parametric unpaired t-tests were used in all comparisons of means. Correlations were calculated as two-tailed Pearson correlations. PRISM (GraphPad Software Inc.) was used to generate all plots and graphs and to conduct comparison of means and correlation analyses of those data. Statistical significance was defined as p-values less than 0.05; additional thresholds reported include $p < 0.01$, 0.001, 0.0001. Mass spectrometry analysis was partially done through the use of the “EASE Score”, a version of the Fisher Exact P-Value test used determine whether a set of genes or proteins is enriched for members of another set of genes or proteins.

TABLES

Table 1 – Details of antibodies used in experiments

Antibody	Source / Catalog or Reference No.	Use	Dilution
anti-GAPDH	ThermoFisher Scientific, MA5-15738	Western blot	1:2000
anti-beta-ACTIN	Cell Signaling Technology, #8457	Western blot	1:2000
anti-cFOS	Santa Cruz Biotechnology, sc-271243	Western blot	1:2000
anti-phospho-cFOS (p-S32)	Cell Signaling Technology, D82C12	Western blot	1:2000
anti-cJUN	Cell Signaling Technology, 60A8	Western blot	1:2000
anti-phospho-cJUN (p-S63)	Cell Signaling Technology, #9261	Western blot	1:2000
anti-JUNB	Sant Cruz Biotechnology, sc-8051	Western blot	1:2000
anti-phospho-JUNB (p-T255)	Invitrogen, PA5-105510	Western blot	1:2000
anti-JNK	Cell Signaling Technology, #9252	Western blot	1:2000
anti-phospho-JNK (p-T184/Y185)	Cell Signaling Technology, #9251	Western blot	1:2000
anti-ERK1/2	Cell Signaling Technology, #4695S	Western blot	1:2000
anti-phospho-ERK1/2 (p-T202/Y-205)	Cell Signaling Technology, #9106	Western blot	1:2000
anti-phospho-p38 (p-T180/Y2182)	Cell Signaling Technology, #9211	Western blot	1:2000
anti-JAK2	Cell Signaling Technology, 3230S	Western blot	1:2000
anti-phospho-JAK2 (p-Y1007/Y1008)	Cell Signaling Technology, 3776S	Western blot	1:2000
anti-STAT3	Cell Signaling Technology, 12640S	Western blot	1:2000
anti-phospho-STAT3 (p-Y705)	Cell Signaling Technology, 9131S	Western blot	1:2000
anti-CD147	ThermoFisher Scientific, MA1-70088	Western blot	1:2000
anti-HSP90AA1	SantaCruz, (F-2), sc-515081	Western blot	1:2000
anti-CALNEXIN	Fisher/EMD Millipore, AB2301MI	Western blot	1:2000
anti-CD81	Cell Signaling Technology, 10037S	Western blot	1:2000
anti-HSC70	Cell Signaling Technology, 4872S	Western blot	1:2000
anti-mouse IgG-HRP	Cell Signaling Technology, 7076S	Western blot	1:2000
anti-rabbit IgG-HRP	Cell Signaling Technology, 7074S	Western blot	1:2000
anti-rat IgG-HRP	Cell Signaling Technology, 7077S	Western blot	1:2000
anti-F4/80	BD Pharmingen, Cat. 565853	Flow cytometry	1:500
anti-CD11B	BioLegend, Cat. 101216	Flow cytometry	1:500
anti-CD11C	BD Horizon, Cat. 585872	Flow cytometry	1:500
anti-CD45	Invitrogen, 12-0451-82	Flow cytometry	1:500

Table 2 – Details of oligonucleotides used in experiments

Oligonucleotide	Sequences	Use
Mlh1 gRNA forward	caccgGGTAGTGAACCGCATAGCGGCGG	CRISPR knockout
Mlh1 gRNA reverse	aaacCCGCCGCTATGCGGTTCACTACCc	CRISPR knockout
Polε gRNA forward	caccgGGCTTGGGCCTATCCGAGAGGGG	CRISPR knockout
Polε gRNA reverse	aaacCCCCTCTCGGATAGGCCCAAGCCc	CRISPR knockout
Rad51 gRNA forward	caccgGCAACGAAGCGCGTTCGAGCCGG	CRISPR knockout
Rad51 gRNA reverse	aaacCCGGCTCGAACGCGCTTCGTTGCc	CRISPR knockout
CD147 shRNA sense	CGACCTGCATACGAAGTACAT	shRNA knockdown
CD147 shRNA anti-sense	ATGTACTTCGTATGCAGGTCG	shRNA knockdown

CHAPTER 3: RESULTS

PURIFICATION OF sEVs FOR *IN VITRO* EXPERIMENTS

Characterization of sEVs to Confirm Purification Success

Nanoparticle Tracking Analysis (NTA) Profile of sEVs

We measured the diameter of sEVs purified from MC38 cell lines bearing mutations in critical DNA repair or genomic instability-related genes in order to confirm if our purifications matched previous research. Nanoparticle Tracking Analysis (NTA) measured sEV diameters between 100-200 nm (Fig.6A), which is near the canonical size of exosomes (30-150 nm). In all our purifications notable populations of large particles persists (200-400 nm), which are likely microvesicles.

Characterization of sEVs Using Transmission Electron Microscopy

Transmission Electron Microscopy (TEM) was also used to determine the physical characteristics of the sEVs we purified (Fig.6D). Sizes of sEVs approximated from the TEM images range between 50-200 nm, which is slightly smaller than measured by NTA. The combination of TEM and NTA confirm that we successfully purified secreted small EVs within the size range of exosomes.

Immunoblot Profile of sEVs

In addition to the physical properties of the sEVs we purified, we measured by immunoblotting the presence and absence of several exosome and sEVs markers, and also CALNEXIN (CANX), a protein not expected to be present in exosomes as

CALNEXIN is found in the endoplasmic reticulum (Fig.6C). Additionally, we measured the expression of CD147 on sEVs purified from MC38 cells, which is indeed frequently identified in exosomes. sEVs purified from MC38 cells express the exosome markers CD147, HSP70, and CD81. CANX, a marker of cellular cytoplasm, is also expressed on the sEVs we purified suggesting that the sEVs we purified are a mix of exosomes with microvesicles.

FBS Depletion of sEVs by Ultracentrifugation

Since we collected sEVs from the cell culture media of MC38 cells, we measured the reduction of sEVs in FBS that is depleted of sEVs (dFBS) by ultracentrifugation (UC) at 100,000g for 20 hours (Fig.6D). We used dFBS in the cell culture media in order to eliminate sEVs of bovine origin from the sEVs purified in downstream processing. We find depletion of FBS sEVs by ultracentrifugation results in a reduction to about half of the original sEV concentration. Nevertheless, a substantial amount of sEVs remain in the dFBS produced by UC sEV depletion.

Comparison of sEV Proteomes from MSI, CIN, and Hypermutable cell lines

Having established and validated an sEV purification method, our first experiment was to conduct qualitative mass-spectrometry to identify proteins present in sEVs from MC38 cells. Furthermore, we aimed to identify proteins uniquely present or absent in any of the DNA repair deficient MC38 cell lines. Two independently purified sets of sEVs from each MC38 cell line were submitted for protein identification mass spectrometry at separate times to ensure biological replicates. Each mass spectrometry experiment was independently conducted, with the cell lines passaged for months in

between to identify proteins durably associated with the DNA repair insufficient genotype of the cells. We only considered proteins that were identified in both mass spectrometry experiments as reliable candidates for further study, any hits not present in both sEV proteomes for a cell line were not included in the final analysis, (See Appendix, Tables 2-10 for all of the individual datasets).

Due to the stringency of our analysis, a total of 12 proteins were found to be shared by the sEVs from all of the MC38 cell lines while variable numbers of other specific proteins was found to differentiate them (Fig.7A). The highest number of individual hits was found in sEVs from Δ*Mlh1* cells. Of note are heat shock cognate 71 kDa protein (HSC71), and heat shock protein 90-alpha (HSP90AA1) in the MC38 Δ*Mlh1* cell line sEVs (Fig.7E).

Functional Analysis of sEV Proteins Identified in all Experiments, Representing a Set of Fundamental sEV Proteins

Gene-ontology cellular component term analysis of our mass spectrometry results further confirmed the robustness of our sEV purification method. Through the DAVID tool, we used the EASE-score, a more conservative version of the Fisher Exact P-value test of significance, to identify enrichment of related proteins in a sample.

12 sEV proteins common to all the sEVs from cell lines tested were identified (Fig.7B), 10 of which are among the most frequently identified exosomal proteins based on the collated data on ExoCarta. The 12 proteins fall into the cellular component gene ontology term for ‘extracellular exosome’ (Fig.7C). Furthermore, nearly all (90.5%-100%) proteins in the MC38 Empty Vector, Δ*Mlh1*, and Δ*Polε* sEVs fall into the

extracellular exosome gene ontology term (Fig.7D-F). Gene ontology cellular component term analysis confirms that the population of sEVs we purified are indeed enriched for exosomes.

CD147 was also identified in the sEVs from each cell, in total in 6 out of 8 mass spectrometry samples (Fig.7B, Table 2-10). Our identification of CD147 in CRC sEVs prompted further investigations into a potential MMP expression-inducing, or activating, role of CD147 expressing sEVs given the known roles of CD147 in inducing MMP expression and MMP activation[153].

FUNCTIONAL MMP ASSAY RESULTS

sEVs induce Dose-Dependent generic-MMP (gMMP) and MMP12 Production in Macrophage Cells

Having transitioned to investigating the potential induction of MMP expression and activity by sEVs expressing CD147, we began testing the induction of MMP expression in macrophage cells by CRC sEVs. We used two functional MMP activity assays as surrogates for MMP protein expression due to technical challenges we faced performing cell lysate and cell culture supernatant immunoblots for MMP proteins (data not shown). Generic MMP (gMMP) activity, which is a measure of MMP1-MMP14 proteolytic activity, in RAW264.7 cell culture supernatants increased with CRC sEV stimulation dose (Fig.8A, D). MMP12 activity specifically also increased with CRC sEV dosage in RAW264.7 cell culture supernatants (Fig.8B, H). The use of functional MMP assays to measure MMP expression relies on the assumption that the sEVs applied to the

macrophage cells are only inducing MMP expression and not also causing the activation of MMPs released by those same macrophage cells.

The Effect of CRC sEV Stimulation on gMMP/MMP12 Production Differs by Cell Type

In order to examine a broader set of sEV responding cells that may be relevant to cancer physiology and conditioning of the premetastatic niche, we applied CRC sEVs to several different cell types representative of those that would be found in the PMN. We specifically stimulated RAW264.7 macrophage cells, the NIH-3T3 mouse fibroblast cell line, bone marrow derived macrophages (BMDM), and bone marrow derived dendritic cells (BMDC) (Fig.8D-K) with CRC sEVs and measured the resulting changes in MMP expression in terms of MMP activity. The RAW264.7 cell line responded to sEV stimulation by increasing MMP and MMP12 expression. In contrast, sEVs did not affect BMDM gMMP expression (Fig.8E), and reduced BMDM MMP12 expression (Fig.8I). Larger doses of sEVs reduced both NIH-3T3 and BMDC gMMP expression (Fig.8F, G), had no effect on NIH-3T3 MMP12 levels (Fig.8J), and reduced BMDC MMP12 expression (Fig.8K). Altogether, the two macrophage cells types we tested responded dissimilarly to CRC sEVs and the remaining cell types we tested expressed unchanged or lowered gMMP/MMP12. This is potentially significant given that RAW264.7 macrophages most closely resemble pro-tumorigenic TAMs[154]. However, as discussed more extensively below, it is difficult to assess the net effect of sEVs on gMMP and MMP12 expression in an *in vivo* context based on these results. Nevertheless, these disparate responses to CRC sEVs in different cell types implies that the net effect of

CRC sEVs on a future PMN depends on cellular composition, environmental signals and the specific properties of the sEVs.

Conventional sEV Depletion with GW4869 is Highly Toxic

In order to further test the role of sEVs in inducing gMMP and MMP12 expression we sought to deplete sEVs from the conditioned media of MC38 CRC cells and apply that depleted conditioned media to macrophages. GW4869 is a widely used exosome release inhibitor. GW4869 acts through inhibition of neutral sphingomyelinase, preventing ceramide dependent exosome secretion. In our hands this drug appeared extremely toxic to RAW264.7 cells (Fig.9A). The majority of cells treated with GW4869 at concentrations typically found in the literature (5-10 μM) were killed, as measured by flow cytometric viability tests. This led us to pursue alternative methods to selectively deplete sEVs from CRC cells.

Depletion of sEVs Ffrom MC38 Conditioned Media Reduces the Induction of MMP12 but not gMMP Expression in Macrophages

As an alternative to GW4869, ultracentrifugation successfully reduced the concentration of sEVs in MC38 conditioned media (Fig.9B). Upon closer inspection of the distribution of sEV sizes remaining after ultracentrifugation, it appears ultracentrifugation pellets mainly larger sEVs although the concentrations of smaller sEVs are also reduced (Fig.9C-E).

RAW264.7 cells treated with conditioned media depleted of sEVs from both vector control and Δ*Mlh1* MC38 CRC cell lines did not reduce gMMP expression however they

did decrease MMP12 expression (Fig.9F, G). In parallel with the dose-response results from Fig.8, CRC sEV stimulation induces both generic MMP and MMP12 expression but MMP12 expression requires a higher dose of CRC sEVs to accomplish this since generic MMP expression was not reduced by partial sEV depletion through ultracentrifugation.

PURIFICATION OF MOUSE KUPFFER CELLS FOR *IN VITRO* STIMULATION WITH SEVS

Flow Cytometry Confirmation of Macrophage Immunophenotype in Purified Kupffer Cells

Kupffer cells are the resident liver macrophages. Kupffer cells are in the liver ducts and exposed to venous blood flow from the colorectal tract. Thus, colorectal cancer sEVs are likely taken up by Kupffer cells *in vivo*. Applying a primary culture model of Kupffer cells was necessary for us to continue testing the role of sEVs in colorectal cancer metastasis and formation of the premetastatic niche. The liver cells we cultured according to the protocol by Li et al.[143], showed a CD11B+CD11C+ phenotype after 3 days of culture, and elevated CD45, and the macrophage marker F4/80, all in keeping with known Kupffer cell immunophenotypes (Fig.10A-C)

TESTING OF MACROPHAGE INVASION-PROMOTING BEHAVIOUR WHEN STIMULATED WITH SEVS AND SEV DEPLETED CONDITIONED MEDIA

RAW264.7 cells and Kupffer cells Stimulated with sEVs Exhibit Invasion-Promoting Behaviour

Having established a Kupffer cell primary culture system, we then tested if MMP induction caused by CRC sEVs might enhance the ability of macrophages to induce invasion-promoting behaviour in CRC cells. For these experiments, we treated macrophages with CRC sEVs, then transferred the conditioned media generated by these stimulated RAW264.7 cells or Kupffer cells to the bottom chamber of trans-well invasion assay systems. By applying MC38 CRC cells to the top chamber and observing their ability to migrate through ECM-coated porous membranes towards the conditioned media, we then evaluated how sEV-stimulated macrophages alter tumor cell invasion. We chose to use this conditioned media system rather than to directly co-culture macrophages and MC38 cells in order to isolate the role of sEV treatment of macrophages. In contrast, a co-culture system would have ongoing feedback occurring between the co-cultured cell types involving numerous other metabolites and secreted factors. At higher doses of sEVs, we detected significant increases in MC38 cell invasion resulting from macrophage treatment with CRC sEVs (Fig.10D, E). While we have not directly linked gMMP or MMP12 expression to this invasion-promoting phenotype, the relationship between MMP degradation of extracellular matrices and cancer cell invasion is clear and represents one possible mechanism for our results. Conditions involving small molecule inhibitors of MMP may be useful for testing the necessity of MMP activity in the invasion assays we have conducted.

STIMULATION OF MACROPHAGES WITH sEVs INCREASES EXPRESSION AND ACTIVATION OF AP-1 PROTEINS AND ACTIVATED MAPK PROTEINS

Expression of AP-1 Proteins and AP-1 Activation Is Increased in Macrophages Treated with sEVs

MMP expression can be induced through AP-1 transcription factor activity. The increased total protein we observed in macrophages cell lysates treated with CRC sEVs (Fig.8C) indicated increased cell activity, leading us to suspected that the MAPK pathway upstream of AP-1 was responsible for the increased expression of gMMP and MMP12 in RAW264.7 cells (Fig.8). In order to test AP-1 protein activation, we stimulated RAW264.7 cells (Fig.9A) and Kupffer cells (Fig.9B) with CRC sEVs over a short time period and immunoblotted the cell lysates to measure the expression and activation of AP-1, MAPK and JAK/STAT proteins. While the AP-1 protein family is diverse, some of the most commonly investigated AP-1 proteins are c-Fos, c-Jun, and JunB. c-Fos and c-Jun also form an AP-1 heterodimer with well known activity.

We detected elevated c-Fos and c-Jun in RAW264.7 cells treated with CRC sEVs by 60 minutes post-stimulation (Fig.9A) while sEV treated Kupffer cells expressed higher c-Jun and c-Fos by 30 minutes post-stimulation (Fig.9B). Treated RAW264.7 cells expressed higher JunB after 60 minutes whereas Kupffer cells did not exhibit obvious changes in JunB expression post-stimulation. Phosphorylated c-Fos was elevated in RAW264.7 cells treated with sEVs by 60 minutes post-stimulation, slightly trailing after the expression of the total c-Fos. However, Kupffer cells showed no clear difference in phosphorylated c-Fos expression post-stimulation. Unlike c-Fos and JunB, c-Jun

appeared to be phosphorylated immediately post-stimulation in both RAW264.7 and Kupffer cells, probably as a consequence of JNK activation. The delayed expression of total c-Jun relative to phosphorylated c-Jun likely reflects the immediate phosphorylation of c-Jun by JNK followed by c-Jun transcription by activated AP-1 dimers.

Activation of the MAPK Pathway Precedes AP-1 Protein Activation and Expression Following sEV Treatment of Macrophages

Before the expression of AP-1 proteins increased post-stimulation, the MAPK proteins JNK, ERK1/2, and P38 were all phosphorylated and thus activated in RAW264.7 cells and Kupffer cells (Fig.9A, B). This increased phosphorylation occurred in every case between 15-30 minutes post stimulation. CRC sEV treatment-induced JNK activation appeared restricted to the first hour post-stimulation in RAW264.7 cells, while increased ERK1/2 and P38 activation continued for to 1-2 hours post-stimulation. In Kupffer cells, increased phosphorylated P38 and phosphorylated JNK expression due to sEV treatment terminated after 30 minutes, while ERK1/2 activation was weakly apparent only 30 minutes post stimulation.

In CRC sEV-treated macrophages, JNK, P38, and ERK1/2 activation began before increased AP-1 protein expression (Fig.8A, B). Given the known function of these MAPK proteins in activating AP-1 signaling, it seems likely that one or all of these MAPKs mediates sEV-induced AP-1 activity. Future experiments could inhibit specific MAPK proteins to explore which are necessary for the AP-1 activation. We also tested the JAK2/STAT3 signalling pathway as an alternative possible mechanism by which CRC sEVs could be activating macrophages. No significant STAT3 activation was

detected in RAW264.7 cells or Kupffer cells. Phosphorylated JAK2 expression was detected in RAW264.7 cells, but not Kupffer cells, 15 minutes post-stimulation. Increased JAK2 phosphorylation as a result of sEV treatment was not detected in later experiments (Fig.12C) thus it seems unlikely that JAK2/STAT3 explains AP-1 activation by CRC sEVs.

KNOCKDOWN OF CD147 ABROGATES THE ABILITY OF MC38 SEVS TO INDUCE INVASION-PROMOTING BEHAVIOUR AND MAPK/AP-1 SIGNALING IN MACROPHAGE CELLS

Knockdown of CD147 Inhibits the Development of Macrophage Invasion-Promoting Phenotypes

We initially hypothesized that CD147 in sEVs from colorectal cancer cells might induce pre-metastatic niche formation. We thus tested if CD147 in MC38 CRC sEVs was necessary for induction of macrophage invasion-promoting behaviour and the induction of MAPK signalling in CRC sEV-treated macrophages. In order to develop sEVs without CD147 we generated knockdowns of CD147 in the MC38 CRC cell line (Fig.12A) and confirmed their phenotype by immunoblotting cell lysates for CD147.

In a preliminary experiment (n=1), we then applied the conditioned media from CD147 knockdown cells or control cells to RAW264.7 macrophages in order to test the role of CD147 on CRC sEVs in generating invasion-promoting behaviour in macrophages (Fig.12B). We observed a reduced ability to induce CRC cell invasion in macrophages treated with conditioned media from CD147 knockdown cells (Fig.12B, left, and middle column). Depletion of sEVs in the conditioned media eliminated any difference between the knockdown and control conditions (Fig.12B, UC conditions), confirming that CD147

expressing sEVs were indeed responsible for a significant amount of the invasion-promoting behaviour induced by macrophages treated with sEVs from MC38 cells.

Knockdown of CD147 in sEVs Abrogates the Ability of sEVs to Induce MAPK/AP-1 Protein Activation

Since we had previously detected MAPK activation in RAW264.7 cells treated with CRC sEVs, we also tested the necessity of CD147 on sEVs to induce MAPK/AP-1 activation in macrophages (Fig.12C). Previously (Fig.11A), we detected the early activation of MAPKs JNK, ERK1/2, and P38, and also c-Jun, followed by total c-Jun and c-Fos expression and phosphorylation in macrophages stimulated with sEVs. sEVs produced by CD147 knockdown cells still induced early phosphorylation of c-Jun (Fig.12C), although much less so compared to control cell sEVs. All MAPKs which are activated by sEV treatment are activated to similar levels in the untreated and CD147 knockdown sEV treated macrophages. Regarding AP-1 protein expression, in macrophages treated with CD147 knockdown CRC sEVs, only c-Fos appears to be expressed at a notably higher level than the untreated macrophages. c-Jun and JunB expression are nearly identical to control levels when CD147 knockdown sEVs are applied to macrophages. Finally, phosphorylated and total JAK2 were similar between the control and CD147 depleted sEV treatments of macrophages while total STAT3 and phosphorylated STAT3 levels do not change in any condition, suggesting no JAK2/STAT3 involvement as we observed earlier. Rapid onset of MAPK activation in macrophages treated with sEVs followed by AP-1 protein expression is dependent on expression of CD147 in the sEV donor cells. The MAPK/AP-1 signalling we observe may be connected to the release of MMP by RAW264.7 cells and the invasion-promoting phenotype of macrophages

treated with sEVs, however further experimentation is required to test these hypotheses.

FIGURES

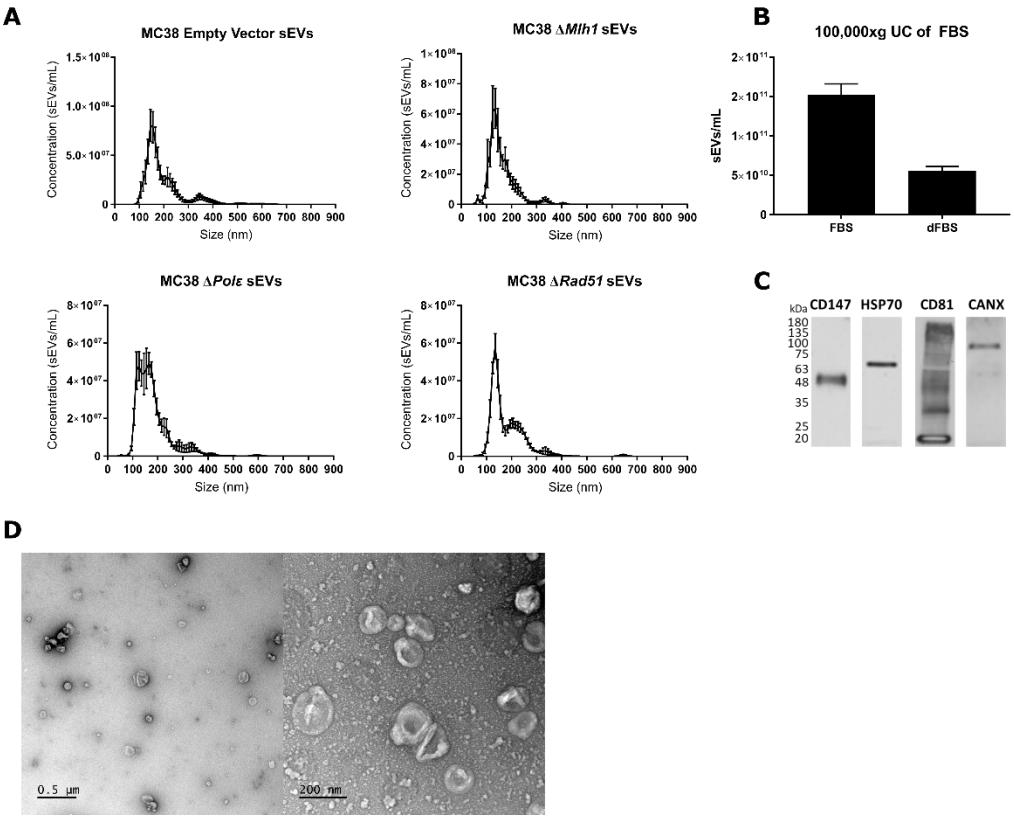

Figure 6 – Purification of sEVs by ultracentrifugation results in particles with characteristics consistent with exosome identity.

sEVs were pelleted by ultracentrifugation at 100,000xg and then measured using the Nanosight Nanoparticle Tracking Analysis (NTA) system to determine the diameter of the purified vesicles. (A) sEVs from the MC38 Empty Vector cell line, and the MC38 *Mlh1*, *Pole,* and *Rad51* mutant cell lines (representative figures). (B) sEV-depleted Fetal Bovine Serum (dFBS) used for the collection of sEVs from MC38 cells was measured using the NTA system to determine residual sEV concentrations in sEV depleted FBS. (n=1) (C) Conventional exosome markers HSP70 and CD81, as well as CD147 and sEV exclusion marker CALNEXIN (CANX) were blotted. (n=1) (D) sEVs were fixed and

imaged using transmission electron microscopy to determine their size and morphology (n=3, representative images). **** : $p < 0.0001$.

A

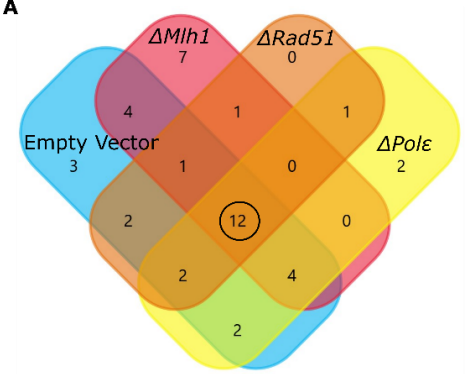

B

UniProt ID	UniProt accession	Protein name
MFGM_MOUSE	P21956	Lactadherin
K2C1_MOUSE	P04104	Keratin, type II cytoskeletal 1
ACTB_MOUSE	P60710	Actin, cytoplasmic 1
GNAI2_MOUSE	P08752	Guanine nucleotide-binding protein G(i) subunit alpha-2
EF1A1_MOUSE	P10126	Elongation factor 1-alpha 1
1433Z_MOUSE	P63101	14-3-3 protein zeta/delta
KPYM_MOUSE	P52480	Pyruvate kinase PKM
PDC6I_MOUSE	Q9WU78	Programmed cell death 6-interacting protein
HS90B_MOUSE	P11499	Heat shock protein HSP 90-beta
ANXA5_MOUSE	P48036	Annexin A5
SERA_MOUSE	Q61753	D-3-phosphoglycerate dehydrogenase
MOES_MOUSE	P26041	Moesin
BASI_MOUSE	P18572	CD-147 (6/8)

C

GO Cellular Component Term	Count	%	PValue
extracellular exosome	12	100	2.89E-10
myelin sheath	6	50	3.71E-08
extracellular vesicle	4	33.33333	2.37E-06
focal adhesion	5	41.66667	4.55E-05
blood microparticle	4	33.33333	4.80E-05
extracellular space	7	58.33333	6.55E-05
cytosol	7	58.33333	1.71E-04
melanosome	3	25	0.001394
cytoplasm	9	75	0.009529
extracellular matrix	3	25	0.011211
cell-cell adherens junction	3	25	0.012868
membrane	9	75	0.013664
cytoskeleton	4	33.33333	0.021195
plasma membrane	7	58.33333	0.032951
nucleus	7	58.33333	0.085301
vesicle	2	16.66667	0.08804

D

Empty Vector sEV proteins

UniProt ID	UniProt accession	Protein name
G3P_MOUSE	P16858	Glyceraldehyde-3-phosphate dehydrogenase
PPIA_MOUSE	P17742	Peptidyl-prolyl cis-trans isomerase A
EF2_MOUSE	P58252	Elongation factor 2

GO Cellular Component Term	Count*	%	PValue
extracellular exosome	26	92.9	5.20E-20

E

ΔMlh1 sEV proteins

UniProt ID	UniProt accession	Protein name
TBB4B_MOUSE	P68372	Tubulin beta-4B chain
HSP7C_MOUSE	P63017	Heat shock cognate 71 kDa protein
ANXA2_MOUSE	P07356	Annexin A2
MVP_MOUSE	Q9EQK5	Major vault protein
HS90A_MOUSE	P07901	Heat shock protein HSP 90-alpha
K2C5_MOUSE	Q922U2	Keratin, type II cytoskeletal 5
1433E_MOUSE	P62259	14-3-3 protein epsilon

GO Cellular Component Term	Count*	%	PValue
extracellular exosome	28	100	3.60E-24

F

ΔPolε sEV proteins

UniProt ID	UniProt accession	Protein name
UBB_MOUSE	P0CG49	Polyubiquitin-B
CSPG4_MOUSE	Q8VHY0	Chondroitin sulfate proteoglycan 4

GO Cellular Component Term	Count*	%	PValue
extracellular exosome	19	90.5	3.50E-14

Figure 7 – Mass spectrometry proteomic profiling of purified sEVs confirms exosome identity and reveals differences between mutant cell lines in their sEV content.

LC-MS/MS mass spectrometry was conducted on two batches of independently purified sEVs from the MC38 mutant cell lines. The results of each mass-spectrometry experiment were pooled and only the consensus proteins identified are reported. (A-F) n=2 for all. (A) Venn diagram displaying the unique and shared proteins identified

between sEVs from the different cell lines. (B) List of the 12 proteins identified in all of the sEVs (circle on panel A). CD147 was also identified in the sEVs from each cell, in total in 6 out of 8 mass spectrometry samples. (C) Gene Ontology cellular component term analysis (DAVID) of the 12 proteins common to sEVs from all the cell lines. (D-F) List of all the unique proteins identified in sEVs from each cell line and of the most significant gene ontology term for all proteins identified in each mutant cell line's sEVs. Blue text: proteins identified in the *ExoCarta* database as among the 100 most frequently identified exosome proteins.

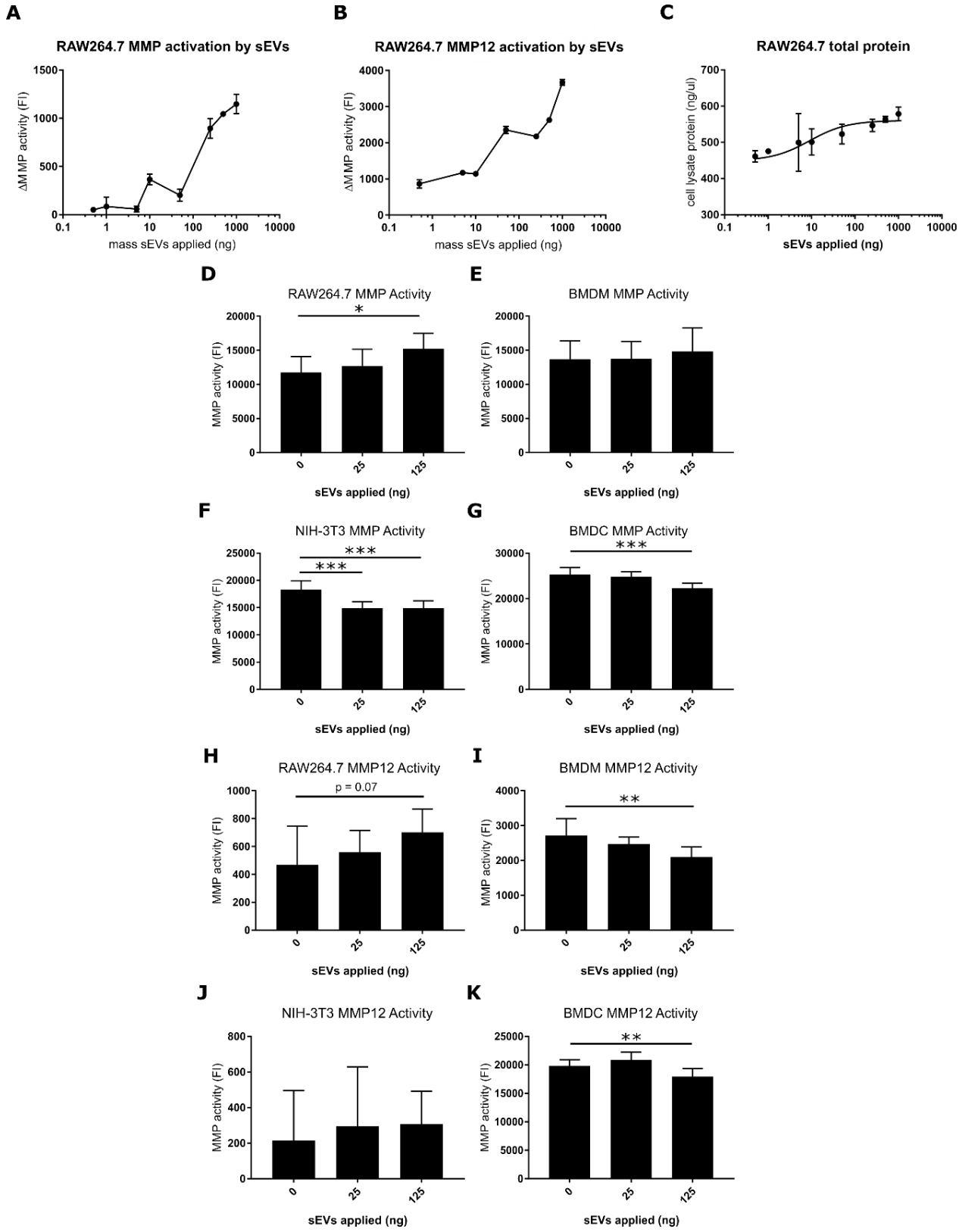
A
RAW264.7 MMP activation by sEVs
ΔMMP activity (FI)
mass sEVs applied (ng)
B
RAW264.7 MMP12 activation by sEVs
ΔMMP activity (FI)
mass sEVs applied (ng)
C
RAW264.7 total protein
cell lysate protein (ng/ul)
sEVs applied (ng)
D
RAW264.7 MMP Activity
*
MMP activity (FI)
sEVs applied (ng)
E
BMDM MMP Activity
MMP activity (FI)
sEVs applied (ng)
F
NIH-3T3 MMP Activity
***
***
MMP activity (FI)
sEVs applied (ng)
G
BMDC MMP Activity
***
MMP activity (FI)
sEVs applied (ng)
H
RAW264.7 MMP12 Activity
p = 0.07
MMP activity (FI)
sEVs applied (ng)
I
BMDM MMP12 Activity
**
MMP activity (FI)
sEVs applied (ng)
J
NIH-3T3 MMP12 Activity
MMP activity (FI)
sEVs applied (ng)
K
BMDC MMP12 Activity
**
MMP activity (FI)
sEVs applied (ng)

Figure 8 – sEVs induce RAW264.7 cell general MMP activity, MMP12 activity, and protein synthesis in a cell type-specific manner.

(A-B) 1 million RAW264.7 macrophage cells were treated with 0 – 1000 ng/mL sEVs for 24 hours, after which the cell culture supernatant was collected and MMP activity in the supernatant was measured using fluorometric generic MMP (ANASPEC: AS-71158, AS-71157) and MMP12 activity assay kits (n=2, each). (C) Protein lysates were collected and measured simultaneously from the treated RAW264.7 cells and protein concentration was determined using the bicinchoninic acid (BCA) assay, n=1. (A) Pearson $R^2 = 0.7759$, $p = 0.0017$, (B) Pearson $R^2 = 0.7841$, $p = 0.0034$, (C) Pearson $R^2 = 0.6215$, $p = 0.0116$. (D-G, H-K) RAW264.7 cells, primary bone marrow derived macrophages (BMDM), fibroblast NIH-3T3 cells, and bone marrow derived dendritic cells (BMDC) were stimulated with concentrations around the EC50 determined in panels A and B (25 ng/mL and 125 ng/mL of sEVs). After 24 hours of stimulation, the cell culture supernatant was measured as in (A) and (B) for general MMP (D-G) and MMP12 (H-K) activity by the fluorescence intensity of cleaved MMP substrates (FI), n=4. * : $p < 0.05$, ** : $p < 0.01$, *** : $p < 0.001$.

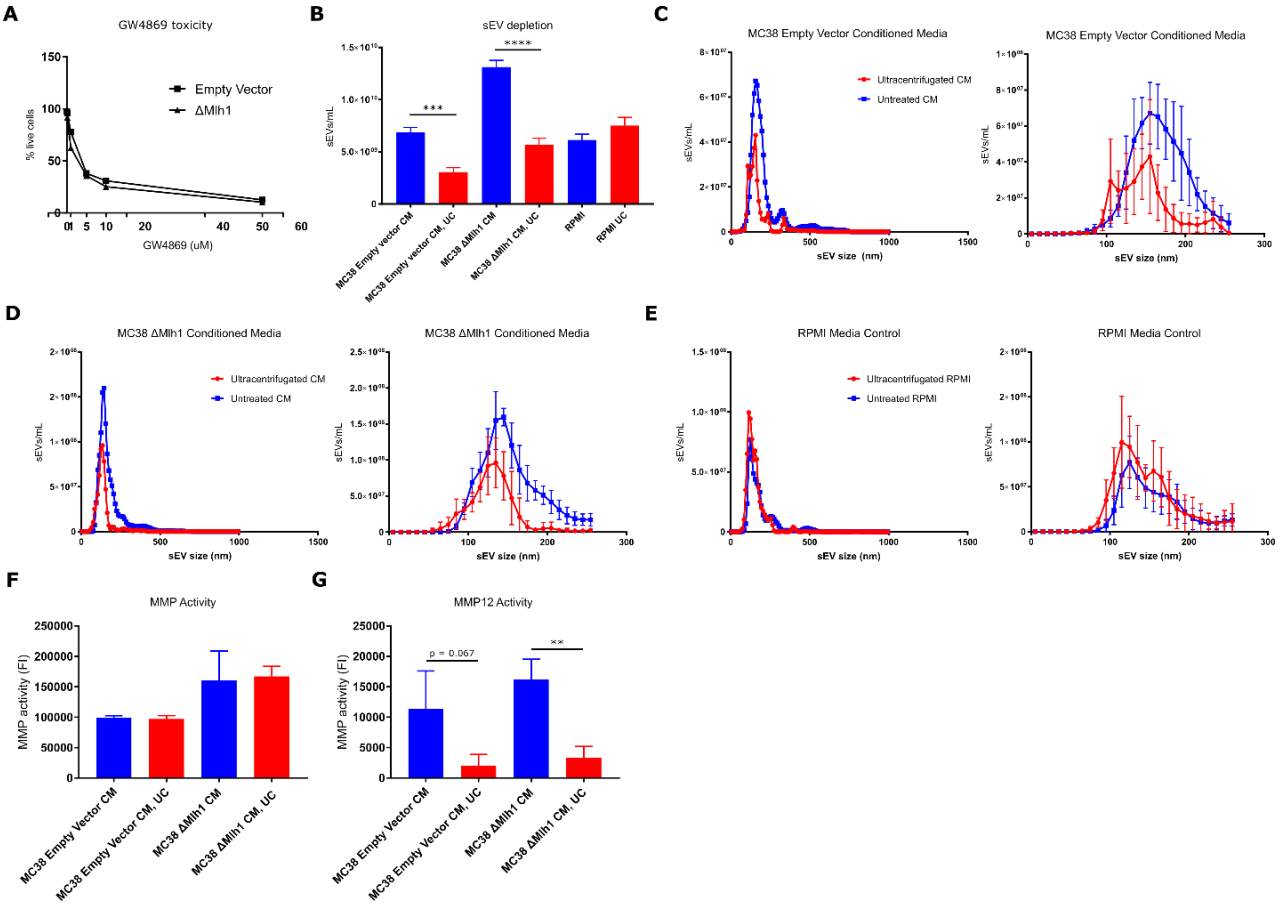

Figure 9 – Depletion of sEVs by ultracentrifugation from the conditioned media of MC38 cells reduces their ability to induce RAW264.7 cell MMP activity

(A) The toxicity of GW4869 on our MC38 cell lines was tested (representative figures) by flow cytometry measurement of live/dead cells using a viability dye. (B-G) Ultracentrifugation is used to deplete sEVs from conditioned media (n=3) (B) sEV concentrations in the conditioned media (CM) of MC38 cells with and without ultracentrifugation (UC), measured by NTA (n=1). (C-E) Histograms of sEV size, determined by NTA, in the conditioned media of MC38 cells before and after ultracentrifugation, left: full histogram, right: close-up on exosome population (n=1). (F-G) RAW264.7 cells were stimulated with the conditioned media generated in (A) for 24

hours, after which fresh media was placed on the RAW264.7 cells and then general MMP activity and MMP12 activity was measured 24 hours later in the RAW264.7 cell supernatants, FI=Fluorescent intensity (n=2). ** : $p < 0.01$, *** : $p < 0.001$, **** : $p < 0.0001$.

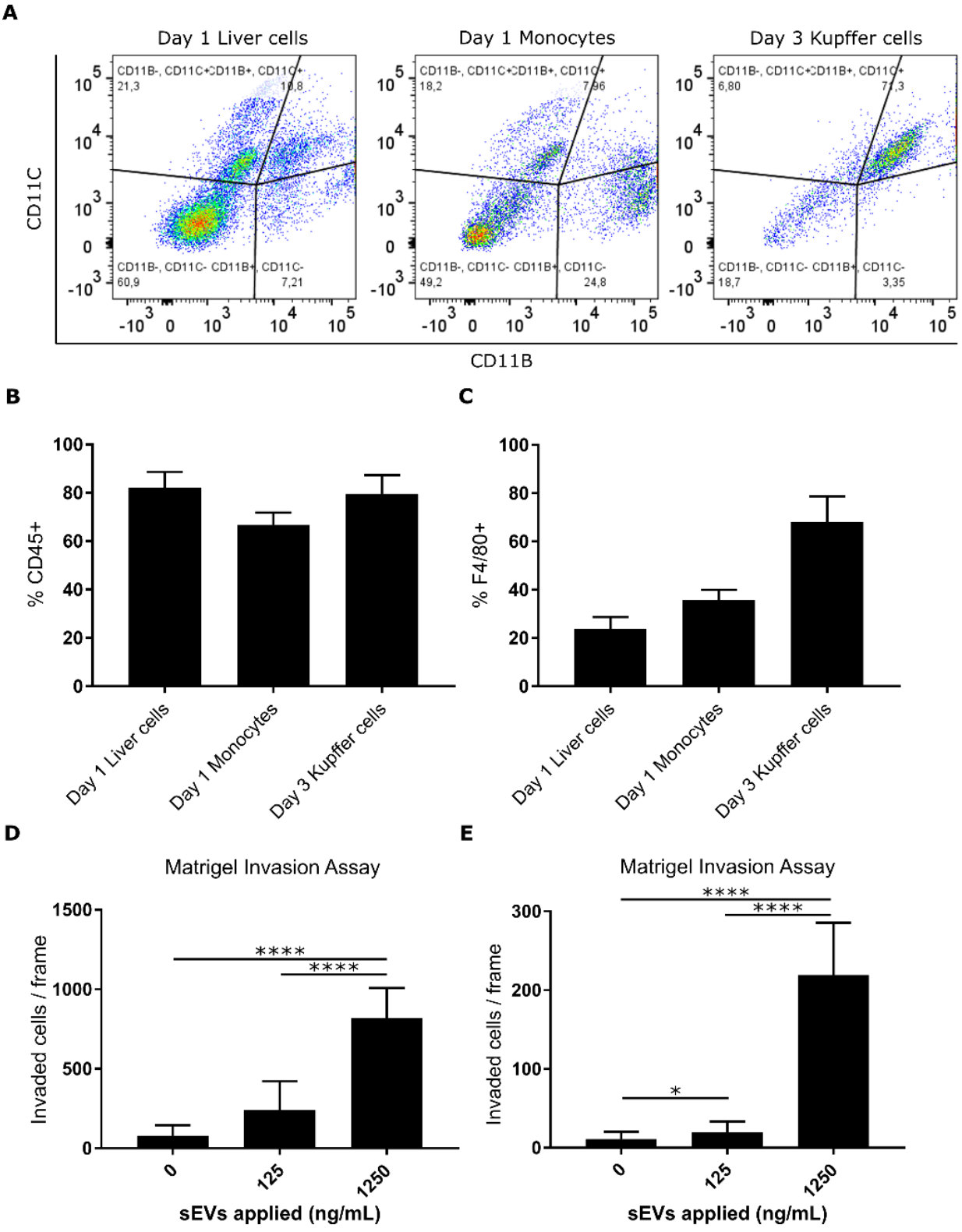
A
Day 1 Liver cells
Day 1 Monocytes
Day 3 Kupffer cells
CD11C
CD11B
CD11B-, CD11C+CD11B+, CD11C+
21,3
CD11B-, CD11C- CD11B+, CD11C-
60,9
7,21
CD11B-, CD11C+CD11B+, CD11C+
18,2
CD11B-, CD11C- CD11B+, CD11C-
49,2
24,8
CD11B-, CD11C+CD11B+, CD11C+
6,80
CD11B-, CD11C- CD11B+, CD11C-
18,7
3,35
B
% CD45+
Day 1 Liver cells
Day 1 Monocytes
Day 3 Kupffer cells
C
% F4/80+
Day 1 Liver cells
Day 1 Monocytes
Day 3 Kupffer cells
D
Matrigel Invasion Assay
Invaded cells / frame
****
****
sEVs applied (ng/mL)
E
Matrigel Invasion Assay
Invaded cells / frame
****
****
*
sEVs applied (ng/mL)

Figure 10 – CRC sEVs enhance an invasion-promoting phenotype in Kupffer cells and RAW264.7 cells that in turn facilitates tumor cell invasion through the ECM.

(A-C) Phenotypic profiling of Kupffer cells purified from the C57BL/6 mouse strain by flow cytometry. Day 1 Liver cells are the initial population of cells from the liver. Day 1 Monocytes are separated from the liver cells on the first day of Kupffer cell purification. Day 3 Kupffer cells are the purified liver macrophage cells after 3 days of culture (n=2). (A) Quadrant gates on the CD11B, and CD11C markers reveal a majority double positive population in the putative Kupffer cell population. (B, C) CD45 and F4/80 positive cells were counted amongst the total population of cells which were live. (D) Kupffer cells were stimulated with CRC sEVs for 24 hours, after which their supernatant was collected and used to induce MC38 cell invasion through ECM-coated transwells. MC38 cells were permitted to migrate through the ECM-coated transwells for 24 hours (n=2, representative figure) (E) RAW264.7 cells were stimulated with CRC sEVs for 24 hours, after which their supernatant was collected and used in Matrigel invasion assays with MC38 cells (n=3). **** : $p < 0.0001$.

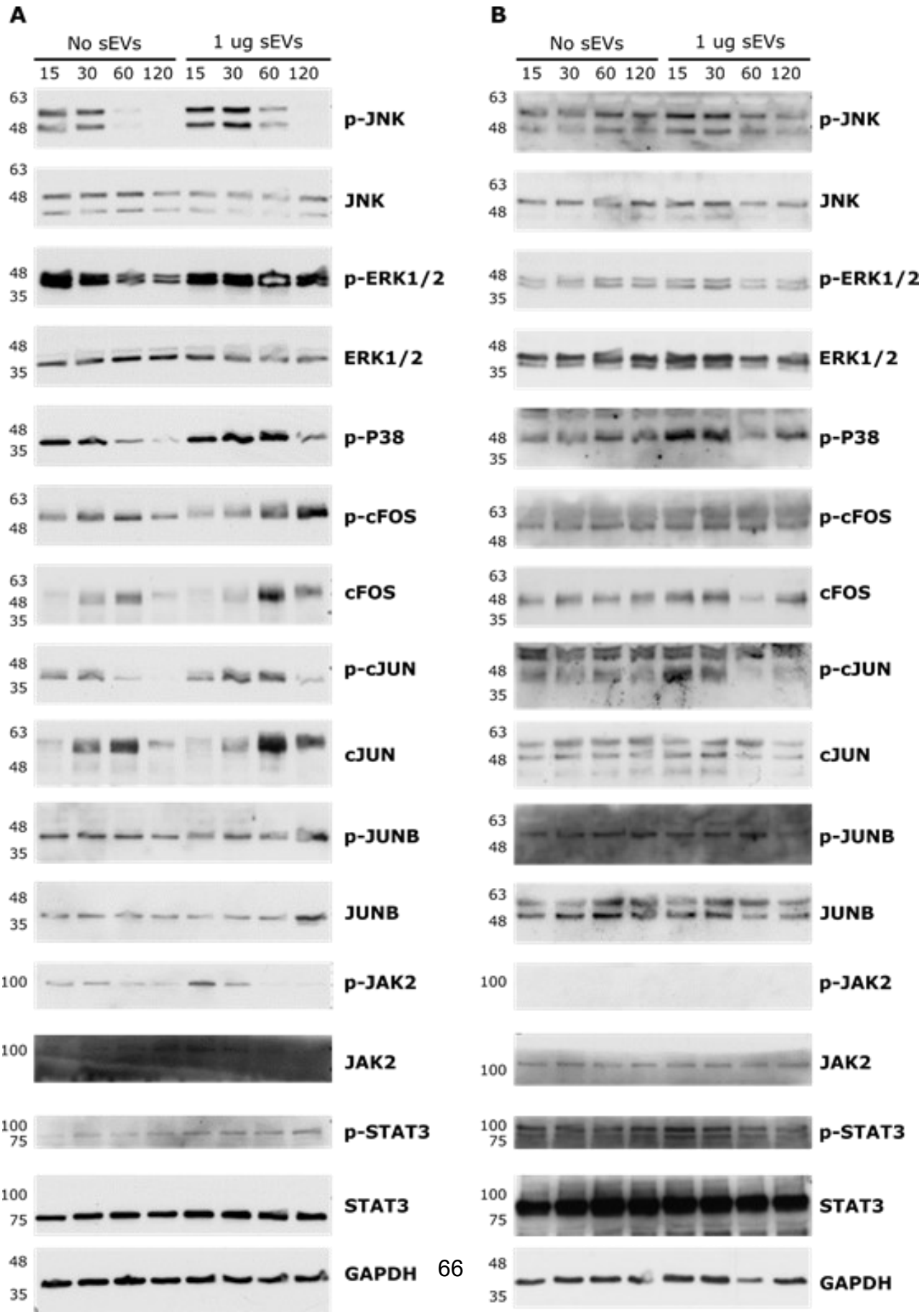
A
No sEVs
1 ug sEVs
15 30 60 120 15 30 60 120
63
48
p-JNK
JNK
48
35
p-ERK1/2
ERK1/2
p-P38
63
48
35
p-cFOS
cFOS
p-cJUN
cJUN
p-JUNB
JUNB
100
p-JAK2
JAK2
100
75
p-STAT3
STAT3
GAPDH
B
No sEVs
1 ug sEVs
15 30 60 120 15 30 60 120
p-JNK
JNK
p-ERK1/2
ERK1/2
p-P38
p-cFOS
cFOS
p-cJUN
cJUN
p-JUNB
JUNB
p-JAK2
JAK2
p-STAT3
STAT3
GAPDH

Figure 11 – sEVs induce MAPK and AP-1 signalling in RAW264.7 and Kupffer cells.

(A) RAW264.7 cells (n=2). and (B) Kupffer cells (n=1) were stimulated for 15, 30, 60, or 120 minutes with no sEVs or 1 µg of sEVs from the MC38 Empty Vector cell line after which cell lysates were collected and measured by western blot for expression and activation of MAPK, AP-1 and JAK/STAT pathways.

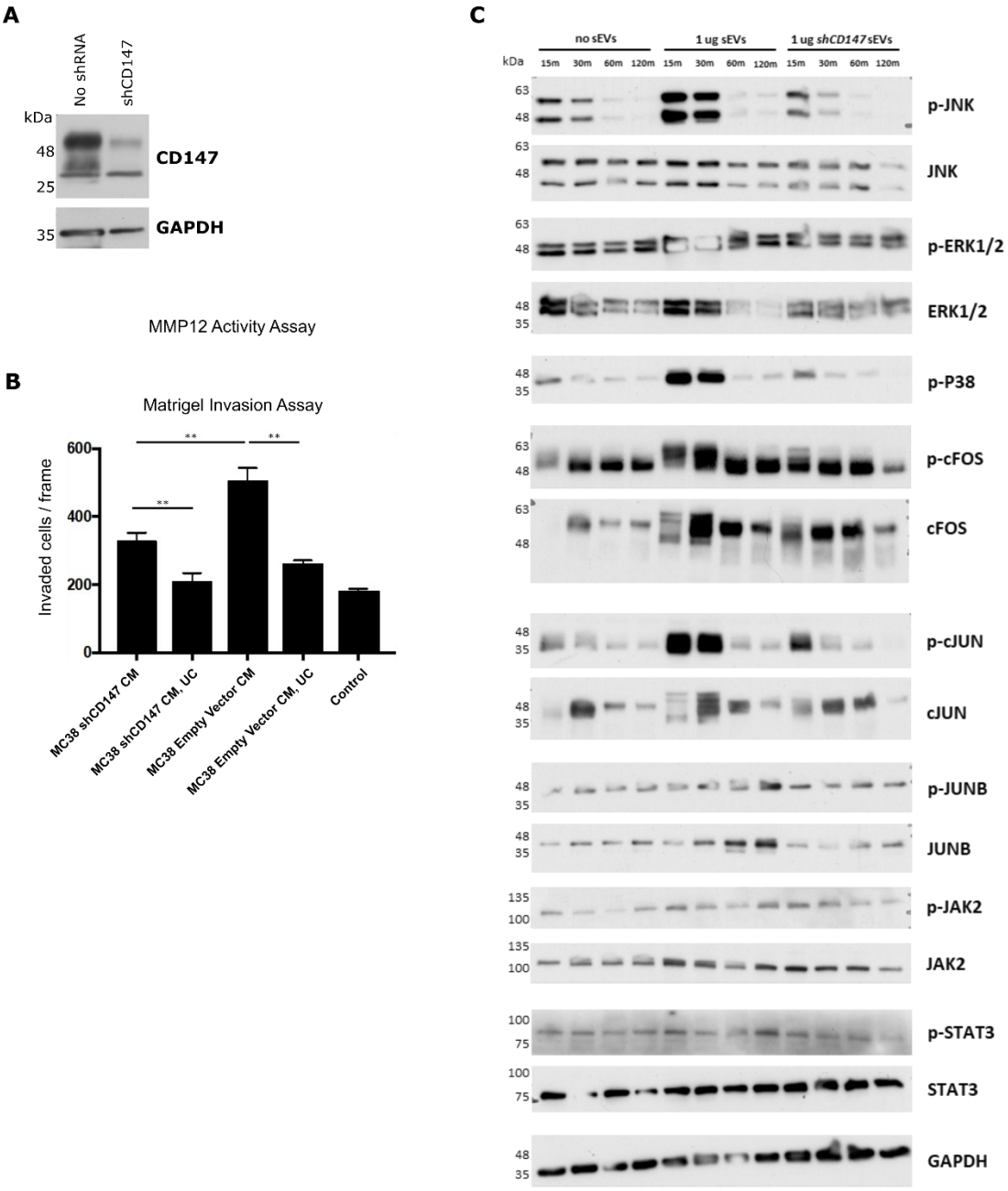

Figure 12 – CD147 on CRC sEVs induce MAPK/AP-1 signalling in RAW264.7 cells, enhancing their invasion-promoting phenotype, MMP12 activation and ability to induce tumor invasion.

(A) MC38 Empty Vector cells were stably transfected with an shRNA for CD147, and then confirmed for knockdown by western blot. (B) Conditioned media (CM) from the

MC38 no shRNA and shCD147 cells was generated over 24 hours. Half of the generated conditioned media was subjected to ultracentrifugation (UC) to deplete sEVs, and then applied for 24 hours to RAW264.7 cells. After a further 24 hours, CRC sEVs were removed and the invasion-promoting phenotype of treated RAW264.7 cells was assessed after a further 24 hours using transwell CRC invasion assays with RPMI media as a control (n=1). (C) RAW264.7 cells were stimulated for 15, 30, 60, or 120 minutes with no sEVs, 1 μg of sEVs from the MC38 Empty Vector cell line, or 1 μg of sEVs from the MC38 Empty Vector shCD147 knockdown cell line (n=2). After 24 hours, cell lysates were western blotted for MAPK/AP-1 proteins. ** : $p < 0.01$.

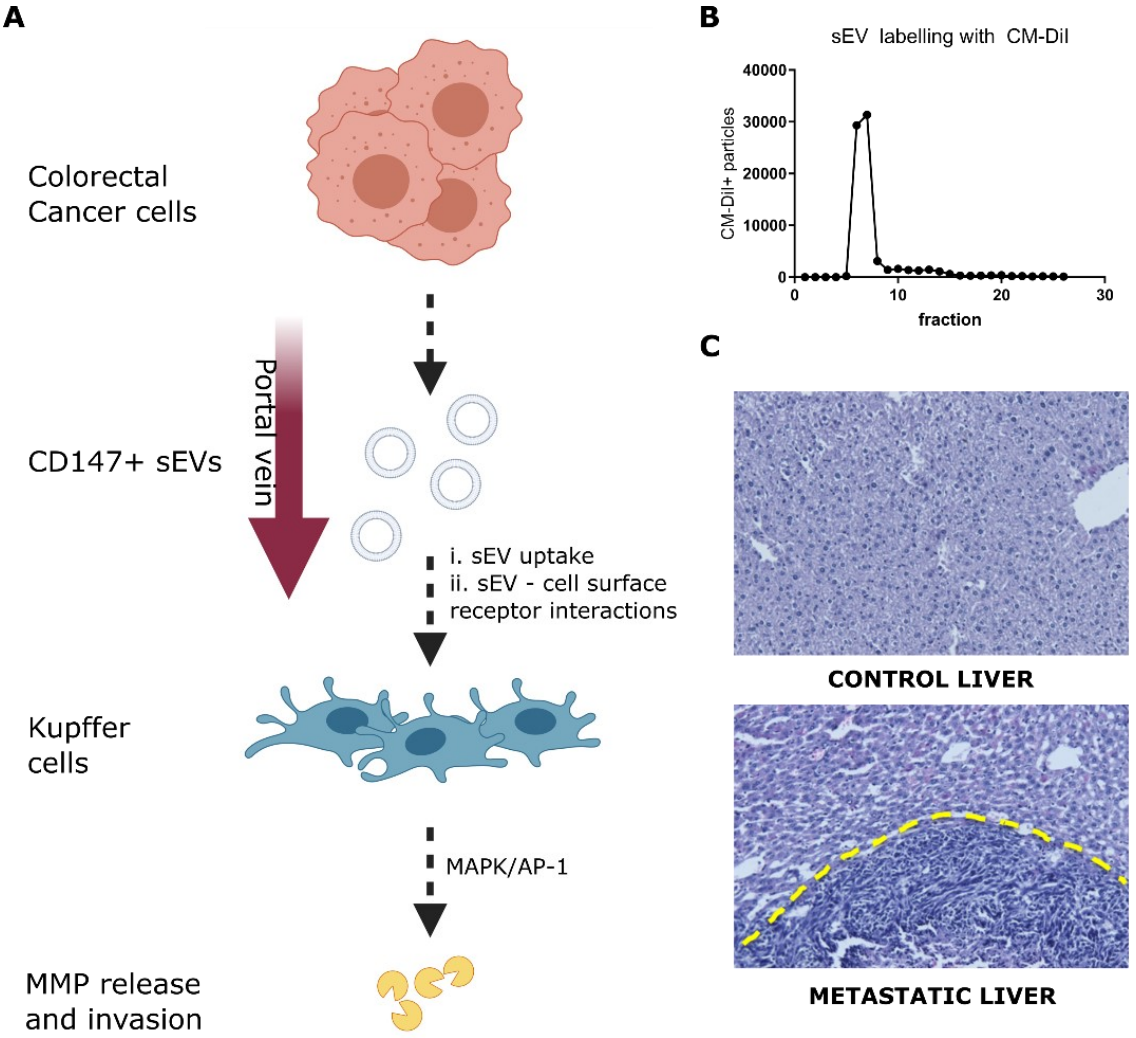

Figure 13 – Working model and future directions for in vivo investigation of the role of sEVs in colorectal cancer metastasis to the liver.

(A) We hypothesized that CD147+ sEVs from CRCs are causing Kupffer cells to release MMP and thus degrade the ECM. (B) In order to test the model proposed in (A), we have generated a method to label sEVs in order to monitor uptake of sEVs by macrophages *in vivo.* sEVs were labelled with CM-DiI and then fractionated using a size-exclusion column into 26 fractions. After fractionation, the CM-DiI+ sEVs+ detected by flow cytometry were measured. (C) To further test our hypothesis, we set up a

protocol for generating liver metastasis in mice. Liver metastases were generated using intrasplenic injection of MC38 tumor cells. 2-3 weeks post-injection, the livers were resected and subjected to H&E staining to detect tumor cells. Injection of fluorescently labelled sEVs will be used to confirm the trafficking of sEVs to the liver during *in vivo* experiments. Fluorescent labelling of sEVs will also be used to assess the uptake of sEVs by different populations of liver cells, especially Kupffer cells.

CHAPTER 4: DISCUSSION

EXAMINING THE PROTEIN CONTENT OF SEVS FROM MOUSE COLORECTAL CANCER CELLS WITH MSI, CIN, OR POLε-DEFICIENCY RELATED GENETIC INSTABILITY

Initially, our research focused on the differences between sEVs from colorectal cancer cells with different mutations in DNA repair pathways. However, the results from our proteomics screen led us in a different direction. The original purpose of using mass spectrometry protein identification was to identify proteins unique to sEVs from the microsatellite instable (MSI) MC38 Δ*Mlh1* cells and cells with other forms of genomic instability such as the hypermutable Δ*Pole* cells, or the chromosomally instable (CIN) Vector control or double strand break repair deficient Δ*Rad51* cells. In fact, we observed the presence of HSC71 and HSP90AA1 only in sEVs from the MC38 Δ*Mlh1* cells and did begin exploring the role of heat shock proteins in sEV function when cells are microsatellite instable. The genetic instability of Δ*Mlh1* cells may have prompted expression of the chaperone proteins HSC71 and HSP90AA1 in sEVs due to an abundance of mutant and mutant and misfolded proteins in MSI cells[18,155]. However, the Δ*Polε* cells are also genetically instable and generate many mutations. That the Δ*Mlh1* and not Δ*Polε* sEVs contained HSC71 and HSP90AA1 suggests some other property of Δ*Mlh1* cells asides from mutability might explain the incorporation of chaperone proteins in sEVs. Alternatively, the specific type of genetic instability may significantly impact the protein content of sEVs. Because of our interest in metastasis, which ultimately kills most CRC patients, we also investigated features of sEVs suggested by the presence of CD147 in sEVs. This line of inquiry proceeded with sufficient speed to attract most of

our attention and is relevant to both MSI and CIN CRCs since there is in fact a lack of difference in prognosis between late stage MSI and CIN colorectal cancers. During the final stages of cancer progression, defined by invasion and metastasis, genetic instability ceases to be relevant to patient prognosis. Accordingly, our work on the contribution of sEVs to metastasis is relevant to all advanced colorectal cancers regardless of the type of genomic instability.

With additional work in the future, it remains possible to achieve our original aim and incorporate some of the findings related to CD147 in CRC sEVs into the work on genetic instability. As noted, we did identify several proteins unique to sEVs from Δ*Mlh1* cells with the proteomics screen. Furthermore, we observed differences in the quantity, size and possibly function of sEVs produced between Δ*Mlh1* and Vector control cells in experiments performed on conditioned media (Fig.9). It is thus possible that the findings we have generated regarding CD147 on CRC sEVs may have specific relevance to colorectal cancers which are either MSI or CIN.

THE ROLE OF CD147+ SEVS IN CANCER

LC-MS/MS of MC38 cell line sEVs revealed that CD147 is present in or on the sEVs we purified from MC38 cells. In addition, other researchers have shared sEV and exosome proteomics data in which they also find CD147. In fact, CD147 is among the frequently identified sEV or microvesicle proteins in both the ExoCarta and Vesiclepedia databases. CD147 expression in colorectal cancer cells is a negative prognostic indicator of survival[156–159] and is an indicator of lymph node metastasis in lung cancer cells[160]. MMP expression is also correlated with CD147 expression and is a negative

prognostic indicator of cumulative survival in colorectal cancer[158]. Several other MMPs are correlated with CD147 expression, which is consistent with the known function of CD147 to induce the expression of several MMPs[158,161–163]. Tumors may be inducing MMP activity in their microenvironment through heterotypic interactions with fibroblasts [164], and potentially other cells in the microenvironment such as endothelial cells, macrophages, and recruited immune cells. We have shown that CRCs can also modulate MMP activity in distant premetastatic niches by secreting CD147+ sEVs. One mechanism by which cell-cell or cell-sEV interactions induce MMP expression through CD147 is homophilic CD147-CD147 interactions[165], downstream of which may be CD147-induced MAPK signalling and MMP transcription through ERK/JNK/P-38[166] and AP-1 transcription factors. We found that CD147 was needed on CRC sEVs for MAPK activation in macrophages treated with the sEVs. Our results suggest that CD147 on CRC sEVs functions in a similar manner as already described with cellular and recombinant CD147 proteins. CD147 positive (CD147+) sEVs appear to induce more MMP expression and cancer cell invasion than CD147 negative (CD147-) sEVs and this is likely mediated through MAPK/AP-1 signalling in macrophage cells since CD147 is known to signal through MAPK/AP-1. Furthermore, stimulation of cells with CD147+ CRC sEVs might initiate a positive feedback loop by promoting expression of CD147 and MMP-9 on the macrophages[167].

Cells in which we knocked-down CD147 by shRNA inhibition may have defects in other aspects of exosome formation, such as cargo loading, that we did not detect. However, there is no indication in the literature that CD147 is essential for exosome formation or secretion. Nonetheless, CD147 binds several membrane proteins in *cis* such as MCTs,

CD44, and β1 intergrins[60,168] and so knockdown of CD147 may cause defects in the trafficking of those proteins where they might otherwise be incorporated into exosomes. In order to determine if knockdown of CD147 specifically affects its trafficking to exosomes and not that of other proteins, some form of total sEV protein analysis, such as Coomassie, silver stain, or even mass spectrometry, should be done to compare CD147+ and CD147- sEVs.

There are some limitations to the CD147 knockdown experiments we have conducted. Ordinarily, a control shRNA that does not target any known mRNAs is used to control for engagement of the shRNA processing machinery in the experimental cells. We did not include a control shRNA in our experiments meaning our results ought to be considered preliminary. More than one shRNA is often used to target a gene in order that off-target effects are ruled out. Additionally, the cargo loaded into sEVs may also change when CD147 is knocked down. Mass spectrometry could be used to identify any changes to the secretome of a cell or to the biogenesis and loading of sEVs in order to determine if the differences we observed exclusively reflect changes in exosome composition. Corroborating experimental results using antibody-based depletion of CD147+ sEVs and also enrichment of CD147+ sEVs would be of more use in confirming our data. We have attempted antibody enrichment and depletion of sEVs however faced technical difficulties related to antibody specificity and sample elution (data not shown).

CD147 could be selectively sorted into exosomes and it could also be diffusing into the plasma membrane regions at which MVBs are formed. In the former case of selective

incorporation into sEVs, CD147 might in fact be sorted into sEVs through *cis* interactions with other proteins. In either case, CD147 as an sEV transmembrane protein is likely able to act in a similar way as cellular or secreted CD147. Through homophilic interactions with cellular CD147, CD147+ sEVs are likely able to induce MAPK/AP-1 activity in cells. In the case of transient induction of MAPK/AP-1 by CD147+ sEVs, cancers very likely take advantage of this activating signal to modify their immediate microenvironment via macrophages. Our results are consistent with the functional properties of CD147, as seen in the literature, and extend these by providing evidence for the first time that CD147+ sEVs are involved in conditioning Kupffer cells in the CRC pre-metastatic niche. We can conclude that CD147+ sEVs behave much like secreted and cellular CD147 in the ability to induce MAPK/AP-1 signalling. Furthermore, we observe concurrent induction of MMPs and a macrophage invasion-promoting phenotype which is likely caused by activation of MAPK/AP-1 in macrophages. In order to connect the MMP expression and MAPK/AP-1 activation we have observed, we are in the process of applying MAPK inhibitors to determine if invasion and MMP expression are dependent on MAPK activation by CD147+ sEVs.

Induction of MMP Production by Cancer sEVs

Through the functional MMP activity assays we conducted, we observed higher general MMP expression and higher MMP12 expression in RAW264.7 macrophage cells treated with sEVs from CRC cells. The generic MMP assays suggest other MMPs might also be activated by sEV treatment. Additionally, our invasion assay experiments show that Kupffer cells and RAW264.7 cells treated with CRC sEVs exhibit an invasion-promoting phenotype, enhancing the invasion of MC38 mouse colorectal cancer cells through the

ECM. Furthermore, CD147+ sEVs in the conditioned media of MC38 CRC cells enhanced the macrophage invasion-promoting phenotype to a much greater degree than CD147- sEVs. Colangelo and Azzam[62,169] have reported that increased CD147 on sEVs as a consequence of irradiation increases MMP expression and invasion, and Millimaggi et al., have shown that microvesicles expressing CD147 induce MMP expression and invasion in endothelial cells[170]. An alternative explanation for the invasion promoting behaviour exhibited by cancer sEV stimulated macrophages is that the macrophages produce factors causing tumor cell chemotaxis. EGF[93,94] and potentially other chemokines[171] released by tumour associated macrophages may explain the invasion promoting behaviour we observed. Given the complex nature of sEVs, it is likely that they stimulate macrophages to produce factors that influence both invasive and chemotactic behavior in cancer cells.

In contrast to previous studies investigating the effect of CD147 and cancer sEVs on macrophages, our specific interest was in the influence of CRC sEVs on liver Kupffer cells. Our results suggest that, much like in other contexts, CD147+ extracellular vesicles enhance MMP production and invasion by a critical cell population in the CRC pre-metastatic niche. The consequences of this to the formation of metastases are clear when the importance of the pre-metastatic niche is considered. Liver Kupffer cells are exposed via the portal vein system to many extracellular vesicles originating from the large intestine. In the case of colorectal cancer, Kupffer cells are directly exposed to cancer exosomes and microvesicles capable of inducing MMP expression and enhancing the rate of metastasis. The negative prognosis of cancers expressing high

CD147 is likely due to a combination of its effects in the local tumor-microenvironment and also the effect of tumor CD147 on extracellular vesicles at distant metastatic sites.

Regulation of MMPs is often detected using western blotting however we were unable to detect any changes in cellular MMP expression levels due to unreliable antibody performance. Subsequent attempts at measuring secreted MMP proteins in cell supernatants via western blotting yielded inconsistent findings. As a result, we turned to functional MMP assays to detect changes in the actual level of functional MMPs. While our results provide details on how CRC sEVs regulate MMP12 activity, our findings do not rule out a contribution for activation of other MMPs by sEVs. We explored the role of MMP12 due to preliminary results (data not shown), as well as the knowledge that macrophages treated with certain types of sEVs express MMP12[172], which degrades elastins into pro-tumorigenic elastin degradation products. Other MMPs such as MMP9 are involved in metastasis and pre-metastatic niche formation[173–175]. For example, MMP2 and MMP9 are known to be expressed in cells stimulated with sEVs so it is likely that these MMPs could also be upregulated in macrophages exposed to CD147+ sEVs in the PMN. While MMPs degrade the ECM, we did not directly tie the invasion-promoting phenotype of macrophages stimulated with CRC sEVs to increased MMP expression. Experiments using macrophages with catalytically inhibiting mutations in one or more MMPs, combined with recombinant MMP proteins as a rescue condition might be effective to directly link the invasion phenotype to macrophage MMP release.

While we have focused on an MMP-mediated and sEV-dependent promotion of metastasis, it is important to consider other mechanisms that could be at play. One of

these is the localization of sEVs to the PMN, which is a prerequisite for many of the processes we have investigated. sEVs from the primary tumor might reach the site of metastasis through integrins that 'home' sEVs to a target organ or tissue, as described in Hoshino et al.[104]. The ability of sEVs to home to the site of metastasis may concentrate sEVs to such an extent that they induce MMP-mediated ECM remodeling in the PMN. Liberation of ECM-bound angiogenic factor VEGF by MMPs is an additional mechanism by which sEVs may promote *in vivo* metastasis[176]. Formation of new blood vessels in the pre-metastatic niche is necessary to support metastatic growth. Finally, while we have addressed secreted MMPs, we did not examine the expression of membrane-tethered (MT) MMPs in macrophages stimulated with CRC sEVs.

The Role of CD147 on sEVs in Conditioning Cells in the Liver Pre-metastatic niche

Our results suggest that some subsets of macrophages are positioned to release MMPs and enhance CRC invasion when stimulated with CRC sEVs. Research into the role of different cell types in the PMN identified a diverse set of cells which contribute to metastasis formation[103]. Our work addresses a novel molecular and physiological mechanism by which colorectal cancer sEVs can induce production of MMPs and invasion-promoting behaviour in liver macrophages that foster a pre-metastatic niche. While the detailed mechanisms for this will require further confirmation, our findings clearly indicate that CD147 on CRC sEVs is important for activating MMP12 in macrophages and that this can enhance tumor cell invasion. Furthermore, our results support and extend those of Hoshino et al.[104], who showed that exosomes guide cancer cell metastasis to organs in a mouse metastasis model, and Milia-Argeiti et al.[61] and Colangelo et al.[62], who both demonstrated that CD147 sEVs can induce MMP

production in fibroblasts and astrocytes but did not show how this could be physiologically relevant.

Macrophages, fibroblasts, endothelial cells, and potentially other cell types have roles to play in PMN formation[103]. While we show that macrophages can respond to cancer sEVs by increasing MMP activation, possible reductions in MMP expression by the other cells in the PMN must be considered. Further work will be needed to show whether CD147 on cancer sEVs contributes to these processes. However, in the context of the liver, Kupffer cells and endothelial cells in the liver ducts will be the main cell types exposed to CRC sEVs circulating in the blood such that the response of Kupffer cells to cancer sEVs is most relevant to PMN formation in colorectal cancer.

Our results suggest that CD147+ sEVs contribute to activation of MAPK signaling in macrophages *in vitro*, leading to MMP expression and enhanced tumor cell invasion. *In vivo*, this population of sEVs might be necessary for some of the macrophage activity that degrades the ECM, releases VEGF, recruits other cells to the PMN, and ultimately enhances metastasis through ECM degradation and PMN modulation. We observed that CRC sEVs also induce an invasion-promoting phenotype in macrophages that may be dependent on CD147.

The possibility that cancers condition macrophages to degrade the ECM and enhance invasion through a specific population of sEVs is an aspect of PMN formation that has not been sufficiently addressed in the literature. Most cancer deaths are a result of metastases, thus it is essential to identify components of the PMN formation process. CD147 is a highly glycosylated protein making it a tricky target for interventions,

however there is evidence that specific glycosylation states of CD147 are essential for to induction of MMP expression[57]. Given that the primary tumor is rarely the cause of death in CRC patients, understanding the formation of the pre-metastatic niche through the influence of sEVs or other secreted factors is critically important for the development of cancer therapies.

DEVELOPMENT OF *IN VIVO* EXPERIMENTAL MODELS FOR FUTURE DIRECTIONS

As a summary of our work we present a model, outlined in Fig.13A, which explains how CRC CD147+ sEVs contribute to the formation of liver metastasis. We propose that CD147 expressing sEVs are released by colorectal cancers and reach liver Kupffer cells, which then produce a pre-metastatic niche through MMP expression mediated by CD147/MAPK signaling. CRC sEVs act either via uptake by macrophage or via interactions between sEV surface proteins and macrophage surface receptors, possibly including homophilic interactions of CD147 proteins on sEVs and on macrophage cell surfaces. We have developed an *in vivo* liver metastasis model (Fig.13C) which will be useful for testing the physiological relevance of our working model (Fig.13A). Specifically, we will precondition mice with CD147+ or CD147- CRC sEVs and determine how this changes establishment of liver metastases in mice. These experiments will establish the extent to which CD147+ CRC sEVs promote metastasis under physiological conditions and indicate if further research in human and clinical settings is justified. Complementary to the *in vivo* metastasis work, we have optimized a method to fluorescently label sEVs in order to detect uptake of sEVs in macrophages and other cells (Fig.13B). Using the above method, we will be able to condition mice with sEVs before and after injection of CRC cells in order to observe any enhancement

of metastasis in mice conditioned with sEVs. The above experimental system can be used with the CD147 knockdown sEVs to directly test the contribution of CD147 on sEVs to any metastasis enhancing phenotypes we observe. Testing the *in vivo* ability of sEVs with and without CD147 to promote liver metastasis formation will move this project forward a significant distance. Further, *in vivo* liver samples from metastatic and pre-metastatic mice provide opportunities for immunohistochemical analysis of how CRC sEVs change cell-recruitment and tissue remodelling during formation of the premetastatic niche. *In vivo* samples can also be analyzed by flow-cytometry to detect changes in expression of relevant proteins (e.g. VEGF, MMPs) and activation of MAPK and AP-1 signaling pathways within different cell populations such as macrophage, parenchymal cells, endothelial cells, and recruited myeloid derived cells. This will enable a more comprehensive view of how CRC sEVs regulate pre-metastatic niche formation.

REVIEW OF THE LIMITATIONS OF THE EXPERIMENTS CONDUCTED

Limitations in our experiments include: (1) Effect sizes of the MMP activity assay results (Fig.8D-K), (2) using MMP activity assays as a proxy for expression, (3) invasion assays potentially measuring changes in macrophages release of chemotactic agents, (4) the use of serum containing media in the sEV stimulation and western blot experiments, (5) lack of a 0 minutes post-stimulation condition in the sEV stimulation and western blot experiments, (6) the number of replicates for the MAPK/AP-1 western blots, (7) the use of a targeted shRNA without an shScramble control.

The MMP activity assays in Figure 8, D-K, showed some different responses to sEV stimulation between different cell types, however those differences were small. With four biological replicates, this experiment was robust. Compared to later experiments however, the dose of sEVs applied was quite low. In later experiments we opted to use about 1 µg/mL for stimulations of macrophages, whereas in these experiments we use 25 ng/mL or 125 ng/mL. We used lower doses to avoid applying excessive amounts of sEVs that would not correspond to physiological conditions. These doses were also based on the preliminary dose-curves shown in Figure 8 A, B. We may have been overly cautious in applying ng/mL range doses of sEVs as many publications in the field use µg/mL amounts of sEVs and the concentration of sEVs in physiological conditions is not known. Furthermore, the effects observed with these low doses are not impressive, suggesting that the cells were not being substantially affected by the ng/mL range stimulations.

MMP activity assays were used as surrogate measurements of MMP expression due to technical issues with early experiments measuring MMP expression by RT-qPCR and western blot. While the MMP activity of cell culture supernatants generated by macrophages is expected to correspond to the expression of MMPs, it may be an underestimate of MMP production as some extracellular MMPs are inactive pro-MMPs and would not be detected by an activity assay. Changes in the rates of secretion and extracellular activation of MMPs may also confound the use of MMP activity assays as surrogate measurements of MMP expression. It could also be argued, however, that a readout of active MMP production is a better of the independent functional contribution of CRC-conditioned macrophages to the PMN.

Although we observed a correlation between sEV treatment and MMP activity in macrophages (Fig.13), it is possible that CRC sEVs contribute MMPs directly to the MMP activity assays, or that sEVs enhance MMP secretion or post-translational MMP activation in the supernatant. We considered the possibility that sEVs contribute MMP directly to our experiments as researchers have found MT1-MMP in exosomes[177] and MT1-MMP has the ability to activate soluble MMPs, MMP2 and MMP13[108]. Given the small doses of sEVs used (0.5 ng-1.0 µg), however, we do not believe that this is a significant factor. Furthermore, we found that signaling pathways that upregulate MMP expression, specifically MAPK and AP-1 (Fig.11, 12), were induced in macrophages upon CRC sEV treatment. This presents a mechanism by which CRC sEVs could be causing MMP production in macrophages. Thus, our evidences supports the idea that sEVs are inducing MMP expression in macrophages and are not directly contributing activated MMPs to the MMP activity assay results. Nonetheless, we have not ruled out the possibility that sEVs directly activate secreted pro-MMPs.

It is also possible that macrophages stimulated with sEVs from our cancer cells cause the production of chemotaxis inducing chemokines. We did not test this possibility, so it is possible that in addition to MMP production, macrophages promoted invasion in our invasion assay experiments by chemokine release that attracted the MC38 cells to invade the ECM. Broad changes in the secretome of macorphages caused by sEV stimulation could be detected using mass-spectrometry, and may be worth measuring in order to understand comprehensively what the effects are of sEV stimulation of macrophages.

One limitation to our experiments was not measuring the expression of proteins at 0 minutes post-stimulation. Since at 15 minutes post-stimulation MAPK proteins were already being phosphorylated (Fig.11, 12C), the 0 minutes post-stimulation condition would provide a clearer picture of the MAPK/AP-1 pathway activation kinetics in our experimental system. At 0 minutes post-stimulation we would expect minimal activation of MAPK or AP-1 proteins. The sEV stimulation experiments where we measure the activation of MAPK/AP-1 proteins have been conducted three times and, in each instance, we observe increased activation at numerous time points by CRC sEVs compared to media controls. Thus, the activation of MAPK/AP-1 in macrophages by CRC sEVs is a consistent experimental result that is likely physiologically relevant although we cannot define precise kinetics from our existing data. It should also be noted that we did not examine unphosphorylated P38 expression by western blot so changes in the phosphorylated P38 signal could reflect changes in the unphosphorylated proteins expression.

The CD147 knockdown experiments could be improved in a few ways. shRNA knockdown is typically done with a scrambled shRNA (shScramble) as a control, and it is best if more than one shRNA targeting the gene of interest is used. These shortcomings of the CD147 knockdown experiments are significant, and thus our experiments using the CD147 knockdown should be considered preliminary. Future experiments should include multiple shRNAs targeting CD147, as well as a scrambled shRNA control. Techniques for establishing a direct causal link between CD147 on CRC sEVs and MMP production by macrophages need to be further developed. We attempted to uncover a causal link between CD147 on sEVs and MMP production by

depleting CD147+ sEVs from purified CRC sEVs to generate CD147- sEVs but our findings were inconclusive. Better depletion methods or methods to otherwise prevent CD147 function in our experiments should also be developed, such as antibody-based depletions of CD147+ sEVs and inhibitors of CD147. Also, the level of CD147 in each batch of purified sEVs should be examined toeliminate batch to batch variability as a source of inconsistency in our experiments.

FINAL CONCLUSIONS AND SIGNIFICANCE

The association of CD147 with MMP activation and expression is not novel, however, to our knowledge, the relevance of this mechanism to the process of tumor-sEVs induced liver metastasis in colorectal cancer has not yet been demonstrated. Our results support the hypothesis that CRC sEVs containing CD147 stimulate liver macrophages to produce MMP production via MAPK signaling thereby promoting CRC liver metastasis. However, future *in vivo* experiments similar to those proposed here are necessary to determine the relevance of our findings for CRC patients. Recent work outlining the role of exosomes in targeting and shaping PMNs in the organs of metastasis[104] suggests that the liver as a site of metastasis will receive a disproportionately high concentration of cancer sEVs before metastasis occurs, although, this may depend on processes governing sEV tissue-localization that are not well understood. Additionally, CD147 is a known negative prognostic marker in colorectal cancer and detection of CD147 expressing sEVs in the serum of CRC patients is also a negative predictor in patients that may serve as a diagnostic or prognostic tool[156,159]. Overall, the evidence suggests CD147 is indeed an important player in colorectal cancer progression, and our data suggest that CD147+ sEVs are one mechanism supporting colorectal cancer

progression. If this is the case, the results of our research may explain a known association of CD147 with poor clinical prognosis. Considering the potential role of CD147 expressing sEVs in colorectal cancer metastasis, it is clear that other populations of sEVs with potential pro-metastatic functions also represent important targets for future anti-cancer therapeutic development.

Metastasis is the final step in cancer progression given that most cancer deaths are associated with metastatic cancer[178]. Consequently, the process of metastasis must be more intensively studied in hope of finding ways to prevent it. Even slowing metastasis will provide valuable time for treatment of the primary tumor and slowing the onset of metastasis and its associated complications. The work presented in this thesis increases our understanding of the metastatic process by demonstrating for the first time how one specific molecule on CRC sEVs activates a specific signaling pathway in macrophage cells in the premetastatic niche in a way that promotes cancer cell invasion.

BIBLIOGRAPHY

1. Canadian Cancer Statistics Advisory Committee. *Canadian Cancer Statistics A 2018 Special Report on Cancer Incidence by Stage*. Toronto, ON; 2018. cancer.ca/Canadian-Cancer-Statistics-2018-EN.

2. Samowitz WS, Curtin K, Lin HH, et al. The colon cancer burden of genetically defined hereditary nonpolyposis colon cancer. *Gastroenterology*. 2001;121(4):830-838. doi:10.1053/gast.2001.27996

3. Jasperson KW, Tuohy TM, Neklason DW, Burt RW. Hereditary and Familial Colon Cancer. *Gastroenterology*. 2010;138(6):2044-2058. doi:10.1053/j.gastro.2010.01.054

4. Hveem TS, Merok MA, Pretorius ME, et al. Prognostic impact of genomic instability in colorectal cancer. *Br J Cancer*. 2014;110(8):2159-2164. doi:10.1038/bjc.2014.133

5. Goel A, Nagasaka T, Arnold CN, et al. The CpG Island Methylator Phenotype and Chromosomal Instability Are Inversely Correlated in Sporadic Colorectal Cancer. *Gastroenterology*. 2007;132(1):127-138. doi:10.1053/j.gastro.2006.09.018

6. Cheng YW, Pincas H, Bacolod MD, et al. CpG island methylator phenotype associates with low-degree chromosomal abnormalities in colorectal cancer. *Clin Cancer Res*. 2008;14(19):6005-6013. doi:10.1158/1078-0432.CCR-08-0216

7. Guinney J, Dienstmann R, Wang X, et al. The consensus molecular subtypes of colorectal cancer. *Nat Med*. 2015;21(11):1350-1356. doi:10.1038/nm.3967

8. Linnekamp JF, Van Hooff SR, Prasetyanti PR, et al. Consensus molecular subtypes of colorectal cancer are recapitulated in in vitro and in vivo models. *Cell Death Differ*. 2018;25(3):616-633. doi:10.1038/s41418-017-0011-5

9. Le DT, Uram JN, Wang H, et al. PD-1 Blockade in Tumors with Mismatch-Repair Deficiency. *N Engl J Med*. 2015;372(26):2509-2520. doi:10.1056/NEJMoa1500596

10. Sinicrope FA, Rego RL, Halling KC, et al. Prognostic Impact of Microsatellite Instability and DNA Ploidy in Human Colon Carcinoma Patients. *Gastroenterology*. 2006;131(3):729-737. doi:10.1053/j.gastro.2006.06.005

11. Xiao Y, Freeman GJ. The microsatellite instable subset of colorectal cancer is a particularly good candidate for checkpoint blockade immunotherapy. *Cancer Discov*. 2015;5(1):16-18. doi:10.1158/2159-8290.CD-14-1397

12. Pino MS, Chung DC. NIH Public Access THE CHROMOSOMAL INSTABILITY PATHWAY IN COLON. 2014;138(6):2059-2072. doi:10.1053/j.gastro.2009.12.065.THE

13. Kuipers EJ, Grady WM, Lieberman D, et al. Colorectal cancer. *Nat Rev Dis Prim*. 2015;1:1-25. doi:10.1038/nrdp.2015.65

14. Sinicrope FA, Sargent DJ. Molecular pathways: Microsatellite instability in

colorectal cancer: Prognostic, predictive, and therapeutic implications. *Clin Cancer Res*. 2012;18(6):1506-1512. doi:10.1158/1078-0432.CCR-11-1469

15. Bae JM, Kim JH, Cho NY, Kim TY, Kang GH. Prognostic implication of the CpG island methylator phenotype in colorectal cancers depends on tumour location. *Br J Cancer*. 2013;109(4):1004-1012. doi:10.1038/bjc.2013.430

16. Gallois C, Laurent-Puig P, Taieb J. Methylator phenotype in colorectal cancer: A prognostic factor or not? *Crit Rev Oncol Hematol*. 2016;99:74-80. doi:10.1016/j.critrevonc.2015.11.001

17. Buckowitz A, Knaebel H-P, Benner A, et al. Microsatellite instability in colorectal cancer is associated with local lymphocyte infiltration and low frequency of distant metastases. *Br J Cancer*. 2005;92(9):1746-1753. doi:10.1038/sj.bjc.6602534

18. Timmermann B, Kerick M, Roehr C, et al. Somatic mutation profiles of MSI and MSS colorectal cancer identified by whole exome next generation sequencing and bioinformatics analysis. *PLoS One*. 2010;5(12):1-10. doi:10.1371/journal.pone.0015661

19. Wolfers J, Lozier A, Raposo G, et al. Tumor-derived exosomes are a source of shared tumor rejection antigens for CTL cross-priming. *Nat Med*. 2001;7(3):297-303. doi:10.1038/85438

20. Mariathasan S, Turley SJ, Nickles D, et al. TGFβ attenuates tumour response to PD-L1 blockade by contributing to exclusion of T cells. *Nature*.

2018;554(7693):544-548. doi:10.1038/nature25501

21. Tauriello DVF, Palomo-Ponce S, Stork D, et al. TGFβ drives immune evasion in genetically reconstituted colon cancer metastasis. *Nature*. 2018;554(7693):538-543. doi:10.1038/nature25492

22. Kalluri R. The biology and function of exosomes in cancer. *J Clin Invest*. 2016;4(2010):1208-1215. doi:10.1172/JCI81135.The

23. Théry C, Witwer KW, Aikawa E, et al. Minimal information for studies of extracellular vesicles 2018 (MISEV2018): a position statement of the International Society for Extracellular Vesicles and update of the MISEV2014 guidelines. *J Extracell Vesicles*. 2018;7(1). doi:10.1080/20013078.2018.1535750

24. Johnstone RM, Adam M, Hammond JR, Orr L, Turbide C. Vesicle formation during reticulocyte maturation. Association of plasma membrane activities with released vesicles (exosomes). *J Biol Chem*. 1987;262(19):9412-9420.

25. Pan B, Teng K, Wu C, Adam M, Johnstone RM. Electron Microscopic Evidence for Externalization of the Transferrin Receptor in Vesicular Form in Sheep Reticulocytes. 1985;101(September).

26. Harding C, Heuser J, Stahl P. Receptor-mediated endocytosis of transferrin and recycling of the transferrin receptor in rat reticulocytes. *J Cell Biol*. 1983;97(2):329-339. doi:10.1083/jcb.97.2.329

27. Ostrowski M, Carmo NB, Krumeich S, et al. Rab27a and Rab27b control different

steps of the exosome secretion pathway. *Nat Cell Biol*. 2010;12(1):19-30. doi:10.1038/ncb2000

28. Baietti MF, Zhang Z, Mortier E, et al. Syndecan–syntenin–ALIX regulates the biogenesis of exosomes. *Nat Cell Biol*. 2012;14(7):677-685. doi:10.1038/ncb2502

29. Savina A, Vidal M, Colombo MI. The exosome pathway in K562 cells is regulated by Rab11. *J Cell Sci*. 2002;115(Pt 12):2505-2515. doi:10.1083/jcb.149.1.1/a

30. Hsu C, Morohashi Y, Yoshimura SI, et al. Regulation of exosome secretion by Rab35 and its GTPase-activating proteins TBC1D10A-C. *J Cell Biol*. 2010;189(2):223-232. doi:10.1083/jcb.200911018

31. Babst M. MVB Vesicle Formation: ESCRT-Dependent, ESCRT-Independent and Everything in Between. 2011;23(4):452-457. doi:10.1016/j.ceb.2011.04.008.MVB

32. Kowal J, Arras G, Colombo M, et al. Proteomic comparison defines novel markers to characterize heterogeneous populations of extracellular vesicle subtypes. *Proc Natl Acad Sci*. 2016;113(8):E968-E977. doi:10.1073/pnas.1521230113

33. Baroni M, Pizzirani C, Pinotti M, et al. Stimulation of P2 (P2X 7) receptors in human dendritic cells induces the release of tissue factor-bearing microparticles . *FASEB J*. 2007;21(8):1926-1933. doi:10.1096/fj.06-7238com

34. Bianco F, Pravettoni E, Colombo A, et al. Astrocyte-Derived ATP Induces Vesicle Shedding and IL-1β Release from Microglia. *J Immunol*. 2005;174(11):7268-7277. doi:10.4049/jimmunol.174.11.7268

35. Bright NA, Gratian MJ, Luzio PJ. Endocytic Delivery to Lysosomes Mediate by Concurrent Fusion and Kissing Events in Living Cells. *Curr Biol*. 2005;15(4):360-365. doi:https://doi.org/10.1016/j.cub.2005.01.049

36. Katzmann DJ, Stefan CJ, Babst M, Emr SD. Vps27 recruits ESCRT machinery to endosomes during MVB sorting. *J Cell Biol*. 2003;162(3):413-423. doi:10.1083/jcb.200302136

37. Reggiori F, Pelham HRB. A transmembrane ubiquitin ligase required to sort membrane proteins into multivesicular bodies. *Nat Cell Biol*. 2002;4(2):117-123. doi:10.1038/ncb743

38. Cheng Y, Schorey JS. Targeting Soluble Proteins to Exosomes Using a Ubiquitin Tag. 2016;113(6):1315-1324. doi:10.1002/bit.25884

39. Bilodeau PS, Winistorfer SC, Kearney WR, Robertson AD, Piper RC. Vps27-Hse1 and ESCRT-I complexes cooperate to increase efficiency of sorting ubiquitinated proteins at the endosome. *J Cell Biol*. 2003;163(2):237-243. doi:10.1083/jcb.200305007

40. Katzmann DJ, Babst M, Emr SD. Ubiquitin-dependent sorting into the multivesicular body pathway requires the function of a conserved endosomal protein sorting complex, ESCRT-I. *Cell*. 2001;106(2):145-155. doi:10.1016/S0092-8674(01)00434-2

41. Babst M. MVB vesicle formation: ESCRT-dependent, ESCRT-independent and

everything in between. *Curr Opin Cell Biol*. 2011;23(4):452-457. doi:10.1016/j.ceb.2011.04.008

42. Hanson PI, Roth R, Lin Y, Heuser JE. Plasma membrane deformation by circular arrays of ESCRT-III protein filaments. *J Cell Biol*. 2008;180(2):389-402. doi:10.1083/jcb.200707031

43. Babst M, Katzmann DJ, Estepa-Sabal EJ, Meerloo T, Emr SD. ESCRT-III: An endosome-associated heterooligomeric protein complex required for MVB sorting. *Dev Cell*. 2002;3(2):271-282. doi:10.1016/S1534-5807(02)00220-4

44. Wollert T, Wunder C, Lippincott-Schwartz J, Hurley JH. Membrane scission by the ESCRT-III complex. *Nature*. 2009;458(7235):172-177. doi:10.1038/nature07836

45. Maity S, Caillat C, Miguet N, et al. VPS4 triggers constriction and cleavage of ESCRT-III helical filaments. *Sci Adv*. 2019;5(4). doi:10.1126/sciadv.aau7198

46. Ghossoub R, Lembo F, Rubio A, et al. Syntenin-ALIX exosome biogenesis and budding into multivesicular bodies are controlled by ARF6 and PLD2. *Nat Commun*. 2014;5. doi:10.1038/ncomms4477

47. Valadi H, Ekström K, Bossios A, Sjöstrand M, Lee JJ, Lötvall JO. Exosome-mediated transfer of mRNAs and microRNAs is a novel mechanism of genetic exchange between cells. *Nat Cell Biol*. 2007;9(6):654-659. doi:10.1038/ncb1596

48. Pegtel DM, Cosmopoulos K, Thorley-Lawson DA, et al. Functional delivery of viral miRNAs via exosomes. *Proc Natl Acad Sci U S A*. 2010;107(14):6328-6333.

doi:10.1073/pnas.0914843107

49. Cheng L, Sharples RA, Scicluna BJ, Hill AF. Exosomes provide a protective and enriched source of miRNA for biomarker profiling compared to intracellular and cell-free blood. *J Extracell Vesicles*. 2014;3(1). doi:10.3402/jev.v3.23743

50. Zhang X, Sai B, Wang F, et al. Hypoxic BMSC-derived exosomal miRNAs promote metastasis of lung cancer cells via STAT3-induced EMT. *Mol Cancer*. 2019;18(1):1-15. doi:10.1186/s12943-019-0959-5

51. Melo SA, Sugimoto H, O'Connell JT, et al. Cancer Exosomes Perform Cell-Independent MicroRNA Biogenesis and Promote Tumorigenesis. *Cancer Cell*. 2014;26(5):707-721. doi:10.1016/j.ccell.2014.09.005

52. Zhou Y, Ren H, Dai B, et al. Hepatocellular carcinoma-derived exosomal miRNA-21 contributes to tumor progression by converting hepatocyte stellate cells to cancer-associated fibroblasts. *J Exp Clin Cancer Res*. 2018;37(1):1-18. doi:10.1186/s13046-018-0965-2

53. Tian Y, Ma L, Gong M, et al. Protein Profiling and Sizing of Extracellular Vesicles from Colorectal Cancer Patients via Flow Cytometry. *ACS Nano*. 2018;12(1):671-680. doi:10.1021/acsnano.7b07782

54. Huang W, Luo WJ, Zhu P, et al. Modulation of CD147-induced matrix metalloproteinase activity: Role of CD147 N-glycosylation. *Biochem J*. 2013;449(2):437-448. doi:10.1042/BJ20120343

55. Le Floch R, Chiche J, Marchiq I, et al. CD147 subunit of lactate/H+ symporters MCT1 and hypoxia-inducible MCT4 is critical for energetics and growth of glycolytic tumors. *Proc Natl Acad Sci U S A*. 2012;109(49):20166. doi:10.1073/pnas.1219161109

56. Li M, Zhai Q, Bharadwaj U, et al. Cyclophilin A is overexpressed in human pancreatic cancer cells and stimulates cell proliferation through CD147. *Cancer*. 2006;106(10):2284-2294. doi:10.1002/cncr.21862

57. Sun J, Hemler ME. Regulation of MMP-1 and MMP-2 production through CD147/extracellular matrix metalloproteinase inducer interactions. *Cancer Res*. 2001;61(5):2276-2281.

58. Lim M, Martinez T, Jablons D, et al. Tumor-derived EMMPRIN (extracellular matrix metalloproteinase inducer) stimulates collagenase transcription through MAPK p38. *FEBS Lett*. 1998;441(1):88-92. doi:10.1016/S0014-5793(98)01474-4

59. Fossum S, Mallett S, Neil Barclay A. The MRC OX-47 antigen is a member of the immunoglobulin superfamily with an unusual transmembrane sequence. *Eur J Immunol*. 1991;21(3):671-679. doi:10.1002/eji.1830210320

60. Slomiany MG, Daniel Grass G, Robertson AD, et al. Hyaluronan, CD44, and emmprin regulate lactate efflux and membrane localization of monocarboxylate transporters in human breast carcinoma cells. *Cancer Res*. 2009;69(4):1293-1301. doi:10.1158/0008-5472.CAN-08-2491

61. Milia-Argeiti E, Mourah S, Vallée B, et al. EMMPRIN/CD147-encriched membrane vesicles released from malignant human testicular germ cells increase MMP production through tumor-stroma interaction. *Biochim Biophys Acta - Gen Subj*. 2014;1840(8):2581-2588. doi:10.1016/j.bbagen.2014.02.026

62. Colangelo N, Toledo S De, Azzam E. Irradiation of Glioblastoma Cells Increases CD147 Levels in their Extracellular Vesicles: Contribution to Increased MMP9 Activity in the Tumor Microenvironment. *Int J Radiat Oncol Biol Phys*. 2017;99(2):E585. doi:10.1016/j.ijrobp.2017.06.2008

63. Fox S, Rossi AG. *Fundamentals of Inflammation, Chapter 8, Macrophages*. 1st ed. (Serhan CN, Ward PA, Gilroy DW, eds.). Cambridge, England: Cambridge: Cambridge University Press; 2010. doi:10.1017/CBO9781139195737.010.

64. Gomez Perdiguero E, Klapproth K, Schulz C, et al. Tissue-resident macrophages originate from yolk-sac-derived erythro-myeloid progenitors. *Nature*. 2015;518(7540):547-551. doi:10.1038/nature13989

65. Ginhoux F, Guilliams M. Tissue-Resident Macrophage Ontogeny and Homeostasis. *Immunity*. 2016;44(3):439-449. doi:10.1016/j.immuni.2016.02.024

66. Dupré-Crochet S, Erard M, Nüβe O. ROS production in phagocytes: why, when, and where? *J Leukoc Biol*. 2013;94(4):657-670. doi:10.1189/jlb.1012544

67. Willman BYCL, Stewart CC, Miller V, Yi T, Tomasi TB. REGULATION OF MHC CLASS II GENE EXPRESSION IN MACROPHAGES BY HEMATOPOIETIC

COLONYSTIMULATING FACTORS (CSF) Induction by Granulocyte / Macrophage CSF and Inhibition by CSF1 The class II MHC molecules expressed on antigen-presenting cells are highly poly-. *J Exp Med*. 1989;170(November):1559-1567.

68. Xue J, Schmidt S V., Sander J, et al. Transcriptome-Based Network Analysis Reveals a Spectrum Model of Human Macrophage Activation. *Immunity*. 2014;40(2):274-288. doi:10.1016/j.immuni.2014.01.006

69. Brown ER, Charles KA, Hoare SA, et al. A clinical study assessing the tolerability and biological effects of infliximab, a TNF-α inhibitor, in patients with advanced cancer. *Ann Oncol*. 2008;19(7):1340-1346. doi:10.1093/annonc/mdn054

70. Grivennikov SI, Greten FR, Karin M. Immunity, Inflammation, and Cancer. *Cell*. 2010;140(6):883-899. doi:10.1016/j.cell.2010.01.025

71. Balkwill F, Charles KA, Mantovani A. Smoldering and polarized inflammation in the initiation and promotion of malignant disease. *Cancer Cell*. 2005;7(3):211-217. doi:10.1016/j.ccr.2005.02.013

72. Deng L, Zhou JF, Sellers RS, et al. A novel mouse model of inflammatory bowel disease links mammalian target of rapamycin-dependent hyperproliferation of colonic epithelium to inflammation-associated tumorigenesis. *Am J Pathol*. 2010;176(2):952-967. doi:10.2353/ajpath.2010.090622

73. Dedon PC, Tannenbaum SR. Reactive nitrogen species in the chemical biology of

inflammation. *Arch Biochem Biophys*. 2004;423(1):12-22. doi:10.1016/j.abb.2003.12.017

74. Jobin C. Colorectal cancer: Looking for answers in the microbiota. *Cancer Discov*. 2013;3(4):384-387. doi:10.1158/2159-8290.CD-13-0042

75. Movahedi K, Laoui D, Gysemans C, et al. Different tumor microenvironments contain functionally distinct subsets of macrophages derived from Ly6C(high) monocytes. *Cancer Res*. 2010;70(14):5728-5739. doi:10.1158/0008-5472.CAN-09-4672

76. Coussens LM, Zitvogel L, Palucka AK. Neutralizing tumor-promoting chronic inflammation: A magic bullet? *Science (80-)*. 2013;339(6117):286-291. doi:10.1126/science.1232227

77. Gocheva V, Wang HW, Gadea BB, et al. IL-4 induces cathepsin protease activity in tumor-associated macrophages to promote cancer growth and invasion. *Genes Dev*. 2010;24(3):241-255. doi:10.1101/gad.1874010

78. Lin EY, Gouon-Evans V, Nguyen A V., Pollard JW. The macrophage growth factor CSF-1 in mammary gland development and tumor progression. *J Mammary Gland Biol Neoplasia*. 2002;7(2):147-162. doi:10.1023/A:1020399802795

79. Loke P, Allison JP. PD-L1 and PD-L2 are differentially regulated by Th1 and Th2 cells. *Proc Natl Acad Sci U S A*. 2003;100(9):5336-5341. doi:10.1073/pnas.0931259100

80. Hla A, Class HL a, Borrego BF, et al. Protection from Natural Killer Cell – mediated Lysis. 1998;187(5).

81. Curiel TJ, Coukos G, Zou L, et al. Specific recruitment of regulatory T cells in ovarian carcinoma fosters immune privilege and predicts reduced survival. *Nat Med*. 2004;10(9):942-949. doi:10.1038/nm1093

82. Liu J, Zhang N, Li Q, et al. Tumor-associated macrophages recruit CCR6+ regulatory T cells and promote the development of colorectal cancer via enhancing CCL20 production in mice. *PLoS One*. 2011;6(4):1-13. doi:10.1371/journal.pone.0019495

83. Schlecker E, Stojanovic A, Eisen C, et al. Tumor-Infiltrating Monocytic Myeloid-Derived Suppressor Cells Mediate CCR5-Dependent Recruitment of Regulatory T Cells Favoring Tumor Growth. *J Immunol*. 2012;189(12):5602-5611. doi:10.4049/jimmunol.1201018

84. Biswas SK, Gangi L, Paul S, et al. A distinct and unique transcriptional program expressed by tumor-associated macrophages (defective NF-κB and enhanced IRF-3/STAT1 activation). *Blood*. 2006;107(5):2112-2122. doi:10.1182/blood-2005-01-0428

85. Savage NDL, de Boer T, Walburg K V., et al. Human Anti-Inflammatory Macrophages Induce Foxp3 + GITR + CD25 + Regulatory T Cells, Which Suppress via Membrane-Bound TGFβ-1 . *J Immunol*. 2008;181(3):2220-2226. doi:10.4049/jimmunol.181.3.2220

86. Biswas SK, Mantovani A. Macrophage plasticity and interaction with lymphocyte subsets: Cancer as a paradigm. *Nat Immunol*. 2010;11(10):889-896. doi:10.1038/ni.1937

87. Sharda DR, Yu S, Ray M, et al. Regulation of Macrophage Arginase Expression and Tumor Growth by the Ron Receptor Tyrosine Kinase. *J Immunol*. 2011;187(5):2181-2192. doi:10.4049/jimmunol.1003460

88. Rodriguez PC, Zea AH, DeSalvo J, et al. l-Arginine Consumption by Macrophages Modulates the Expression of CD3ζ Chain in T Lymphocytes. *J Immunol*. 2003;171(3):1232-1239. doi:10.4049/jimmunol.171.3.1232

89. Rodriguez PC, Quiceno DG, Zabaleta J, et al. Arginase I production in the tumor microenvironment by mature myeloid cells inhibits T-cell receptor expression and antigen-specific T-cell responses. *Cancer Res*. 2004;64(16):5839-5849. doi:10.1158/0008-5472.CAN-04-0465

90. Lin EY, Pollard JW. Tumor-associated macrophages press the angiogenic switch in breast cancer. *Cancer Res*. 2007;67(11):5064-5066. doi:10.1158/0008-5472.CAN-07-0912

91. Eubank TD, Galloway M, Montague CM, Waldman WJ, Marsh CB. M-CSF Induces Vascular Endothelial Growth Factor Production and Angiogenic Activity From Human Monocytes. *J Immunol*. 2003;171(5):2637-2643. doi:10.4049/jimmunol.171.5.2637

92. Shojaei F, Wu X, Zhong C, et al. Bv8 regulates myeloid-cell-dependent tumour angiogenesis. *Nature*. 2007;450(7171):825-831. doi:10.1038/nature06348

93. Wyckoff JB, Wang Y, Lin EY, et al. Direct visualization of macrophage-assisted tumor cell intravasation in mammary tumors. *Cancer Res*. 2007;67(6):2649-2656. doi:10.1158/0008-5472.CAN-06-1823

94. Condeelis J, Pollard JW. Macrophages: Obligate partners for tumor cell migration, invasion, and metastasis. *Cell*. 2006;124(2):263-266. doi:10.1016/j.cell.2006.01.007

95. Fuxe J, Karlsson MCI. TGF-β-induced epithelial-mesenchymal transition: A link between cancer and inflammation. *Semin Cancer Biol*. 2012;22(5-6):455-461. doi:10.1016/j.semcancer.2012.05.004

96. Willis BC, Borok Z. TGF-β-induced EMT: Mechanisms and implications for fibrotic lung disease. *Am J Physiol - Lung Cell Mol Physiol*. 2007;293(3). doi:10.1152/ajplung.00163.2007

97. Bonde AK, Tischler V, Kumar S, Soltermann A, Schwendener RA. Intratumoral macrophages contribute to epithelial-mesenchymal transition in solid tumors. *BMC Cancer*. 2012;12. doi:10.1186/1471-2407-12-35

98. Quail DF, Joyce JA. Microenvironmental regulation of tumor progression and metastasis. *Nat Med*. 2013;19(11):1423-1437. doi:10.1038/nm.3394

99. Qian B, Deng Y, Im JH, et al. A distinct macrophage population mediates

metastatic breast cancer cell extravasation, establishment and growth. *PLoS One*. 2009;4(8). doi:10.1371/journal.pone.0006562

100. Qian BZ, Li J, Zhang H, et al. CCL2 recruits inflammatory monocytes to facilitate breast-tumour metastasis. *Nature*. 2011;475(7355):222-225. doi:10.1038/nature10138

101. Headley MB, Bins A, Nip A, et al. Visualization of immediate immune responses to pioneer metastatic cells in the lung. *Nature*. 2016;531(7595):513-517. doi:10.1038/nature16985

102. Riihimäki M, Hemminki A, Sundquist J, Hemminki K. Patterns of metastasis in colon and rectal cancer. *Sci Rep*. 2016;6(1):29765. doi:10.1038/srep29765

103. Peinado H, Zhang H, Matei IR, et al. Pre-metastatic niches: Organ-specific homes for metastases. *Nat Rev Cancer*. 2017;17(5):302-317. doi:10.1038/nrc.2017.6

104. Hoshino A, Costa-Silva B, Shen TL, et al. Tumour exosome integrins determine organotropic metastasis. *Nature*. 2015;527(7578):329-335. doi:10.1038/nature15756

105. Costa-Silva B, Aiello NM, Ocean AJ, et al. Pancreatic cancer exosomes initiate pre-metastatic niche formation in the liver. *Nat Cell Biol*. 2015;17(6):816-826. doi:10.1038/ncb3169

106. Birkedal-Hansen H, Moore WGI, Bodden MK, et al. Matrix Metalloproteinases: A Review Matrix Metalloproteinases: A Review. *Crit Rev Oral Biol Med*.

1993;4(2):197-250. doi:10.1177/1045441193004002040l

107. Visse R, Nagase H. Matrix metalloproteinases and tissue inhibitors of metalloproteinases: Structure, function, and biochemistry. *Circ Res*. 2003;92(8):827-839. doi:10.1161/01.RES.0000070112.80711.3D

108. Gifford V, Itoh Y. MT1-MMP-dependent cell migration: Proteolytic and non-proteolytic mechanisms. *Biochem Soc Trans*. 2019;47(3):811-826. doi:10.1042/BST20180363

109. Tang Y, Nakada MT, Kesavan P, et al. Extracellular matrix metalloproteinase inducer stimulates tumor angiogenesis by elevating vascular endothelial cell growth factor and matrix metalloproteinases. *Cancer Res*. 2005;65(8):3193-3199. doi:10.1158/0008-5472.CAN-04-3605

110. Wells JM, Gaggar A, Blalock JE. MMP generated matrikines. *Matrix Biol*. 2015;44-46:122-129. doi:10.1016/j.matbio.2015.01.016

111. Cui N, Hu M, Khalil RA, Mol P, Transl B, Author S. Biochemical and Biological Attributes of Matrix Metalloproteinases. *Prog Mol Biol Transl Sci*. 2017;147(617):1-73. doi:10.1016/bs.pmbts.2017.02.005

112. Leeman MF, McKay JA, Murray GI. Matrix metalloproteinase 13 activity is associated with poor prognosis in colorectal cancer. *J Clin Pathol*. 2002;55(10):758-762. doi:10.1136/jcp.55.10.758

113. Maurel J, Nadal C, Garcia-Albeniz X, et al. Serum matrix metalloproteinase 7

levels identifies poor prognosis advanced colorectal cancer patients. *Int J Cancer*. 2007;121(5):1066-1071. doi:10.1002/ijc.22799

114. Curran S, Dundas SR, Buxton J, Leeman MF, Ramsay R, Murray GI. Matrix metalloproteinase/tissue inhibitors of matrix metalloproteinase phenotype identifies poor prognosis colorectal cancers. *Clin Cancer Res*. 2004;10(24):8229-8234. doi:10.1158/1078-0432.CCR-04-0424

115. Bergers G, Brekken R, McMahon G, et al. Matrix metalloproteinase-9 triggers the angiogenic switch during carcinogenesis. *Nat Cell Biol*. 2000;2(10):737-744. doi:10.1038/35036374

116. D'Haese A, Wuyts A, Dillen C, et al. In vivo neutrophil recruitment by granulocyte chemotactic protein-2 is assisted by gelatinase B/MMP-9 in the mouse. *J Interf Cytokine Res*. 2000;20(7):667-674. doi:10.1089/107999000414853

117. Van Den Steen PE, Proost P, Wuyts A, Van Damme J, Opdenakker G. Neutrophil gelatinase B potentiates interleukin-8 tenfold by aminoterminal processing, whereas it degrades CTAP-III, PF-4, and GRO-α and leaves RANTES and MCP-2 intact. *Blood*. 2000;96(8):2673-2681. doi:10.1182/blood.v96.8.2673.h8002673_2673_2681

118. Overall CM, McQuibban GA, Clark-Lewis I. Discovery of chemokine substrates for matrix metalloproteinases by exosite scanning: A new tool for degradomics. *Biol Chem*. 2002;383(7-8):1059-1066. doi:10.1515/BC.2002.114

119. Nackman GB, Karkowski FJ, Halpern VJ, Gaetz HP, Tilson MD. Elastin degradation products induce adventitial angiogenesis in the Anidjar/Dobrin rat aneurysm model. *Surgery*. 1997;122(1):39-44. doi:10.1016/S0039-6060(97)90262-2

120. Jung S, Rutka JT, Hinek A. Tropoelastin and Elastin Degradation Products Promote Proliferation of Human Astrocytoma Cell Lines. *J Neuropathol Exp Neurol*. 1998;57(5):439-448. http://dx.doi.org/10.1016/j.jsames.2011.03.003%0Ahttps://doi.org/10.1016/j.gr.2017.08.001%0Ahttp://dx.doi.org/10.1016/j.precamres.2014.12.018%0Ahttp://dx.doi.org/10.1016/j.precamres.2011.08.005%0Ahttp://dx.doi.org/10.1080/00206814.2014.902757%0Ahttp://dx.

121. Murray GI, Duncan ME, O'Neil P, Melvin WT, Fothergill JE. Matrix metalloproteinase-1 is associated with poor prognosis in colorectal cancer. *Nat Med*. 1996;2(4):461-462.

122. Brassart B, Fuchs P, Huet E, et al. Conformational Dependence of Collagenase (Matrix Metalloproteinase-1) Up-regulation by Elastin Peptides in Cultured Fibroblasts. *J Biol Chem*. 2001;276(7):5222-5227. doi:10.1074/jbc.M003642200

123. Liu C, Zhang C, Jia L, et al. Interleukin-3 stimulates matrix metalloproteinase 12 production from macrophages promoting thoracic aortic aneurysm/dissection. *Clin Sci*. 2018;132(6):655-668. doi:10.1042/CS20171529

124. Yan C, Boyd DD. Regulation of Matrix Metalloproteinase Gene Expression. *J Cell*

Physiol. 2006;211(1):19-26. doi:10.1002/JCP

125. Benbow U, Brinckerhoff CE. The AP-1 site and MMP gene regulation: What is all the fuss about? *Matrix Biol*. 1997;15(8-9):519-526. doi:10.1016/S0945-053X(97)90026-3

126. Santos SDM, Verveer PJ, Bastiaens PIH. Growth factor-induced MAPK network topology shapes Erk response determining PC-12 cell fate. *Nat Cell Biol*. 2007;9(3):324-330. doi:10.1038/ncb1543

127. Seufferlein T, Rozengurt E. Galanin, neurotensin, and phorbol esters rapidly stimulate activation of mitogen-activated protein kinase in small cell lung cancer cells. *Cancer Res*. 1996;56(24):5758-5764.

128. Venkatakrishnan CD, Tewari AK, Moldovan L, et al. Heat shock protects cardiac cells from doxorubicin-induced toxicity by activating p38 MAPK and phosphorylation of small heat shock protein 27. *Am J Physiol - Hear Circ Physiol*. 2006;291(6):2680-2691. doi:10.1152/ajpheart.00395.2006

129. Cannell IG, Kong YW, Johnston SJ, et al. p38 MAPK/MK2-mediated induction of miR-34c following DNA damage prevents Myc-dependent DNA replication. *Proc Natl Acad Sci U S A*. 2010;107(12):5375-5380. doi:10.1073/pnas.0910015107

130. Matsuda S, Kawasaki H, Moriguchi T, Gotoh Y, Nishida E. Activation of protein kinase cascades by osmotic shock. *J Biol Chem*. 1995;270(21):12781-12786. doi:10.1074/jbc.270.21.12781

131. Minet E, Arnould T, Michel G, et al. ERK activation upon hypoxia: Involvement in HIF-1 activation. *FEBS Lett*. 2000;468(1):53-58. doi:10.1016/S0014-5793(00)01181-9

132. Karin M, Liu ZG, Zandi E. AP-1 function and regulation. *Curr Opin Cell Biol*. 1997;9(2):240-246. doi:10.1016/S0955-0674(97)80068-3

133. Hess J, Angel P, Schorpp-Kistner M. AP-1 subunits: Quarrel and harmony among siblings. *J Cell Sci*. 2004;117(25):5965-5973. doi:10.1242/jcs.01589

134. Nakabeppu Y, Ryder K, Nathans D. DNA binding activities of three murine Jun proteins: Stimulation by Fos. *Cell*. 1988;55(5):907-915. doi:10.1016/0092-8674(88)90146-8

135. Dérijard B, Hibi M, Wu IH, et al. JNK1: A protein kinase stimulated by UV light and Ha-Ras that binds and phosphorylates the c-Jun activation domain. *Cell*. 1994;76(6):1025-1037. doi:10.1016/0092-8674(94)90380-8

136. Halazonetis TD, Georgopoulos K, Greenberg ME, Leder P. c-Jun dimerizes with itself and with c-Fos, forming complexes of different DNA binding affinities. *Cell*. 1988;55(5):917-924. doi:10.1016/0092-8674(88)90147-X

137. Smeal T, Angel P, Meek J, Karin M. Different requirements for formation of Jun : Jun and Jun : Fos complexes. *Genes Dev*. 1989;3(12 B):2091-2100. doi:10.1101/gad.3.12b.2091

138. Chida K, Nagamori S, Kuroki T. Nuclear translocation of Fos is stimulated by

interaction with Jun through the leucine zipper. *Cell Mol Life Sci*. 1999;55(2):297-302. doi:10.1007/s000180050291

139. Rahmsdorf HJ. Jun: Transcription factor and oncoprotein. *J Mol Med*. 1996;74(12):725-747. doi:10.1007/s001090050077

140. Henne WM, Buchkovich NJ, Emr SD. The ESCRT Pathway. *Dev Cell*. 2011;21(1):77-91. doi:10.1016/j.devcel.2011.05.015

141. Pfeffer SR. Two Rabs for exosome release. *Nat Cell Biol*. 2010;12(1):3-4. doi:10.1038/ncb0110-3

142. Corbett TH, Griswold DP, Roberts BJ, Peckham JC, Schabel FM. Tumor Induction Relationships in Development of Transplantable Cancers of the Colon in Mice for Chemotherapy Assays, with a Note on Carcinogen Structure. *Cancer Res*. 1975;35(9):2434-2439.

143. Li P zhi, Li J zheng, Li M, Gong J ping, He K. An efficient method to isolate and culture mouse Kupffer cells. *Immunol Lett*. 2014;158(1-2):52-56. doi:10.1016/j.imlet.2013.12.002

144. Théry C, Amigorena S, Raposo G, et al. Isolation and Characterization of Exosomes from Cell Culture Supernatants. *Curr Protoc Cell Biol*. 2006;Chapter 3:1-29. doi:10.1002/0471143030.cb0322s30

145. Dragovic RA, Gardiner C, Brooks AS, et al. Sizing and phenotyping of cellular vesicles using Nanoparticle Tracking Analysis. *Nanomedicine Nanotechnology,*

Biol Med. 2011;7(6):780-788. doi:10.1016/j.nano.2011.04.003

146. Pathan M, Keerthikumar S, Ang C, et al. FunRich : An open access standalone functional. 2015:2597-2601. doi:10.1002/pmic.201400515

147. Huang DW, Sherman BT, Lempicki RA. Systematic and integrative analysis of large gene lists using DAVID bioinformatics resources. *Nat Protoc*. 2009;4(1):44-57. doi:10.1038/nprot.2008.211

148. Keerthikumar S, Chisanga D, Ariyaratne D, et al. ExoCarta: A Web-Based Compendium of Exosomal Cargo. *J Mol Biol*. 2016;428(4):688-692. doi:10.1016/j.jmb.2015.09.019

149. Simpson RJ, Kalra H, Mathivanan S. Exocarta as a resource for exosomal research. *J Extracell Vesicles*. 2012;1(1). doi:10.3402/jev.v1i0.18374

150. Mathivanan S, Fahner CJ, Reid GE, Simpson RJ. ExoCarta 2012: Database of exosomal proteins, RNA and lipids. *Nucleic Acids Res*. 2012;40(D1):1241-1244. doi:10.1093/nar/gkr828

151. Mathivanan S, Simpson RJ. ExoCarta: A compendium of exosomal proteins and RNA. *Proteomics*. 2009;9(21):4997-5000. doi:10.1002/pmic.200900351

152. Kuruppu D, Christophi C, Bertram JF, O'Brien PE. Characterization of an animal model of hepatic metastasis. *J Gastroenterol Hepatol*. 1996;11(1):26-32. doi:10.1111/j.1440-1746.1996.tb00006.x

153. Gabison EE, Hoang-xuan T, Mauviel A, Menashi S. EMMPRIN / CD147 , an MMP modulator in cancer , development and tissue repair. 2005;87:361-368. doi:10.1016/j.biochi.2004.09.023

154. Raschke WC, Baird S, Ralph P, Nakoinz I. Functional Macrophage Cell Lines Transformed by Abelson Leukemia Virus. *Cell*. 1978;15(September):261-267. doi:10.1016/0092-8674(78)90101-0

155. McGrail DJ, Garnett J, Yin J, et al. Proteome Instability Is a Therapeutic Vulnerability in Mismatch Repair-Deficient Cancer. *Cancer Cell*. 2020;37(3):371-386.e12. doi:10.1016/j.ccell.2020.01.011

156. Stenzinger A, Wittschieber D, Von Winterfeld M, et al. High extracellular matrix metalloproteinase inducer/CD147 expression is strongly and independently associated with poor prognosis in colorectal cancer. *Hum Pathol*. 2012;43(9):1471-1481. doi:10.1016/j.humpath.2011.10.023

157. Zhu S, Chu D, Zhang Y, et al. EMMPRIN/CD147 expression is associated with disease-free survival of patients with colorectal cancer. *Med Oncol*. 2013;30(1). doi:10.1007/s12032-012-0369-7

158. Tian X, Ye C, Yang Y, et al. Expression of CD147 and matrix metalloproteinase - 11 in colorectal cancer and their relationship to clinicopathological features. *J Transl Med*. 2015:1-11. doi:10.1186/s12967-015-0702-y

159. Xin X, Zeng X, Gu H, et al. CD147/EMMPRIN overexpression and prognosis in

cancer: A systematic review and meta-analysis. *Sci Rep*. 2016;6(113):1-12. doi:10.1038/srep32804

160. Liu B, Wan Z, Sheng B, et al. Overexpression of EMMPRIN is associated with lymph node metastasis and advanced stage of non-small cell lung cancer: A retrospective study. *BMC Pulm Med*. 2017;17(1):1-9. doi:10.1186/s12890-017-0540-1

161. Aoki M, Koga K, Miyazaki M, et al. CD73 complexes with emmprin to regulate MMP-2 production from co-cultured sarcoma cells and fibroblasts. *BMC Cancer*. 2019;19(1):1-13. doi:10.1186/s12885-019-6127-x

162. Zhong W De, Han ZD, He HC, et al. CD147, MMP-1, MMP-2 and MMP-9 protein expression as significant prognostic factors in human prostate cancer. *Oncology*. 2008;75(3-4):230-236. doi:10.1159/000163852

163. Reddy VS, Prabhu SD, Mummidi S, et al. Interleukin-18 induces EMMPRIN expression in primary cardiomyocytes via JNK/Sp1 signaling and MMP-9 in part via EMMPRIN and through AP-1 and NF-κB activation. *Am J Physiol - Hear Circ Physiol*. 2010;299(4):1242-1254. doi:10.1152/ajpheart.00451.2010

164. Nabeshima K, Iwasaki H, Koga K, Hojo H, Suzumiya J, Kikuchi M. Emmprin (basigin / CD147): Matrix metalloproteinase modulator and multifunctional cell recognition molecule that plays a critical role in cancer progression. 2006;(November 2005):359-367. doi:10.1111/j.1440-1827.2006.01972.x

165. Sun J, Hemler ME. Regulation of MMP-1 and MMP-2 Production through CD147 / Extracellular Matrix Metalloproteinase Inducer Interactions 1. 2001:2276-2281.

166. Y MLY, Y TM, Jablons D, et al. Tumor-derived EMMPRIN (extracellular matrix metalloproteinase inducer) stimulates collagenase transcription through MAPK p38. 1998;441:88-92.

167. Tang Y, Kesavan P, Nakada MT, Yan L. Tumor-Stroma Interaction: Positive Feedback Regulation of Extracellular Matrix Metalloproteinase Inducer (EMMPRIN) Expression and Matrix Metalloproteinase-Dependent Generation of Soluble EMMPRIN. *Mol Cancer Res*. 2004;2(2):73-80.

168. Berditchevski F, Chang S, Bodorova J, Hemler ME. Generation of Monoclonal Antibodies to Integrin-associated Proteins. *J Biol Chem*. 1997;272(46):29174-29180. doi:10.1074/jbc.272.46.29174

169. Colangelo NW, Azzam EI. Extracellular vesicles originating from glioblastoma cells increase metalloproteinase release by astrocytes: The role of CD147 (EMMPRIN) and ionizing radiation. *Cell Commun Signal*. 2020;18(1):1-14. doi:10.1186/s12964-019-0494-4

170. Millimaggi D, Mari M, D'Ascenzo S, et al. Tumor vesicle-associated CD147 modulates the angiogenic capability of endothelial cells. *Neoplasia*. 2007;9(4):349-357. doi:10.1593/neo.07133

171. Roussos ET, Condeelis JS, Patsialou A. Chemotaxis in cancer. *Nat Rev Cancer*.

2011;11(8):573-587. doi:10.1038/nrc3078

172. Domenis R, Zanutel R, Caponnetto F, et al. Characterization of the Proinflammatory Profile of Synovial Fluid-Derived Exosomes of Patients with Osteoarthritis. 2017;2017. doi:10.1155/2017/4814987

173. Psaila B, Lyden D. The metastatic niche: Adapting the foreign soil. *Nat Rev Cancer*. 2009;9(4):285-293. doi:10.1038/nrc2621

174. Brodt P. Role of the microenvironment in liver metastasis: From pre- to prometastatic niches. *Clin Cancer Res*. 2016;22(24):5971-5982. doi:10.1158/1078-0432.CCR-16-0460

175. Mu W, Rana S, Zöller M. Host Matrix Modulation by Tumor Exosomes Promotes Motility and Invasiveness. *Neoplasia*. 2013;15(8):875-IN4. doi:10.1593/neo.13786

176. Ozawa C, McDonald DM, Blau HM. Microenvironmental VEGF concentration, not total dose, determines a threshold between normal and aberrant angiogenesis. *J Clin Invest*. 2004;113(4):516-527. doi:10.1172/JCI200418420.Introduction

177. Hakulinen J, Sankkila L, Sugiyama N, Lehti K, Keski-Oja J. Secretion of active membrane type 1 matrix metalloproteinase (MMP-14) into extracellular space in microvesicular exosomes. *J Cell Biochem*. 2008;105(5):1211-1218. doi:10.1002/jcb.21923

178. Dillekås H, Rogers MS, Straume O. Are 90% of deaths from cancer caused by metastases? *Cancer Med*. 2019;8(12):5574-5576. doi:10.1002/cam4.2474

APPENDIX

TABLES

Table 3 – MC38 Empty Vector H2 cell sEV LC-MS/MS, Round 1: Identified Proteins and Peptides List

Accession	Description	Score	Coverage	Proteins (no.)	Unique Peptides (no.)	Peptides (no.)	PSMs	AAs (no.)	MW [kDa]	calc. pI
P21956	Lactadherin OS=Mus musculus GN=Mfge8 PE=1 SV=3 - [MFGM_MOUSE]	264.75	35.64	1	14	14	89	463	51.2	6.52
P03336	Gag polyprotein OS=AKV murine leukemia virus GN=gag PE=1 SV=3 - [GAG_MLVAV]	218.82	20.86	1	9	9	82	537	60.5	8.03
P01837	Ig kappa chain C region OS=Mus musculus PE=1 SV=1 - [IGKC_MOUSE]	178.27	76.42	1	5	5	151	106	11.8	5.41
P63017	Heat shock cognate 71 kDa protein OS=Mus musculus GN=Hspa8 PE=1 SV=1 - [HSP7C_MOUSE]	126.61	36.38	1	17	17	44	646	70.8	5.52
P07356	Annexin A2 OS=Mus musculus GN=Anxa2 PE=1 SV=2 - [ANXA2_MOUSE]	101.08	40.41	1	13	13	33	339	38.7	7.69
P17182	Alpha-enolase OS=Mus musculus GN=Eno1 PE=1 SV=3 - [ENOA_MOUSE]	89.13	30.88	1	10	10	34	434	47.1	6.80
P10126	Elongation factor 1-alpha 1 OS=Mus musculus GN=Eef1a1 PE=1 SV=3 - [EF1A1_MOUSE]	69.99	31.39	1	9	9	25	462	50.1	9.01
P62806	Histone H4 OS=Mus musculus GN=Hist1h4a PE=1 SV=2 - [H4_MOUSE]	64.55	50.49	1	5	5	26	103	11.4	11.36
P60710	Actin, cytoplasmic 1 OS=Mus musculus GN=Actb PE=1 SV=1 - [ACTB_MOUSE]	59.12	20.53	2	7	7	22	375	41.7	5.48
P16858	Glyceraldehyde-3-phosphate dehydrogenase OS=Mus musculus GN=Gapdh PE=1 SV=2 - [G3P_MOUSE]	53.91	25.83	1	7	7	19	333	35.8	8.25
P08752	Guanine nucleotide-binding protein G(i) subunit alpha-2 OS=Mus musculus GN=Gnai2 PE=1 SV=5 - [GNAI2_MOUSE]	51.79	30.70	1	5	9	19	355	40.5	5.45

P52480	Pyruvate kinase PKM OS=Mus musculus GN=Pkm PE=1 SV=4 - [KPYM_MOUSE]	49.32	27.31	1	10	10	15	531	57.8	7.47
P48036	Annexin A5 OS=Mus musculus GN=Anxa5 PE=1 SV=1 - [ANXA5_MOUSE]	49.05	28.84	1	9	9	21	319	35.7	4.96
P03386	Envelope glycoprotein OS=AKV murine leukemia virus GN=env PE=1 SV=1 - [ENV_MLVAV]	48.18	13.30	1	7	7	16	669	73.7	8.05
P10107	Annexin A1 OS=Mus musculus GN=Anxa1 PE=1 SV=2 - [ANXA1_MOUSE]	45.22	30.64	1	8	8	16	346	38.7	7.37
P99024	Tubulin beta-5 chain OS=Mus musculus GN=Tubb5 PE=1 SV=1 - [TBB5_MOUSE]	44.05	27.93	1	9	9	15	444	49.6	4.89
Q8VDN2	Sodium/potassium-transporting ATPase subunit alpha-1 OS=Mus musculus GN=Atp1a1 PE=1 SV=1 - [AT1A1_MOUSE]	40.20	16.13	1	12	12	14	1023	112.9	5.45
P17742	Peptidyl-prolyl cis-trans isomerase A OS=Mus musculus GN=Ppia PE=1 SV=2 - [PPIA_MOUSE]	38.92	35.37	1	5	5	15	164	18.0	7.90
P62880	Guanine nucleotide-binding protein G(I)/G(S)/G(T) subunit beta-2 OS=Mus musculus GN=Gnb2 PE=1 SV=3 - [GBB2_MOUSE]	38.39	18.82	1	3	6	14	340	37.3	6.00
P0CG49	Polyubiquitin-B OS=Mus musculus GN=Ubb PE=2 SV=1 - [UBB_MOUSE]	36.13	61.64	4	4	4	14	305	34.3	7.53
Q9DC51	Guanine nucleotide-binding protein G(k) subunit alpha OS=Mus musculus GN=Gnai3 PE=1 SV=3 - [GNAI3_MOUSE]	35.21	19.21	1	2	6	13	354	40.5	5.69
Q99JI6	Ras-related protein Rap-1b OS=Mus musculus GN=Rap1b PE=1 SV=2 - [RAP1B_MOUSE]	33.61	33.15	1	5	5	12	184	20.8	5.78
P62874	Guanine nucleotide-binding protein G(I)/G(S)/G(T) subunit beta-1 OS=Mus musculus GN=Gnb1 PE=1 SV=3 - [GBB1_MOUSE]	31.51	18.53	1	2	5	12	340	37.4	6.00
P63101	14-3-3 protein zeta/delta OS=Mus musculus GN=Ywhaz PE=1 SV=1 - [1433Z_MOUSE]	29.47	19.59	1	3	4	11	245	27.8	4.79
P10852	4F2 cell-surface antigen heavy chain OS=Mus musculus GN=Slc3a2 PE=1 SV=1 - [4F2_MOUSE]	28.33	11.22	1	5	5	11	526	58.3	5.91
Q9WU78	Programmed cell death 6-interacting protein OS=Mus musculus GN=Pdcd6ip PE=1 SV=3 - [PDC6I_MOUSE]	27.56	13.23	1	7	7	10	869	96.0	6.52
P63094	Guanine nucleotide-binding protein G(s) subunit alpha isoforms short OS=Mus musculus GN=Gnas PE=1 SV=1 - [GNAS2_MOUSE]	26.60	15.23	2	3	4	10	394	45.6	5.96
P26041	Moesin OS=Mus musculus GN=Msn PE=1 SV=3 - [MOES_MOUSE]	25.85	14.73	1	6	6	9	577	67.7	6.60
Q9WV91	Prostaglandin F2 receptor negative regulator OS=Mus musculus GN=Ptgfrn PE=1 SV=2 - [FPRP_MOUSE]	25.61	10.24	1	6	6	9	879	98.7	6.61

P61205	ADP-ribosylation factor 3 OS=Mus musculus GN=Arf3 PE=2 SV=2 - [ARF3_MOUSE]	24.51	19.89	2	3	3	9	181	20.6	7.43
P68373	Tubulin alpha-1C chain OS=Mus musculus GN=Tuba1c PE=1 SV=1 - [TBA1C_MOUSE]	24.03	14.92	2	4	4	7	449	49.9	5.10
Q6PHN9	Ras-related protein Rab-35 OS=Mus musculus GN=Rab35 PE=1 SV=1 - [RAB35_MOUSE]	23.41	16.42	2	3	3	10	201	23.0	8.29
P06151	L-lactate dehydrogenase A chain OS=Mus musculus GN=Ldha PE=1 SV=3 - [LDHA_MOUSE]	22.75	22.59	1	6	6	8	332	36.5	7.74
P97449	Aminopeptidase N OS=Mus musculus GN=Anpep PE=1 SV=4 - [AMPN_MOUSE]	22.58	7.45	1	5	5	8	966	109.6	5.90
P63001	Ras-related C3 botulinum toxin substrate 1 OS=Mus musculus GN=Rac1 PE=1 SV=1 - [RAC1_MOUSE]	22.21	13.02	1	3	3	8	192	21.4	8.50
P01868	Ig gamma-1 chain C region secreted form OS=Mus musculus GN=Ighg1 PE=1 SV=1 - [IGHG1_MOUSE]	21.44	22.84	2	4	4	11	324	35.7	7.40
P09411	Phosphoglycerate kinase 1 OS=Mus musculus GN=Pgk1 PE=1 SV=4 - [PGK1_MOUSE]	21.19	20.62	1	6	6	7	417	44.5	7.90
Q9Z127	Large neutral amino acids transporter small subunit 1 OS=Mus musculus GN=Slc7a5 PE=1 SV=2 - [LAT1_MOUSE]	20.43	8.40	1	3	3	8	512	55.8	7.90
P68254	14-3-3 protein theta OS=Mus musculus GN=Ywhaq PE=1 SV=1 - [1433T_MOUSE]	20.39	17.96	1	2	4	8	245	27.8	4.78
P05064	Fructose-bisphosphate aldolase A OS=Mus musculus GN=Aldoa PE=1 SV=2 - [ALDOA_MOUSE]	20.11	15.38	1	4	4	9	364	39.3	8.09
O08992	Syntenin-1 OS=Mus musculus GN=Sdcbp PE=1 SV=1 - [SDCB1_MOUSE]	20.09	14.38	1	3	3	8	299	32.4	7.15
P11499	Heat shock protein HSP 90-beta OS=Mus musculus GN=Hsp90ab1 PE=1 SV=3 - [HS90B_MOUSE]	19.18	7.18	1	4	4	6	724	83.2	5.03
P61982	14-3-3 protein gamma OS=Mus musculus GN=Ywhag PE=1 SV=2 - [1433G_MOUSE]	18.59	17.00	1	2	4	7	247	28.3	4.89
P18572	Basigin OS=Mus musculus GN=Bsg PE=1 SV=2 - [BASI_MOUSE]	18.20	9.77	1	3	3	7	389	42.4	5.85
P15379	CD44 antigen OS=Mus musculus GN=Cd44 PE=1 SV=3 - [CD44_MOUSE]	16.85	4.63	1	3	3	7	778	85.6	4.96
P04104	Keratin, type II cytoskeletal 1 OS=Mus musculus GN=Krt1 PE=1 SV=4 - [K2C1_MOUSE]	16.17	3.61	1	2	2	5	637	65.6	8.15
P68510	14-3-3 protein eta OS=Mus musculus GN=Ywhah PE=1 SV=2 - [1433F_MOUSE]	15.72	17.89	1	2	4	6	246	28.2	4.89

Q9CQV8	14-3-3 protein beta/alpha OS=Mus musculus GN=Ywhab PE=1 SV=3 - [1433B_MOUSE]	14.97	19.92	1	2	4	6	246	28.1	4.83
P97429	Annexin A4 OS=Mus musculus GN=Anxa4 PE=1 SV=4 - [ANXA4_MOUSE]	14.78	19.12	1	5	5	6	319	35.9	5.57
Q9QUI0	Transforming protein RhoA OS=Mus musculus GN=Rhoa PE=1 SV=1 - [RHOA_MOUSE]	12.51	18.13	1	3	3	5	193	21.8	6.10
Q62470	Integrin alpha-3 OS=Mus musculus GN=Itga3 PE=1 SV=1 - [ITA3_MOUSE]	11.83	4.65	1	4	4	4	1053	116.7	6.57
G5E829	Plasma membrane calcium-transporting ATPase 1 OS=Mus musculus GN=Atp2b1 PE=1 SV=1 - [AT2B1_MOUSE]	11.82	5.16	1	4	4	4	1220	134.7	5.91
Q8R366	Immunoglobulin superfamily member 8 OS=Mus musculus GN=Igsf8 PE=1 SV=2 - [IGSF8_MOUSE]	11.44	7.86	1	3	3	4	611	65.0	7.99
P97370	Sodium/potassium-transporting ATPase subunit beta-3 OS=Mus musculus GN=Atp1b3 PE=1 SV=1 - [AT1B3_MOUSE]	11.16	9.35	1	2	2	4	278	31.8	8.51
P58252	Elongation factor 2 OS=Mus musculus GN=Eef2 PE=1 SV=2 - [EF2_MOUSE]	10.30	4.31	1	3	3	4	858	95.3	6.83
Q9Z1Q5	Chloride intracellular channel protein 1 OS=Mus musculus GN=Clic1 PE=1 SV=3 - [CLIC1_MOUSE]	10.15	12.45	1	2	2	3	241	27.0	5.17
Q03145	Ephrin type-A receptor 2 OS=Mus musculus GN=Epha2 PE=1 SV=3 - [EPHA2_MOUSE]	9.89	3.48	1	3	3	4	977	108.8	6.23
P28667	MARCKS-related protein OS=Mus musculus GN=Marcksl1 PE=1 SV=2 - [MRP_MOUSE]	9.74	31.00	1	3	3	3	200	20.2	4.61
Q91W53	Golgin subfamily A member 7 OS=Mus musculus GN=Golga7 PE=1 SV=1 - [GOGA7_MOUSE]	9.66	13.87	1	2	2	4	137	15.8	7.05
P35278	Ras-related protein Rab-5C OS=Mus musculus GN=Rab5c PE=1 SV=2 - [RAB5C_MOUSE]	9.54	17.13	1	3	3	4	216	23.4	8.41
Q9WVA4	Transgelin-2 OS=Mus musculus GN=Tagln2 PE=1 SV=4 - [TAGL2_MOUSE]	9.38	13.07	1	2	2	3	199	22.4	8.24
P51912	Neutral amino acid transporter B(0) OS=Mus musculus GN=Slc1a5 PE=1 SV=2 - [AAAT_MOUSE]	9.12	5.79	1	2	2	3	553	58.4	7.84
P40237	CD82 antigen OS=Mus musculus GN=Cd82 PE=1 SV=1 - [CD82_MOUSE]	8.72	8.65	1	2	2	3	266	29.6	5.02
P17751	Triosephosphate isomerase OS=Mus musculus GN=Tpi1 PE=1 SV=4 - [TPIS_MOUSE]	7.97	8.36	1	2	2	3	299	32.2	5.74

P16045	Galectin-1 OS=Mus musculus GN=Lgals1 PE=1 SV=3 - [LEG1_MOUSE]	7.84	17.04	1	2	2	3	135	14.9	5.49
Q62465	Synaptic vesicle membrane protein VAT-1 homolog OS=Mus musculus GN=Vat1 PE=1 SV=3 - [VAT1_MOUSE]	7.77	7.39	1	2	2	3	406	43.1	6.37
P08228	Superoxide dismutase [Cu-Zn] OS=Mus musculus GN=Sod1 PE=1 SV=2 - [SODC_MOUSE]	7.20	14.94	1	2	2	3	154	15.9	6.51
Q91VI7	Ribonuclease inhibitor OS=Mus musculus GN=Rnh1 PE=1 SV=1 - [RINI_MOUSE]	7.10	8.55	1	3	3	3	456	49.8	4.78
P62965	Cellular retinoic acid-binding protein 1 OS=Mus musculus GN=Crabp1 PE=1 SV=2 - [RABP1_MOUSE]	7.05	13.87	1	2	2	3	137	15.6	5.38
P60843	Eukaryotic initiation factor 4A-I OS=Mus musculus GN=Eif4a1 PE=1 SV=1 - [IF4A1_MOUSE]	6.44	5.91	2	2	2	2	406	46.1	5.48
P70296	Phosphatidylethanolamine-binding protein 1 OS=Mus musculus GN=Pebp1 PE=1 SV=3 - [PEBP1_MOUSE]	6.33	14.44	1	2	2	2	187	20.8	5.40
Q99K85	Phosphoserine aminotransferase OS=Mus musculus GN=Psat1 PE=1 SV=1 - [SERC_MOUSE]	6.21	6.49	1	2	2	2	370	40.4	8.03
Q8R0J7	Vacuolar protein sorting-associated protein 37B OS=Mus musculus GN=Vps37b PE=1 SV=1 - [VP37B_MOUSE]	5.99	10.18	1	2	2	2	285	31.0	7.05
Q9CYL5	Golgi-associated plant pathogenesis-related protein 1 OS=Mus musculus GN=Glipr2 PE=1 SV=3 - [GAPR1_MOUSE]	5.97	16.88	1	2	2	2	154	17.1	9.51
Q9WTI7	Unconventional myosin-Ic OS=Mus musculus GN=Myo1c PE=1 SV=2 - [MYO1C_MOUSE]	5.82	3.29	1	2	2	2	1063	121.9	9.35
P21278	Guanine nucleotide-binding protein subunit alpha-11 OS=Mus musculus GN=Gna11 PE=1 SV=1 - [GNA11_MOUSE]	5.78	7.24	1	2	2	2	359	42.0	5.97
Q61753	D-3-phosphoglycerate dehydrogenase OS=Mus musculus GN=Phgdh PE=1 SV=3 - [SERA_MOUSE]	5.44	5.25	1	2	2	2	533	56.5	6.54
Q60854	Serpin B6 OS=Mus musculus GN=Serpinb6 PE=1 SV=1 - [SPB6_MOUSE]	5.38	6.61	1	2	2	2	378	42.6	5.74
P63321	Ras-related protein Ral-A OS=Mus musculus GN=Rala PE=1 SV=1 - [RALA_MOUSE]	5.24	12.62	1	2	2	2	206	23.5	7.11
O35639	Annexin A3 OS=Mus musculus GN=Anxa3 PE=1 SV=4 - [ANXA3_MOUSE]	5.14	6.50	1	2	2	2	323	36.4	5.76
P51150	Ras-related protein Rab-7a OS=Mus musculus GN=Rab7a PE=1 SV=2 - [RAB7A_MOUSE]	4.94	10.14	1	2	2	2	207	23.5	6.70

O35474	EGF-like repeat and discoidin I-like domain-containing protein 3 OS=Mus musculus GN=Edil3 PE=1 SV=2 - [EDIL3_MOUSE]	4.70	5.83	1	2	2	2	480	53.7	7.58
P47757	F-actin-capping protein subunit beta OS=Mus musculus GN=Capzb PE=1 SV=3 - [CAPZB_MOUSE]	4.68	8.66	1	2	2	2	277	31.3	5.74
Q02788	Collagen alpha-2(VI) chain OS=Mus musculus GN=Col6a2 PE=1 SV=3 - [CO6A2_MOUSE]	4.68	2.51	1	2	2	2	1034	110.3	6.42
Q60605	Myosin light polypeptide 6 OS=Mus musculus GN=Myl6 PE=1 SV=3 - [MYL6_MOUSE]	4.65	14.57	1	2	2	2	151	16.9	4.65
Q02013	Aquaporin-1 OS=Mus musculus GN=Aqp1 PE=1 SV=3 - [AQP1_MOUSE]	4.59	7.06	1	2	2	2	269	28.8	7.43
Q01768	Nucleoside diphosphate kinase B OS=Mus musculus GN=Nme2 PE=1 SV=1 - [NDKB_MOUSE]	4.27	17.76	1	2	2	2	152	17.4	7.50

Table 4 – MC38 Empty Vector H2 cell sEV LC-MS/MS, Round 2: Identified Proteins and Peptides List

Accession	Description	Score	Coverage	Proteins (no.)	Unique Peptides (no.)	Peptides (no.)	PSMs	AAs (no.)	MW [kDa]	calc. pI
P21956	Lactadherin OS=Mus musculus GN=Mfge8 PE=1 SV=3 - [MFGM_MOUSE]	171.42	31.97	1	15	15	81	463	51.2	6.52
Q504P4	Heat shock cognate 71 kDa protein OS=Mus musculus GN=Hspa8 PE=2 SV=1 - [Q504P4_MOUSE]	103.69	24.24	2	14	14	48	627	68.7	5.52
P04104	Keratin, type II cytoskeletal 1 OS=Mus musculus GN=Krt1 PE=1 SV=4 - [K2C1_MOUSE]	95.72	3.77	1	3	3	35	637	65.6	8.15
P03336	Gag polyprotein OS=AKV murine leukemia virus GN=gag PE=1 SV=3 - [GAG_MLVAV]	88.29	13.78	1	7	7	35	537	60.5	8.03
A2A513	Keratin, type I cytoskeletal 10 OS=Mus musculus GN=Krt10 PE=4 SV=1 - [A2A513_MOUSE]	81.64	10.87	2	4	6	33	561	57	5.07
P62806	Histone H4 OS=Mus musculus GN=Hist1h4a PE=1 SV=2 - [H4_MOUSE]	61.29	50.49	1	5	5	25	103	11.4	11.36
P08249	Malate dehydrogenase, mitochondrial OS=Mus musculus GN=Mdh2 PE=1 SV=3 - [MDHM_MOUSE]	55.77	42.31	1	10	10	20	338	35.6	8.68
P16858	Glyceraldehyde-3-phosphate dehydrogenase OS=Mus musculus GN=Gapdh PE=1 SV=2 - [G3P_MOUSE]	55.16	28.83	1	7	7	22	333	35.8	8.25

P60710	Actin, cytoplasmic 1 OS=Mus musculus GN=Actb PE=1 SV=1 - [ACTB_MOUSE]	52.63	21.07	2	6	6	23	375	41.7	5.48
P99024	Tubulin beta-5 chain OS=Mus musculus GN=Tubb5 PE=1 SV=1 - [TBB5_MOUSE]	50.48	25	1	9	9	21	444	49.6	4.89
Q3TTY5	Keratin, type II cytoskeletal 2 epidermal OS=Mus musculus GN=Krt2 PE=1 SV=1 - [K22E_MOUSE]	50.36	4.53	1	3	3	20	707	70.9	8.06
P08752	Guanine nucleotide-binding protein G(i) subunit alpha-2 OS=Mus musculus GN=Gnai2 PE=1 SV=5 - [GNAI2_MOUSE]	46.57	8.45	1	3	3	19	355	40.5	5.45
P10126	Elongation factor 1-alpha 1 OS=Mus musculus GN=Eef1a1 PE=1 SV=3 - [EF1A1_MOUSE]	43.81	8.66	1	4	4	19	462	50.1	9.01
P68369	Tubulin alpha-1A chain OS=Mus musculus GN=Tuba1a PE=1 SV=1 - [TBA1A_MOUSE]	35.66	15.3	1	5	5	13	451	50.1	5.06
B0V2N8	Annexin A2 (Fragment) OS=Mus musculus GN=Anxa2 PE=2 SV=1 - [B0V2N8_MOUSE]	31.99	22.73	3	4	4	13	176	19.6	5.96
P97449	Aminopeptidase N OS=Mus musculus GN=Anpep PE=1 SV=4 - [AMPN_MOUSE]	31.14	6.73	1	5	5	12	966	109.6	5.9
P63101	14-3-3 protein zeta/delta OS=Mus musculus GN=Ywhaz PE=1 SV=1 - [1433Z_MOUSE]	31.01	26.94	1	4	5	12	245	27.8	4.79
P56480	ATP synthase subunit beta, mitochondrial OS=Mus musculus GN=Atp5b PE=1 SV=2 - [ATPB_MOUSE]	25.47	17.01	1	6	6	9	529	56.3	5.34
Q9ESU7	Neutral amino acid transporter ASCT2 OS=Mus musculus GN=Slc1a5 PE=2 SV=1 - [Q9ESU7_MOUSE]	25.05	8.11	1	3	3	9	555	58.4	7.12
P14152	Malate dehydrogenase, cytoplasmic OS=Mus musculus GN=Mdh1 PE=1 SV=3 - [MDHC_MOUSE]	24.86	26.05	1	7	7	11	334	36.5	6.58
J3QQ16	Protein Col6a3 OS=Mus musculus GN=Col6a3 PE=4 SV=1 - [J3QQ16_MOUSE]	24.47	2.95	2	7	7	10	2677	288.5	8.53
Q61414	Keratin, type I cytoskeletal 15 OS=Mus musculus GN=Krt15 PE=1 SV=2 - [K1C15_MOUSE]	23.57	7.52	2	3	5	11	452	49.1	4.86
P10852	4F2 cell-surface antigen heavy chain OS=Mus musculus GN=Slc3a2 PE=1 SV=1 - [4F2_MOUSE]	23.36	9.51	2	6	6	10	526	58.3	5.91
D3Z1M1	Guanine nucleotide-binding protein G(I)/G(S)/G(T) subunit beta-2 (Fragment) OS=Mus musculus GN=Gnb2 PE=2 SV=1 - [D3Z1M1_MOUSE]	22.83	14.54	4	3	3	10	227	25	7.34
P09055	Integrin beta-1 OS=Mus musculus GN=Itgb1 PE=1 SV=1 - [ITB1_MOUSE]	22.36	9.4	1	7	7	10	798	88.2	5.94
P52480	Pyruvate kinase isozymes M1/M2 OS=Mus musculus GN=Pkm PE=1 SV=4 - [KPYM_MOUSE]	21.91	13.18	1	7	7	9	531	57.8	7.47

Q8VDN2	Sodium/potassium-transporting ATPase subunit alpha-1 OS=Mus musculus GN=Atp1a1 PE=1 SV=1 - [AT1A1_MOUSE]	21.33	5.96	1	5	5	9	1023	112.9	5.45
P62259	14-3-3 protein epsilon OS=Mus musculus GN=Ywhae PE=1 SV=1 - [1433E_MOUSE]	20.17	13.33	1	2	3	9	255	29.2	4.74
P17182	Alpha-enolase OS=Mus musculus GN=Eno1 PE=1 SV=3 - [ENOA_MOUSE]	19.89	25.12	1	8	8	8	434	47.1	6.8
Q9WU78	Programmed cell death 6-interacting protein OS=Mus musculus GN=Pdcd6ip PE=1 SV=3 - [PDC6I_MOUSE]	18.21	4.72	1	4	4	8	869	96	6.52
K3W4Q8	Basigin OS=Mus musculus GN=Bsg PE=4 SV=1 - [K3W4Q8_MOUSE]	16.8	22.48	2	4	4	7	218	24.1	5.36
P53986	Monocarboxylate transporter 1 OS=Mus musculus GN=Slc16a1 PE=1 SV=1 - [MOT1_MOUSE]	15.39	4.46	1	2	2	6	493	53.2	7.47
P11499	Heat shock protein HSP 90-beta OS=Mus musculus GN=Hsp90ab1 PE=1 SV=3 - [HS90B_MOUSE]	13.85	6.08	1	4	4	6	724	83.2	5.03
P06151	L-lactate dehydrogenase A chain OS=Mus musculus GN=Ldha PE=1 SV=3 - [LDHA_MOUSE]	13.66	12.65	2	3	4	6	332	36.5	7.74
Q8C4U8	EGF-like repeat and discoidin I-like domain-containing protein 3 OS=Mus musculus GN=Edil3 PE=2 SV=1 - [Q8C4U8_MOUSE]	13.4	10	2	4	4	6	470	52.7	7.8
F8WIX8	Histone H2A OS=Mus musculus GN=Hist1h2al PE=2 SV=1 - [F8WIX8_MOUSE]	13.34	12.8	13	2	2	6	125	13.6	10.74
Q9WV91	Prostaglandin F2 receptor negative regulator OS=Mus musculus GN=Ptgfrn PE=1 SV=2 - [FPRP_MOUSE]	13.26	4.66	1	4	4	6	879	98.7	6.61
P17742	Peptidyl-prolyl cis-trans isomerase A OS=Mus musculus GN=Ppia PE=1 SV=2 - [PPIA_MOUSE]	12.35	17.07	1	3	3	5	164	18	7.9
Q04447	Creatine kinase B-type OS=Mus musculus GN=Ckb PE=1 SV=1 - [KCRB_MOUSE]	12.26	12.6	1	3	3	4	381	42.7	5.67
Q60932	Voltage-dependent anion-selective channel protein 1 OS=Mus musculus GN=Vdac1 PE=1 SV=3 - [VDAC1_MOUSE]	11.69	11.49	1	2	3	5	296	32.3	8.43
Q03145	Ephrin type-A receptor 2 OS=Mus musculus GN=Epha2 PE=1 SV=3 - [EPHA2_MOUSE]	11.43	3.48	1	3	3	5	977	108.8	6.23
D3Z6F5	ATP synthase subunit alpha OS=Mus musculus GN=Atp5a1 PE=3 SV=1 - [D3Z6F5_MOUSE]	10.97	13.12	2	4	4	4	503	54.6	8.24
Q62470	Integrin alpha-3 OS=Mus musculus GN=Itga3 PE=1 SV=1 - [ITA3_MOUSE]	9.67	1.9	1	2	2	4	1053	116.7	6.57
P05064	Fructose-bisphosphate aldolase A OS=Mus musculus GN=Aldoa PE=1 SV=2 - [ALDOA_MOUSE]	9.39	9.07	2	3	3	4	364	39.3	8.09

J3QPE8	MCG16555 OS=Mus musculus GN=Vdac3-ps1 PE=4 SV=1 - [J3QPE8_MOUSE]	9.38	8.13	3	1	2	4	283	30.7	8.66
P03386	Envelope glycoprotein OS=AKV murine leukemia virus GN=env PE=1 SV=1 - [ENV_MLVAV]	9.36	3.59	1	2	2	4	669	73.7	8.05
P48036	Annexin A5 OS=Mus musculus GN=Anxa5 PE=1 SV=1 - [ANXA5_MOUSE]	9.21	10.03	1	3	3	4	319	35.7	4.96
Q8VHY0	Chondroitin sulfate proteoglycan 4 OS=Mus musculus GN=Cspg4 PE=1 SV=3 - [CSPG4_MOUSE]	8.98	1.38	1	3	3	4	2327	252.2	5.44
P10107	Annexin A1 OS=Mus musculus GN=Anxa1 PE=1 SV=2 - [ANXA1_MOUSE]	8.88	8.67	1	3	3	4	346	38.7	7.37
Q61753	D-3-phosphoglycerate dehydrogenase OS=Mus musculus GN=Phgdh PE=1 SV=3 - [SERA_MOUSE]	8.66	7.32	1	3	3	4	533	56.5	6.54
Q3U4F0	Sideroflexin-3 OS=Mus musculus GN=Sfxn3 PE=2 SV=1 - [Q3U4F0_MOUSE]	8.37	21.35	2	3	3	3	281	30.9	8.98
Q9EQK5	Major vault protein OS=Mus musculus GN=Mvp PE=1 SV=4 - [MVP_MOUSE]	7.72	2.44	2	2	2	3	861	95.9	5.59
P16125	L-lactate dehydrogenase B chain OS=Mus musculus GN=Ldhb PE=1 SV=2 - [LDHB_MOUSE]	7.31	10.78	1	2	3	3	334	36.5	6.05
P61264	Syntaxin-1B OS=Mus musculus GN=Stx1b PE=1 SV=1 - [STX1B_MOUSE]	7.01	13.19	1	3	3	3	288	33.2	5.38
Q9Z127	Large neutral amino acids transporter small subunit 1 OS=Mus musculus GN=Slc7a5 PE=1 SV=2 - [LAT1_MOUSE]	6.97	5.86	1	2	2	3	512	55.8	7.9
P58252	Elongation factor 2 OS=Mus musculus GN=Eef2 PE=1 SV=2 - [EF2_MOUSE]	6.84	3.61	1	3	3	3	858	95.3	6.83
P11798	Calcium/calmodulin-dependent protein kinase type II subunit alpha OS=Mus musculus GN=Camk2a PE=1 SV=2 - [KCC2A_MOUSE]	6.83	5.02	2	2	2	3	478	54.1	7.08
Q60770	Syntaxin-binding protein 3 OS=Mus musculus GN=Stxbp3 PE=1 SV=1 - [STXB3_MOUSE]	6.3	4.22	1	2	2	3	592	67.9	8.02
P26041	Moesin OS=Mus musculus GN=Msn PE=1 SV=3 - [MOES_MOUSE]	6.27	4.51	1	3	3	3	577	67.7	6.6
P57746	V-type proton ATPase subunit D OS=Mus musculus GN=Atp6v1d PE=1 SV=1 - [VATD_MOUSE]	6.16	11.34	1	2	2	2	247	28.4	9.45
Q9D051	Pyruvate dehydrogenase E1 component subunit beta, mitochondrial OS=Mus musculus GN=Pdhb PE=1 SV=1 - [ODPB_MOUSE]	5.47	8.91	1	2	2	2	359	38.9	6.87
P84084	ADP-ribosylation factor 5 OS=Mus musculus GN=Arf5 PE=2 SV=2 - [ARF5_MOUSE]	5.33	11.67	3	2	2	2	180	20.5	6.79
Q04857	Collagen alpha-1(VI) chain OS=Mus musculus GN=Col6a1 PE=2 SV=1 - [CO6A1_MOUSE]	4.89	2.44	1	2	2	2	1025	108.4	5.36

P45376	Aldose reductase OS=Mus musculus GN=Akr1b1 PE=1 SV=3 - [ALDR_MOUSE]	4.33	6.01	1	2	2	2	316	35.7	7.18
Q9WVK4	EH domain-containing protein 1 OS=Mus musculus GN=Ehd1 PE=1 SV=1 - [EHD1_MOUSE]	4.2	3.75	1	2	2	2	534	60.6	6.83
P10853	Histone H2B type 1-F/J/L OS=Mus musculus GN=Hist1h2bf PE=1 SV=2 - [H2B1F_MOUSE]	4.13	15.87	13	2	2	2	126	13.9	10.32
Q3U6K9	Phosphoserine aminotransferase OS=Mus musculus GN=Psat1 PE=2 SV=1 - [Q3U6K9_MOUSE]	4	5.45	2	2	2	2	367	40.2	7.65

Table 5 – MC38 Δ*Mlh1* cell sEV LC-MS/MS Round 1: Identified Proteins and Peptides List

Accession	Description	Score	Coverage	Proteins (no.)	Unique Peptides (no.)	Peptides (no.)	PSMs	AAs (no.)	MW [kDa]	calc. pI
P21956	Lactadherin OS=Mus musculus GN=Mfge8 PE=1 SV=3 - [MFGM_MOUSE]	444.83	40.39	1	16	16	149	463	51.2	6.52
P03336	Gag polyprotein OS=AKV murine leukemia virus GN=gag PE=1 SV=3 - [GAG_MLVAV]	216.32	15.83	1	8	8	79	537	60.5	8.03
P63017	Heat shock cognate 71 kDa protein OS=Mus musculus GN=Hspa8 PE=1 SV=1 - [HSP7C_MOUSE]	179.76	40.09	1	21	21	61	646	70.8	5.52
P07356	Annexin A2 OS=Mus musculus GN=Anxa2 PE=1 SV=2 - [ANXA2_MOUSE]	131.17	49.26	1	17	17	44	339	38.7	7.69
P60710	Actin, cytoplasmic 1 OS=Mus musculus GN=Actb PE=1 SV=1 - [ACTB_MOUSE]	106.4	26.67	2	8	8	39	375	41.7	5.48
P17182	Alpha-enolase OS=Mus musculus GN=Eno1 PE=1 SV=3 - [ENOA_MOUSE]	89.78	32.26	1	9	9	34	434	47.1	6.8
P0CG49	Polyubiquitin-B OS=Mus musculus GN=Ubb PE=2 SV=1 - [UBB_MOUSE]	89.17	61.64	4	4	4	35	305	34.3	7.53
P04104	Keratin, type II cytoskeletal 1 OS=Mus musculus GN=Krt1 PE=1 SV=4 - [K2C1_MOUSE]	80.76	3.77	1	3	3	24	637	65.6	8.15
P99024	Tubulin beta-5 chain OS=Mus musculus GN=Tubb5 PE=1 SV=1 - [TBB5_MOUSE]	71.39	39.86	1	4	12	25	444	49.6	4.89
P10126	Elongation factor 1-alpha 1 OS=Mus musculus GN=Eef1a1 PE=1 SV=3 - [EF1A1_MOUSE]	69.21	31.39	1	10	10	24	462	50.1	9.01
P11499	Heat shock protein HSP 90-beta OS=Mus musculus GN=Hsp90ab1 PE=1 SV=3 - [HS90B_MOUSE]	65.66	21.41	1	8	14	24	724	83.2	5.03
P02535	Keratin, type I cytoskeletal 10 OS=Mus musculus GN=Krt10 PE=1 SV=3 - [K1C10_MOUSE]	61.76	5.26	1	2	3	22	570	57.7	5.11
P52480	Pyruvate kinase PKM OS=Mus musculus GN=Pkm PE=1 SV=4 - [KPYM_MOUSE]	58.15	27.68	1	12	12	17	531	57.8	7.47
P11268	Envelope glycoprotein OS=Radiation murine leukemia virus GN=env PE=3 SV=2 - [ENV_MLVRD]	55.12	12.18	1	1	6	19	665	73	7.72
P16858	Glyceraldehyde-3-phosphate dehydrogenase OS=Mus musculus GN=Gapdh PE=1 SV=2 - [G3P_MOUSE]	53	25.83	1	7	7	19	333	35.8	8.25
P62880	Guanine nucleotide-binding protein G(I)/G(S)/G(T) subunit beta-2 OS=Mus musculus GN=Gnb2 PE=1 SV=3 - [GBB2_MOUSE]	52.38	18.82	1	3	6	19	340	37.3	6

P03386	Envelope glycoprotein OS=AKV murine leukemia virus GN=env PE=1 SV=1 - [ENV_MLVAV]	51.07	13.9	1	2	7	18	669	73.7	8.05
P10107	Annexin A1 OS=Mus musculus GN=Anxa1 PE=1 SV=2 - [ANXA1_MOUSE]	48.8	36.13	1	11	11	17	346	38.7	7.37
P63101	14-3-3 protein zeta/delta OS=Mus musculus GN=Ywhaz PE=1 SV=1 - [1433Z_MOUSE]	46.69	19.59	1	3	4	17	245	27.8	4.79
Q9WU78	Programmed cell death 6-interacting protein OS=Mus musculus GN=Pdcd6ip PE=1 SV=3 - [PDC6I_MOUSE]	44.85	17.84	1	11	11	16	869	96	6.52
P68372	Tubulin beta-4B chain OS=Mus musculus GN=Tubb4b PE=1 SV=1 - [TBB4B_MOUSE]	44.53	29.89	1	1	9	16	445	49.8	4.89
P08752	Guanine nucleotide-binding protein G(i) subunit alpha-2 OS=Mus musculus GN=Gnai2 PE=1 SV=5 - [GNAI2_MOUSE]	43.32	20.56	1	4	6	15	355	40.5	5.45
P62874	Guanine nucleotide-binding protein G(I)/G(S)/G(T) subunit beta-1 OS=Mus musculus GN=Gnb1 PE=1 SV=3 - [GBB1_MOUSE]	42.28	15.29	1	2	5	16	340	37.4	6
P63094	Guanine nucleotide-binding protein G(s) subunit alpha isoforms short OS=Mus musculus GN=Gnas PE=1 SV=1 - [GNAS2_MOUSE]	42	20.56	2	5	6	17	394	45.6	5.96
P62806	Histone H4 OS=Mus musculus GN=Hist1h4a PE=1 SV=2 - [H4_MOUSE]	41.36	38.83	1	4	4	17	103	11.4	11.36
P07901	Heat shock protein HSP 90-alpha OS=Mus musculus GN=Hsp90aa1 PE=1 SV=4 - [HS90A_MOUSE]	41.31	11.87	1	1	7	14	733	84.7	5.01
P15379	CD44 antigen OS=Mus musculus GN=Cd44 PE=1 SV=3 - [CD44_MOUSE]	40.43	8.1	1	5	5	17	778	85.6	4.96
Q8VDN2	Sodium/potassium-transporting ATPase subunit alpha-1 OS=Mus musculus GN=Atp1a1 PE=1 SV=1 - [AT1A1_MOUSE]	38.55	13.69	1	10	10	12	1023	112.9	5.45
Q99JI6	Ras-related protein Rap-1b OS=Mus musculus GN=Rap1b PE=1 SV=2 - [RAP1B_MOUSE]	38.35	27.17	1	4	4	13	184	20.8	5.78
P23242	Gap junction alpha-1 protein OS=Mus musculus GN=Gja1 PE=1 SV=2 - [CXA1_MOUSE]	37.83	24.87	1	6	6	11	382	43	8.76
P05213	Tubulin alpha-1B chain OS=Mus musculus GN=Tuba1b PE=1 SV=2 - [TBA1B_MOUSE]	35.83	29.27	1	9	9	12	451	50.1	5.06
P48036	Annexin A5 OS=Mus musculus GN=Anxa5 PE=1 SV=1 - [ANXA5_MOUSE]	35.39	25.71	1	8	8	14	319	35.7	4.96
P63001	Ras-related C3 botulinum toxin substrate 1 OS=Mus musculus GN=Rac1 PE=1 SV=1 - [RAC1_MOUSE]	35.27	27.6	1	6	6	13	192	21.4	8.5
P06151	L-lactate dehydrogenase A chain OS=Mus musculus GN=Ldha PE=1 SV=3 - [LDHA_MOUSE]	33.36	25.6	1	8	8	12	332	36.5	7.74

Q9WV91	Prostaglandin F2 receptor negative regulator OS=Mus musculus GN=Ptgfrn PE=1 SV=2 - [FPRP_MOUSE]	33.02	16.27	1	10	10	11	879	98.7	6.61
Q9DC51	Guanine nucleotide-binding protein G(k) subunit alpha OS=Mus musculus GN=Gnai3 PE=1 SV=3 - [GNAI3_MOUSE]	31.68	12.71	1	2	4	11	354	40.5	5.69
P51912	Neutral amino acid transporter B(0) OS=Mus musculus GN=Slc1a5 PE=1 SV=2 - [AAAT_MOUSE]	28.44	10.85	1	4	4	11	553	58.4	7.84
P26041	Moesin OS=Mus musculus GN=Msn PE=1 SV=3 - [MOES_MOUSE]	27.79	17.85	1	7	7	12	577	67.7	6.6
P97449	Aminopeptidase N OS=Mus musculus GN=Anpep PE=1 SV=4 - [AMPN_MOUSE]	27.35	8.39	1	6	6	9	966	109.6	5.9
Q9Z1Q5	Chloride intracellular channel protein 1 OS=Mus musculus GN=Clic1 PE=1 SV=3 - [CLIC1_MOUSE]	24.79	17.43	1	3	3	8	241	27	5.17
P10852	4F2 cell-surface antigen heavy chain OS=Mus musculus GN=Slc3a2 PE=1 SV=1 - [4F2_MOUSE]	24.45	13.69	1	7	7	9	526	58.3	5.91
P61205	ADP-ribosylation factor 3 OS=Mus musculus GN=Arf3 PE=2 SV=2 - [ARF3_MOUSE]	23.87	24.31	2	4	4	9	181	20.6	7.43
P58252	Elongation factor 2 OS=Mus musculus GN=Eef2 PE=1 SV=2 - [EF2_MOUSE]	23.5	10.14	1	7	7	9	858	95.3	6.83
P53986	Monocarboxylate transporter 1 OS=Mus musculus GN=Slc16a1 PE=1 SV=1 - [MOT1_MOUSE]	23.38	6.69	1	2	2	8	493	53.2	7.47
P09411	Phosphoglycerate kinase 1 OS=Mus musculus GN=Pgk1 PE=1 SV=4 - [PGK1_MOUSE]	22.39	17.75	1	5	5	8	417	44.5	7.9
P27601	Guanine nucleotide-binding protein subunit alpha-13 OS=Mus musculus GN=Gna13 PE=1 SV=1 - [GNA13_MOUSE]	21.69	5.57	1	1	2	8	377	44	8.21
Q9Z127	Large neutral amino acids transporter small subunit 1 OS=Mus musculus GN=Slc7a5 PE=1 SV=2 - [LAT1_MOUSE]	21.67	8.4	1	3	3	8	512	55.8	7.9
P07091	Protein S100-A4 OS=Mus musculus GN=S100a4 PE=1 SV=1 - [S10A4_MOUSE]	21.16	24.75	1	4	4	9	101	11.7	5.31
P61982	14-3-3 protein gamma OS=Mus musculus GN=Ywhag PE=1 SV=2 - [1433G_MOUSE]	21.14	13.77	1	2	3	8	247	28.3	4.89
P62259	14-3-3 protein epsilon OS=Mus musculus GN=Ywhae PE=1 SV=1 - [1433E_MOUSE]	20.79	17.25	1	4	5	9	255	29.2	4.74
P68510	14-3-3 protein eta OS=Mus musculus GN=Ywhah PE=1 SV=2 - [1433F_MOUSE]	20.41	14.63	1	2	3	8	246	28.2	4.89
P40240	CD9 antigen OS=Mus musculus GN=Cd9 PE=1 SV=2 - [CD9_MOUSE]	20.38	10.18	1	2	2	8	226	25.2	7.23
Q922U2	Keratin, type II cytoskeletal 5 OS=Mus musculus GN=Krt5 PE=1 SV=1 - [K2C5_MOUSE]	20.05	5.52	1	3	3	6	580	61.7	7.75

O08992	Syntenin-1 OS=Mus musculus GN=Sdcbp PE=1 SV=1 - [SDCB1_MOUSE]	19.4	7.02	1	2	2	8	299	32.4	7.15
Q68FD5	Clathrin heavy chain 1 OS=Mus musculus GN=Cltc PE=1 SV=3 - [CLH1_MOUSE]	18.92	3.52	1	5	5	7	1675	191.4	5.69
Q61414	Keratin, type I cytoskeletal 15 OS=Mus musculus GN=Krt15 PE=1 SV=2 - [K1C15_MOUSE]	18.88	5.97	1	2	3	8	452	49.1	4.86
Q9WTI7	Unconventional myosin-Ic OS=Mus musculus GN=Myo1c PE=1 SV=2 - [MYO1C_MOUSE]	18.38	8.09	1	6	6	6	1063	121.9	9.35
G5E829	Plasma membrane calcium-transporting ATPase 1 OS=Mus musculus GN=Atp2b1 PE=1 SV=1 - [AT2B1_MOUSE]	17.93	6.64	1	5	5	6	1220	134.7	5.91
Q9CQV8	14-3-3 protein beta/alpha OS=Mus musculus GN=Ywhab PE=1 SV=3 - [1433B_MOUSE]	17.4	14.63	1	2	3	7	246	28.1	4.83
P18572	Basigin OS=Mus musculus GN=Bsg PE=1 SV=2 - [BASI_MOUSE]	17.37	9.51	1	3	3	6	389	42.4	5.85
P35700	Peroxiredoxin-1 OS=Mus musculus GN=Prdx1 PE=1 SV=1 - [PRDX1_MOUSE]	17.37	27.64	1	5	5	7	199	22.2	8.12
P61027	Ras-related protein Rab-10 OS=Mus musculus GN=Rab10 PE=1 SV=1 - [RAB10_MOUSE]	16.17	17	1	1	3	7	200	22.5	8.38
Q04857	Collagen alpha-1(VI) chain OS=Mus musculus GN=Col6a1 PE=1 SV=1 - [CO6A1_MOUSE]	16.12	5.76	1	4	4	6	1025	108.4	5.36
Q6PHN9	Ras-related protein Rab-35 OS=Mus musculus GN=Rab35 PE=1 SV=1 - [RAB35_MOUSE]	16.02	15.92	1	1	3	7	201	23	8.29
Q64314	Hematopoietic progenitor cell antigen CD34 OS=Mus musculus GN=Cd34 PE=1 SV=1 - [CD34_MOUSE]	15.58	9.69	1	2	2	7	382	41	5.3
Q9QUI0	Transforming protein RhoA OS=Mus musculus GN=Rhoa PE=1 SV=1 - [RHOA_MOUSE]	15.53	25.39	1	4	4	6	193	21.8	6.1
P17751	Triosephosphate isomerase OS=Mus musculus GN=Tpi1 PE=1 SV=4 - [TPIS_MOUSE]	14.64	21.4	1	5	5	5	299	32.2	5.74
Q9DAS9	Guanine nucleotide-binding protein G(I)/G(S)/G(O) subunit gamma-12 OS=Mus musculus GN=Gng12 PE=1 SV=3 - [GBG12_MOUSE]	14.34	25	1	2	2	6	72	8	8.97
O35874	Neutral amino acid transporter A OS=Mus musculus GN=Slc1a4 PE=1 SV=1 - [SATT_MOUSE]	14.17	10.9	1	3	3	6	532	56	5.87
P28667	MARCKS-related protein OS=Mus musculus GN=Marcksl1 PE=1 SV=2 - [MRP_MOUSE]	13.38	41.5	1	3	3	5	200	20.2	4.61
Q03145	Ephrin type-A receptor 2 OS=Mus musculus GN=Epha2 PE=1 SV=3 - [EPHA2_MOUSE]	13.38	3.48	1	3	3	5	977	108.8	6.23
Q9WVA4	Transgelin-2 OS=Mus musculus GN=Tagln2 PE=1 SV=4 - [TAGL2_MOUSE]	13.28	11.56	1	2	2	5	199	22.4	8.24

P63321	Ras-related protein Ral-A OS=Mus musculus GN=Rala PE=1 SV=1 - [RALA_MOUSE]	13.18	19.42	1	3	3	4	206	23.5	7.11
P29391	Ferritin light chain 1 OS=Mus musculus GN=Ftl1 PE=1 SV=2 - [FRIL1_MOUSE]	13.15	20.22	1	3	3	5	183	20.8	6
P62492	Ras-related protein Rab-11A OS=Mus musculus GN=Rab11a PE=1 SV=3 - [RB11A_MOUSE]	12.11	24.54	2	5	5	5	216	24.4	6.57
O35474	EGF-like repeat and discoidin I-like domain-containing protein 3 OS=Mus musculus GN=Edil3 PE=1 SV=2 - [EDIL3_MOUSE]	11.6	13.33	1	4	4	4	480	53.7	7.58
Q62470	Integrin alpha-3 OS=Mus musculus GN=Itga3 PE=1 SV=1 - [ITA3_MOUSE]	11.23	4.65	1	4	4	4	1053	116.7	6.57
P05064	Fructose-bisphosphate aldolase A OS=Mus musculus GN=Aldoa PE=1 SV=2 - [ALDOA_MOUSE]	11.11	9.07	1	3	3	4	364	39.3	8.09
O09044	Synaptosomal-associated protein 23 OS=Mus musculus GN=Snap23 PE=1 SV=1 - [SNP23_MOUSE]	10.95	30.48	1	4	4	7	210	23.2	4.98
Q99PT1	Rho GDP-dissociation inhibitor 1 OS=Mus musculus GN=Arhgdia PE=1 SV=3 - [GDIR1_MOUSE]	10.9	14.22	1	2	2	4	204	23.4	5.2
P35278	Ras-related protein Rab-5C OS=Mus musculus GN=Rab5c PE=1 SV=2 - [RAB5C_MOUSE]	10.5	17.13	1	3	3	4	216	23.4	8.41
P97429	Annexin A4 OS=Mus musculus GN=Anxa4 PE=1 SV=4 - [ANXA4_MOUSE]	10.38	11.29	1	3	3	4	319	35.9	5.57
P09055	Integrin beta-1 OS=Mus musculus GN=Itgb1 PE=1 SV=1 - [ITB1_MOUSE]	10.21	3.51	1	2	2	3	798	88.2	5.94
Q9WV92	Band 4.1-like protein 3 OS=Mus musculus GN=Epb41l3 PE=1 SV=1 - [E41L3_MOUSE]	10.2	6.24	1	3	3	3	929	103.3	5.31
O35639	Annexin A3 OS=Mus musculus GN=Anxa3 PE=1 SV=4 - [ANXA3_MOUSE]	9.86	13.31	1	4	4	4	323	36.4	5.76
Q8R422	CD109 antigen OS=Mus musculus GN=Cd109 PE=1 SV=1 - [CD109_MOUSE]	9.84	3.26	1	4	4	4	1442	161.6	5.57
P26645	Myristoylated alanine-rich C-kinase substrate OS=Mus musculus GN=Marcks PE=1 SV=2 - [MARCS_MOUSE]	9.64	15.53	1	2	2	3	309	29.6	4.34
P62965	Cellular retinoic acid-binding protein 1 OS=Mus musculus GN=Crabp1 PE=1 SV=2 - [RABP1_MOUSE]	9.4	23.36	1	3	3	4	137	15.6	5.38
Q02788	Collagen alpha-2(VI) chain OS=Mus musculus GN=Col6a2 PE=1 SV=3 - [CO6A2_MOUSE]	9.17	3	1	2	2	3	1034	110.3	6.42
P40237	CD82 antigen OS=Mus musculus GN=Cd82 PE=1 SV=1 - [CD82_MOUSE]	8.99	8.65	1	2	2	3	266	29.6	5.02

P70296	Phosphatidylethanolamine-binding protein 1 OS=Mus musculus GN=Pebp1 PE=1 SV=3 - [PEBP1_MOUSE]	8.89	14.44	1	2	2	3	187	20.8	5.4
Q60854	Serpin B6 OS=Mus musculus GN=Serpinb6 PE=1 SV=1 - [SPB6_MOUSE]	8.58	6.61	1	2	2	3	378	42.6	5.74
Q8R0J7	Vacuolar protein sorting-associated protein 37B OS=Mus musculus GN=Vps37b PE=1 SV=1 - [VP37B_MOUSE]	8.18	10.18	1	2	2	3	285	31	7.05
Q01768	Nucleoside diphosphate kinase B OS=Mus musculus GN=Nme2 PE=1 SV=1 - [NDKB_MOUSE]	7.91	28.29	1	3	3	3	152	17.4	7.5
P08556	GTPase NRas OS=Mus musculus GN=Nras PE=1 SV=1 - [RASN_MOUSE]	7.9	20.11	1	3	3	3	189	21.2	5.17
Q61753	D-3-phosphoglycerate dehydrogenase OS=Mus musculus GN=Phgdh PE=1 SV=3 - [SERA_MOUSE]	7.89	8.26	1	3	3	3	533	56.5	6.54
P53994	Ras-related protein Rab-2A OS=Mus musculus GN=Rab2a PE=1 SV=1 - [RAB2A_MOUSE]	7.81	14.15	1	2	2	8	212	23.5	6.54
P62827	GTP-binding nuclear protein Ran OS=Mus musculus GN=Ran PE=1 SV=3 - [RAN_MOUSE]	7.57	15.74	1	3	3	3	216	24.4	7.49
Q64337	Sequestosome-1 OS=Mus musculus GN=Sqstm1 PE=1 SV=1 - [SQSTM_MOUSE]	7.29	11.09	1	2	2	2	442	48.1	5.21
P17809	Solute carrier family 2, facilitated glucose transporter member 1 OS=Mus musculus GN=Slc2a1 PE=1 SV=4 - [GTR1_MOUSE]	7.02	3.66	1	2	2	3	492	53.9	8.87
P50543	Protein S100-A11 OS=Mus musculus GN=S100a11 PE=1 SV=1 - [S10AB_MOUSE]	6.99	23.47	1	2	2	3	98	11.1	5.45
Q61598	Rab GDP dissociation inhibitor beta OS=Mus musculus GN=Gdi2 PE=1 SV=1 - [GDIB_MOUSE]	6.92	6.74	1	2	2	2	445	50.5	6.25
P21278	Guanine nucleotide-binding protein subunit alpha-11 OS=Mus musculus GN=Gna11 PE=1 SV=1 - [GNA11_MOUSE]	6.34	7.24	1	2	2	2	359	42	5.97
P60843	Eukaryotic initiation factor 4A-I OS=Mus musculus GN=Eif4a1 PE=1 SV=1 - [IF4A1_MOUSE]	6.3	5.91	2	2	2	2	406	46.1	5.48
P70290	55 kDa erythrocyte membrane protein OS=Mus musculus GN=Mpp1 PE=1 SV=1 - [EM55_MOUSE]	6.22	8.58	1	2	2	2	466	52.2	7.2
Q8VHY0	Chondroitin sulfate proteoglycan 4 OS=Mus musculus GN=Cspg4 PE=1 SV=3 - [CSPG4_MOUSE]	6.04	1.55	1	2	2	2	2327	252.2	5.44
P97370	Sodium/potassium-transporting ATPase subunit beta-3 OS=Mus musculus GN=Atp1b3 PE=1 SV=1 - [AT1B3_MOUSE]	5.92	9.35	1	2	2	2	278	31.8	8.51
Q9EQK5	Major vault protein OS=Mus musculus GN=Mvp PE=1 SV=4 - [MVP_MOUSE]	5.73	3.83	1	2	2	2	861	95.9	5.59

Q99K85	Phosphoserine aminotransferase OS=Mus musculus GN=Psat1 PE=1 SV=1 - [SERC_MOUSE]	5.58	6.49	1	2	2	2	370	40.4	8.03
Q8K2Y3	Protein eva-1 homolog B OS=Mus musculus GN=Eva1b PE=1 SV=1 - [EVA1B_MOUSE]	5.4	25.61	1	2	2	2	164	18.3	4.68
P63028	Translationally-controlled tumor protein OS=Mus musculus GN=Tpt1 PE=1 SV=1 - [TCTP_MOUSE]	5.32	13.37	1	2	2	2	172	19.4	4.86
Q02257	Junction plakoglobin OS=Mus musculus GN=Jup PE=1 SV=3 - [PLAK_MOUSE]	5.28	3.49	1	2	2	2	745	81.7	6.14
Q6P9J9	Anoctamin-6 OS=Mus musculus GN=Ano6 PE=1 SV=1 - [ANO6_MOUSE]	5.24	2.74	1	2	2	2	911	106.2	6.76
P47754	F-actin-capping protein subunit alpha-2 OS=Mus musculus GN=Capza2 PE=1 SV=3 - [CAZA2_MOUSE]	5.22	8.74	1	2	2	2	286	32.9	5.85
P51150	Ras-related protein Rab-7a OS=Mus musculus GN=Rab7a PE=1 SV=2 - [RAB7A_MOUSE]	5.17	11.11	1	2	2	2	207	23.5	6.7
F8VPU2	FERM, RhoGEF and pleckstrin domain-containing protein 1 OS=Mus musculus GN=Farp1 PE=1 SV=1 - [FARP1_MOUSE]	5.12	2.77	1	2	2	2	1048	118.8	7.88
P61022	Calcineurin B homologous protein 1 OS=Mus musculus GN=Chp1 PE=1 SV=2 - [CHP1_MOUSE]	5.09	10.26	1	2	2	2	195	22.4	5.1
Q61171	Peroxiredoxin-2 OS=Mus musculus GN=Prdx2 PE=1 SV=3 - [PRDX2_MOUSE]	4.97	9.6	1	2	2	2	198	21.8	5.41
P19157	Glutathione S-transferase P 1 OS=Mus musculus GN=Gstp1 PE=1 SV=2 - [GSTP1_MOUSE]	4.81	16.67	1	2	2	6	210	23.6	7.87
P62242	40S ribosomal protein S8 OS=Mus musculus GN=Rps8 PE=1 SV=2 - [RS8_MOUSE]	4.76	11.54	1	2	2	2	208	24.2	10.32
P62071	Ras-related protein R-Ras2 OS=Mus musculus GN=Rras2 PE=1 SV=1 - [RRAS2_MOUSE]	4.7	11.27	1	2	2	2	204	23.4	6.01
Q8R366	Immunoglobulin superfamily member 8 OS=Mus musculus GN=Igsf8 PE=1 SV=2 - [IGSF8_MOUSE]	4.68	3.6	1	2	2	2	611	65	7.99
P47757	F-actin-capping protein subunit beta OS=Mus musculus GN=Capzb PE=1 SV=3 - [CAPZB_MOUSE]	4.53	8.66	1	2	2	2	277	31.3	5.74
P14069	Protein S100-A6 OS=Mus musculus GN=S100a6 PE=1 SV=3 - [S10A6_MOUSE]	4.33	19.1	1	2	2	2	89	10	5.48

Table 6 – MC38 Δ*Mlh1* cell sEV LC-MS/MS Round 2: Identified Proteins and Peptides List

Accession	Description	Score	Coverage	Proteins (no.)	Unique Peptides (no.)	Peptides (no.)	PSMs	AAs (no.)	MW [kDa]	calc. pI
P21956	Lactadherin OS=Mus musculus GN=Mfge8 PE=1 SV=3 - [MFGM_MOUSE]	167.72	31.53	1	12	12	72	463	51.2	6.52
P04104	Keratin, type II cytoskeletal 1 OS=Mus musculus GN=Krt1 PE=1 SV=4 - [K2C1_MOUSE]	108.41	3.77	1	3	3	43	637	65.6	8.15
P68369	Tubulin alpha-1A chain OS=Mus musculus GN=Tuba1a PE=1 SV=1 - [TBA1A_MOUSE]	101.85	32.15	1	6	10	36	451	50.1	5.06
P68372	Tubulin beta-4B chain OS=Mus musculus GN=Tubb4b PE=1 SV=1 - [TBB4B_MOUSE]	94.09	32.13	1	1	11	39	445	49.8	4.89
P63017	Heat shock cognate 71 kDa protein OS=Mus musculus GN=Hspa8 PE=1 SV=1 - [HSP7C_MOUSE]	91.18	24.15	1	12	12	39	646	70.8	5.52
Q9D6F9	Tubulin beta-4A chain OS=Mus musculus GN=Tubb4a PE=1 SV=3 - [TBB4A_MOUSE]	86.92	33.11	1	3	11	36	444	49.6	4.88
P99024	Tubulin beta-5 chain OS=Mus musculus GN=Tubb5 PE=1 SV=1 - [TBB5_MOUSE]	85.72	32.21	1	3	11	36	444	49.6	4.89
Q7TMM9	Tubulin beta-2A chain OS=Mus musculus GN=Tubb2a PE=1 SV=1 - [TBB2A_MOUSE]	83.22	27.42	1	2	9	34	445	49.9	4.89
A2A513	Keratin, type I cytoskeletal 10 OS=Mus musculus GN=Krt10 PE=4 SV=1 - [A2A513_MOUSE]	69.15	10.87	2	5	6	28	561	57	5.07
P68368	Tubulin alpha-4A chain OS=Mus musculus GN=Tuba4a PE=1 SV=1 - [TBA4A_MOUSE]	62.59	25.89	1	4	8	23	448	49.9	5.06
O08553	Dihydropyrimidinase-related protein 2 OS=Mus musculus GN=Dpysl2 PE=1 SV=2 - [DPYL2_MOUSE]	55.04	34.44	1	13	13	23	572	62.2	6.38
P60710	Actin, cytoplasmic 1 OS=Mus musculus GN=Actb PE=1 SV=1 - [ACTB_MOUSE]	54.13	24.53	2	7	7	25	375	41.7	5.48
P52480	Pyruvate kinase isozymes M1/M2 OS=Mus musculus GN=Pkm PE=1 SV=4 - [KPYM_MOUSE]	42.79	23.54	1	10	10	17	531	57.8	7.47
P07356	Annexin A2 OS=Mus musculus GN=Anxa2 PE=1 SV=2 - [ANXA2_MOUSE]	42.4	15.04	1	5	5	18	339	38.7	7.69
Q9EQK5	Major vault protein OS=Mus musculus GN=Mvp PE=1 SV=4 - [MVP_MOUSE]	33.31	4.99	2	4	4	14	861	95.9	5.59
Q3TTY5	Keratin, type II cytoskeletal 2 epidermal OS=Mus musculus GN=Krt2 PE=1 SV=1 - [K22E_MOUSE]	30.87	3.25	1	2	2	12	707	70.9	8.06

Q9QWL7	Keratin, type I cytoskeletal 17 OS=Mus musculus GN=Krt17 PE=1 SV=3 - [K1C17_MOUSE]	29.48	8.78	1	4	5	13	433	48.1	5.06
P08752	Guanine nucleotide-binding protein G(i) subunit alpha-2 OS=Mus musculus GN=Gnai2 PE=1 SV=5 - [GNAI2_MOUSE]	28.07	6.2	1	2	2	11	355	40.5	5.45
P46660	Alpha-internexin OS=Mus musculus GN=Ina PE=1 SV=2 - [AINX_MOUSE]	26.46	9.52	1	3	4	9	504	55.7	5.27
P08551	Neurofilament light polypeptide OS=Mus musculus GN=Nefl PE=1 SV=5 - [NFL_MOUSE]	25.67	12.34	1	4	5	9	543	61.5	4.64
P56480	ATP synthase subunit beta, mitochondrial OS=Mus musculus GN=Atp5b PE=1 SV=2 - [ATPB_MOUSE]	23.51	18.71	1	7	7	9	529	56.3	5.34
Q04447	Creatine kinase B-type OS=Mus musculus GN=Ckb PE=1 SV=1 - [KCRB_MOUSE]	22.36	27.03	1	7	7	8	381	42.7	5.67
P07901	Heat shock protein HSP 90-alpha OS=Mus musculus GN=Hsp90aa1 PE=1 SV=4 - [HS90A_MOUSE]	22.35	8.05	1	1	5	9	733	84.7	5.01
P11499	Heat shock protein HSP 90-beta OS=Mus musculus GN=Hsp90ab1 PE=1 SV=3 - [HS90B_MOUSE]	22.33	8.01	1	1	5	9	724	83.2	5.03
O08599	Syntaxin-binding protein 1 OS=Mus musculus GN=Stxbp1 PE=1 SV=2 - [STXB1_MOUSE]	20.83	12.63	1	6	6	9	594	67.5	6.96
P11269	Gag polyprotein OS=Radiation murine leukemia virus GN=gag PE=1 SV=3 - [GAG_MLVRD]	20.6	11.55	1	4	4	8	537	60.7	7.77
Q8C4U8	EGF-like repeat and discoidin I-like domain-containing protein 3 OS=Mus musculus GN=Edil3 PE=2 SV=1 - [Q8C4U8_MOUSE]	20.33	12.13	2	5	5	12	470	52.7	7.8
P10852	4F2 cell-surface antigen heavy chain OS=Mus musculus GN=Slc3a2 PE=1 SV=1 - [4F2_MOUSE]	19.39	9.89	2	5	5	9	526	58.3	5.91
P10126	Elongation factor 1-alpha 1 OS=Mus musculus GN=Eef1a1 PE=1 SV=3 - [EF1A1_MOUSE]	18.95	6.28	2	3	3	8	462	50.1	9.01
P07724	Serum albumin OS=Mus musculus GN=Alb PE=1 SV=3 - [ALBU_MOUSE]	16.01	6.74	1	3	3	6	608	68.6	6.07
Q03265	ATP synthase subunit alpha, mitochondrial OS=Mus musculus GN=Atp5a1 PE=1 SV=1 - [ATPA_MOUSE]	14.82	13.2	1	5	5	6	553	59.7	9.19
P48036	Annexin A5 OS=Mus musculus GN=Anxa5 PE=1 SV=1 - [ANXA5_MOUSE]	13.18	9.09	1	3	3	6	319	35.7	4.96
Q922U2	Keratin, type II cytoskeletal 5 OS=Mus musculus GN=Krt5 PE=1 SV=1 - [K2C5_MOUSE]	12	3.45	1	2	2	5	580	61.7	7.75
P17182	Alpha-enolase OS=Mus musculus GN=Eno1 PE=1 SV=3 - [ENOA_MOUSE]	11.76	14.52	1	3	4	4	434	47.1	6.8

Q9ESU7	Neutral amino acid transporter ASCT2 OS=Mus musculus GN=Slc1a5 PE=2 SV=1 - [Q9ESU7_MOUSE]	11.75	5.95	1	2	2	4	555	58.4	7.12
P10107	Annexin A1 OS=Mus musculus GN=Anxa1 PE=1 SV=2 - [ANXA1_MOUSE]	11.48	6.36	1	2	2	5	346	38.7	7.37
P26041	Moesin OS=Mus musculus GN=Msn PE=1 SV=3 - [MOES_MOUSE]	10.68	6.24	1	4	4	5	577	67.7	6.6
D3YWD1	Protein Col6a3 (Fragment) OS=Mus musculus GN=Col6a3 PE=4 SV=2 - [D3YWD1_MOUSE]	10.6	3.17	3	5	5	5	1703	185.6	5.53
P46096	Synaptotagmin-1 OS=Mus musculus GN=Syt1 PE=1 SV=1 - [SYT1_MOUSE]	10.35	7.6	1	3	3	4	421	47.4	8.53
D3Z6E4	Enolase OS=Mus musculus GN=Eno2 PE=2 SV=1 - [D3Z6E4_MOUSE]	10.23	18.73	2	3	4	4	315	34.8	4.94
P53986	Monocarboxylate transporter 1 OS=Mus musculus GN=Slc16a1 PE=1 SV=1 - [MOT1_MOUSE]	9.87	6.69	1	2	2	4	493	53.2	7.47
Q61753	D-3-phosphoglycerate dehydrogenase OS=Mus musculus GN=Phgdh PE=1 SV=3 - [SERA_MOUSE]	9.48	9.57	1	4	4	4	533	56.5	6.54
Q8VDN2	Sodium/potassium-transporting ATPase subunit alpha-1 OS=Mus musculus GN=Atp1a1 PE=1 SV=1 - [AT1A1_MOUSE]	9.16	2.74	1	2	2	4	1023	112.9	5.45
F8WJL5	Glyceraldehyde-3-phosphate dehydrogenase OS=Mus musculus GN=Gapdh PE=2 SV=1 - [F8WJL5_MOUSE]	7.84	8.94	3	2	2	3	302	32.5	8.19
P05064	Fructose-bisphosphate aldolase A OS=Mus musculus GN=Aldoa PE=1 SV=2 - [ALDOA_MOUSE]	7.05	6.87	2	2	2	3	364	39.3	8.09
D3Z1M1	Guanine nucleotide-binding protein G(I)/G(S)/G(T) subunit beta-2 (Fragment) OS=Mus musculus GN=Gnb2 PE=2 SV=1 - [D3Z1M1_MOUSE]	6.84	9.69	4	2	2	3	227	25	7.34
P62259	14-3-3 protein epsilon OS=Mus musculus GN=Ywhae PE=1 SV=1 - [1433E_MOUSE]	6.37	7.45	1	1	2	3	255	29.2	4.74
P63101	14-3-3 protein zeta/delta OS=Mus musculus GN=Ywhaz PE=1 SV=1 - [1433Z_MOUSE]	6.34	13.88	1	2	3	3	245	27.8	4.79
P97449	Aminopeptidase N OS=Mus musculus GN=Anpep PE=1 SV=4 - [AMPN_MOUSE]	5.82	2.9	1	2	2	2	966	109.6	5.9
Q9R045	Angiopoietin-related protein 2 OS=Mus musculus GN=Angptl2 PE=2 SV=2 - [ANGL2_MOUSE]	5.42	5.88	1	2	2	2	493	57.1	7.75
Q9WU78	Programmed cell death 6-interacting protein OS=Mus musculus GN=Pdcd6ip PE=1 SV=3 - [PDC6I_MOUSE]	4.99	2.53	1	2	2	2	869	96	6.52
P03386	Envelope glycoprotein OS=AKV murine leukemia virus GN=env PE=1 SV=1 - [ENV_MLVAV]	4.9	3.59	1	2	2	2	669	73.7	8.05

Q8BH59	Calcium-binding mitochondrial carrier protein Aralar1 OS=Mus musculus GN=Slc25a12 PE=1 SV=1 - [CMC1_MOUSE]	4.18	3.69	1	2	2	2	677	74.5	8.25
P06151	L-lactate dehydrogenase A chain OS=Mus musculus GN=Ldha PE=1 SV=3 - [LDHA_MOUSE]	4.14	6.02	2	2	2	2	332	36.5	7.74

Table 7 – MC38 Δ*Polε* cell sEV LC-MS/MS Round 1: Identified Proteins and Peptides List

Accession	Description	Score	Coverage	Proteins (no.)	Unique Peptides (no.)	Peptides (no.)	PSMs	AAs (no.)	MW [kDa]	calc. pI
P21956	Lactadherin OS=Mus musculus GN=Mfge8 PE=1 SV=3 - [MFGM_MOUSE]	294.03	27	1	11	11	108	463	51.2	6.52
P03336	Gag polyprotein OS=AKV murine leukemia virus GN=gag PE=1 SV=3 - [GAG_MLVAV]	159.24	13.78	1	7	7	59	537	60.5	8.03
P63017	Heat shock cognate 71 kDa protein OS=Mus musculus GN=Hspa8 PE=1 SV=1 - [HSP7C_MOUSE]	125.76	28.64	1	16	16	45	646	70.8	5.52
P60710	Actin, cytoplasmic 1 OS=Mus musculus GN=Actb PE=1 SV=1 - [ACTB_MOUSE]	85.03	19.47	2	6	6	32	375	41.7	5.48
Q9WU78	Programmed cell death 6-interacting protein OS=Mus musculus GN=Pdcd6ip PE=1 SV=3 - [PDC6I_MOUSE]	62.72	20.02	1	13	13	22	869	96	6.52
P0CG49	Polyubiquitin-B OS=Mus musculus GN=Ubb PE=2 SV=1 - [UBB_MOUSE]	52.24	61.64	4	4	4	19	305	34.3	7.53
P07356	Annexin A2 OS=Mus musculus GN=Anxa2 PE=1 SV=2 - [ANXA2_MOUSE]	43.76	19.47	1	7	7	17	339	38.7	7.69
P10852	4F2 cell-surface antigen heavy chain OS=Mus musculus GN=Slc3a2 PE=1 SV=1 - [4F2_MOUSE]	39.03	13.69	1	7	7	14	526	58.3	5.91
P63101	14-3-3 protein zeta/delta OS=Mus musculus GN=Ywhaz PE=1 SV=1 - [1433Z_MOUSE]	38.63	15.51	1	3	3	14	245	27.8	4.79
P11499	Heat shock protein HSP 90-beta OS=Mus musculus GN=Hsp90ab1 PE=1 SV=3 - [HS90B_MOUSE]	37.95	12.29	1	7	7	13	724	83.2	5.03
Q8VDN2	Sodium/potassium-transporting ATPase subunit alpha-1 OS=Mus musculus GN=Atp1a1 PE=1 SV=1 - [AT1A1_MOUSE]	37.03	13.78	1	10	10	12	1023	112.9	5.45
P99024	Tubulin beta-5 chain OS=Mus musculus GN=Tubb5 PE=1 SV=1 - [TBB5_MOUSE]	33.89	10.36	1	4	4	12	444	49.6	4.89
P08752	Guanine nucleotide-binding protein G(i) subunit alpha-2 OS=Mus musculus GN=Gnai2 PE=1 SV=5 - [GNAI2_MOUSE]	31.62	15.77	1	5	5	12	355	40.5	5.45
P09055	Integrin beta-1 OS=Mus musculus GN=Itgb1 PE=1 SV=1 - [ITB1_MOUSE]	30.39	11.78	1	7	7	11	798	88.2	5.94
Q9WV91	Prostaglandin F2 receptor negative regulator OS=Mus musculus GN=Ptgfrn PE=1 SV=2 - [FPRP_MOUSE]	26.14	10.47	1	7	7	9	879	98.7	6.61
Q62470	Integrin alpha-3 OS=Mus musculus GN=Itga3 PE=1 SV=1 - [ITA3_MOUSE]	24.47	3.32	1	4	4	9	1053	116.7	6.57

P10126	Elongation factor 1-alpha 1 OS=Mus musculus GN=Eef1a1 PE=1 SV=3 - [EF1A1_MOUSE]	24.45	9.09	1	4	4	9	462	50.1	9.01
P15379	CD44 antigen OS=Mus musculus GN=Cd44 PE=1 SV=3 - [CD44_MOUSE]	24.43	6.04	1	5	5	10	778	85.6	4.96
P04104	Keratin, type II cytoskeletal 1 OS=Mus musculus GN=Krt1 PE=1 SV=4 - [K2C1_MOUSE]	23.12	3.77	1	2	2	7	637	65.6	8.15
P16858	Glyceraldehyde-3-phosphate dehydrogenase OS=Mus musculus GN=Gapdh PE=1 SV=2 - [G3P_MOUSE]	22.78	17.42	1	4	4	8	333	35.8	8.25
P51912	Neutral amino acid transporter B(0) OS=Mus musculus GN=Slc1a5 PE=1 SV=2 - [AAAT_MOUSE]	22.45	8.5	1	3	3	7	553	58.4	7.84
Q04857	Collagen alpha-1(VI) chain OS=Mus musculus GN=Col6a1 PE=1 SV=1 - [CO6A1_MOUSE]	21.24	5.66	1	4	4	7	1025	108.4	5.36
Q02788	Collagen alpha-2(VI) chain OS=Mus musculus GN=Col6a2 PE=1 SV=3 - [CO6A2_MOUSE]	19.25	6.38	1	5	5	6	1034	110.3	6.42
P11268	Envelope glycoprotein OS=Radiation murine leukemia virus GN=env PE=3 SV=2 - [ENV_MLVRD]	18.41	4.51	1	1	2	5	665	73	7.72
Q9Z127	Large neutral amino acids transporter small subunit 1 OS=Mus musculus GN=Slc7a5 PE=1 SV=2 - [LAT1_MOUSE]	18.28	8.4	1	3	3	7	512	55.8	7.9
P97449	Aminopeptidase N OS=Mus musculus GN=Anpep PE=1 SV=4 - [AMPN_MOUSE]	18.02	7.66	1	5	5	6	966	109.6	5.9
P26041	Moesin OS=Mus musculus GN=Msn PE=1 SV=3 - [MOES_MOUSE]	16.7	8.15	1	5	5	6	577	67.7	6.6
Q9WTI7	Unconventional myosin-Ic OS=Mus musculus GN=Myo1c PE=1 SV=2 - [MYO1C_MOUSE]	16.59	5.64	1	4	4	5	1063	121.9	9.35
P40237	CD82 antigen OS=Mus musculus GN=Cd82 PE=1 SV=1 - [CD82_MOUSE]	15.22	8.65	1	2	2	5	266	29.6	5.02
P18572	Basigin OS=Mus musculus GN=Bsg PE=1 SV=2 - [BASI_MOUSE]	14.92	5.66	1	2	2	5	389	42.4	5.85
P61205	ADP-ribosylation factor 3 OS=Mus musculus GN=Arf3 PE=2 SV=2 - [ARF3_MOUSE]	14.74	10.5	3	2	2	6	181	20.6	7.43
O35874	Neutral amino acid transporter A OS=Mus musculus GN=Slc1a4 PE=1 SV=1 - [SATT_MOUSE]	13.58	10.71	1	3	3	6	532	56	5.87
Q8VHY0	Chondroitin sulfate proteoglycan 4 OS=Mus musculus GN=Cspg4 PE=1 SV=3 - [CSPG4_MOUSE]	13.21	2.75	1	5	5	5	2327	252.2	5.44
P03386	Envelope glycoprotein OS=AKV murine leukemia virus GN=env PE=1 SV=1 - [ENV_MLVAV]	12.98	6.28	1	2	3	4	669	73.7	8.05
P17182	Alpha-enolase OS=Mus musculus GN=Eno1 PE=1 SV=3 - [ENOA_MOUSE]	12.82	8.29	1	3	3	5	434	47.1	6.8

P40240	CD9 antigen OS=Mus musculus GN=Cd9 PE=1 SV=2 - [CD9_MOUSE]	12.65	10.18	1	2	2	5	226	25.2	7.23
Q68FD5	Clathrin heavy chain 1 OS=Mus musculus GN=Cltc PE=1 SV=3 - [CLH1_MOUSE]	12.3	2.15	1	3	3	4	1675	191.4	5.69
P62835	Ras-related protein Rap-1A OS=Mus musculus GN=Rap1a PE=1 SV=1 - [RAP1A_MOUSE]	12.02	17.93	2	3	3	5	184	21	6.67
G5E829	Plasma membrane calcium-transporting ATPase 1 OS=Mus musculus GN=Atp2b1 PE=1 SV=1 - [AT2B1_MOUSE]	11.26	5.25	1	4	4	4	1220	134.7	5.91
P62880	Guanine nucleotide-binding protein G(I)/G(S)/G(T) subunit beta-2 OS=Mus musculus GN=Gnb2 PE=1 SV=3 - [GBB2_MOUSE]	11.13	9.71	1	3	3	4	340	37.3	6
Q8K2Q7	BRO1 domain-containing protein BROX OS=Mus musculus GN=Brox PE=1 SV=1 - [BROX_MOUSE]	11.13	9.49	1	3	3	4	411	46.2	7.69
Q03145	Ephrin type-A receptor 2 OS=Mus musculus GN=Epha2 PE=1 SV=3 - [EPHA2_MOUSE]	10.47	2.35	1	2	2	4	977	108.8	6.23
P06151	L-lactate dehydrogenase A chain OS=Mus musculus GN=Ldha PE=1 SV=3 - [LDHA_MOUSE]	10.32	9.94	1	3	3	4	332	36.5	7.74
Q8R422	CD109 antigen OS=Mus musculus GN=Cd109 PE=1 SV=1 - [CD109_MOUSE]	10.27	3.54	1	4	4	4	1442	161.6	5.57
P62806	Histone H4 OS=Mus musculus GN=Hist1h4a PE=1 SV=2 - [H4_MOUSE]	9.69	31.07	1	3	3	4	103	11.4	11.36
Q9QUI0	Transforming protein RhoA OS=Mus musculus GN=Rhoa PE=1 SV=1 - [RHOA_MOUSE]	9.54	11.92	1	2	2	4	193	21.8	6.1
Q9R118	Serine protease HTRA1 OS=Mus musculus GN=Htra1 PE=1 SV=2 - [HTRA1_MOUSE]	9.47	4.58	1	2	2	4	480	51.2	7.65
P68254	14-3-3 protein theta OS=Mus musculus GN=Ywhaq PE=1 SV=1 - [1433T_MOUSE]	9.23	10.61	1	2	2	3	245	27.8	4.78
P52480	Pyruvate kinase PKM OS=Mus musculus GN=Pkm PE=1 SV=4 - [KPYM_MOUSE]	8.89	4.52	1	2	2	3	531	57.8	7.47
Q9QYJ0	DnaJ homolog subfamily A member 2 OS=Mus musculus GN=Dnaja2 PE=1 SV=1 - [DNJA2_MOUSE]	8.29	5.1	1	2	2	3	412	45.7	6.48
Q9CX00	IST1 homolog OS=Mus musculus GN=Ist1 PE=1 SV=1 - [IST1_MOUSE]	8.29	6.63	1	3	3	3	362	39.4	5.44
P62259	14-3-3 protein epsilon OS=Mus musculus GN=Ywhae PE=1 SV=1 - [1433E_MOUSE]	8.06	9.02	1	2	2	3	255	29.2	4.74
Q9D8B3	Charged multivesicular body protein 4b OS=Mus musculus GN=Chmp4b PE=1 SV=2 - [CHM4B_MOUSE]	7.9	10.71	1	2	2	3	224	24.9	4.82

F8VPU2	FERM, RhoGEF and pleckstrin domain-containing protein 1 OS=Mus musculus GN=Farp1 PE=1 SV=1 - [FARP1_MOUSE]	7.84	4.01	1	3	3	3	1048	118.8	7.88
O35474	EGF-like repeat and discoidin I-like domain-containing protein 3 OS=Mus musculus GN=Edil3 PE=1 SV=2 - [EDIL3_MOUSE]	7.69	7.92	1	3	3	3	480	53.7	7.58
P10107	Annexin A1 OS=Mus musculus GN=Anxa1 PE=1 SV=2 - [ANXA1_MOUSE]	7.63	10.69	1	3	3	3	346	38.7	7.37
P48036	Annexin A5 OS=Mus musculus GN=Anxa5 PE=1 SV=1 - [ANXA5_MOUSE]	7.61	6.27	1	2	2	3	319	35.7	4.96
P35278	Ras-related protein Rab-5C OS=Mus musculus GN=Rab5c PE=1 SV=2 - [RAB5C_MOUSE]	7.29	10.65	1	2	2	3	216	23.4	8.41
P61226	Ras-related protein Rap-2b OS=Mus musculus GN=Rap2b PE=1 SV=1 - [RAP2B_MOUSE]	7.09	10.93	1	2	2	3	183	20.5	4.81
Q9D1C8	Vacuolar protein sorting-associated protein 28 homolog OS=Mus musculus GN=Vps28 PE=1 SV=1 - [VPS28_MOUSE]	7.08	9.05	1	2	2	3	221	25.4	5.54
P68510	14-3-3 protein eta OS=Mus musculus GN=Ywhah PE=1 SV=2 - [1433F_MOUSE]	6.67	10.57	1	2	2	2	246	28.2	4.89
Q80W68	Kin of IRRE-like protein 1 OS=Mus musculus GN=Kirrel PE=1 SV=1 - [KIRR1_MOUSE]	6.55	3.93	1	2	2	2	789	87.1	5.92
Q69ZN7	Myoferlin OS=Mus musculus GN=Myof PE=1 SV=2 - [MYOF_MOUSE]	5.97	1.12	1	2	2	2	2048	233.2	6.16
P61982	14-3-3 protein gamma OS=Mus musculus GN=Ywhag PE=1 SV=2 - [1433G_MOUSE]	5.57	9.72	1	2	2	2	247	28.3	4.89
P55012	Solute carrier family 12 member 2 OS=Mus musculus GN=Slc12a2 PE=1 SV=2 - [S12A2_MOUSE]	5.34	2.49	1	2	2	2	1205	131	7.33
Q6P9J9	Anoctamin-6 OS=Mus musculus GN=Ano6 PE=1 SV=1 - [ANO6_MOUSE]	5.23	2.74	1	2	2	2	911	106.2	6.76
Q61753	D-3-phosphoglycerate dehydrogenase OS=Mus musculus GN=Phgdh PE=1 SV=3 - [SERA_MOUSE]	5.08	4.5	1	2	2	2	533	56.5	6.54
P17742	Peptidyl-prolyl cis-trans isomerase A OS=Mus musculus GN=Ppia PE=1 SV=2 - [PPIA_MOUSE]	4.92	14.02	1	2	2	2	164	18	7.9
P17809	Solute carrier family 2, facilitated glucose transporter member 1 OS=Mus musculus GN=Slc2a1 PE=1 SV=4 - [GTR1_MOUSE]	4.71	3.66	1	2	2	2	492	53.9	8.87
P28667	MARCKS-related protein OS=Mus musculus GN=Marcksl1 PE=1 SV=2 - [MRP_MOUSE]	4.66	14	1	2	2	2	200	20.2	4.61
P17751	Triosephosphate isomerase OS=Mus musculus GN=Tpi1 PE=1 SV=4 - [TPIS_MOUSE]	4.53	8.36	1	2	2	2	299	32.2	5.74

Table 8 – MC38 Δ*Polε* cell sEV LC-MS/MS Round 2: Identified Proteins and Peptides List

Accession	Description	Score	Coverage	Proteins (no.)	Unique Peptides (no.)	Peptides (no.)	PSMs	AAs (no.)	MW [kDa]	calc. pI
P21956	Lactadherin OS=Mus musculus GN=Mfge8 PE=1 SV=3 - [MFGM_MOUSE]	119.17	16.41	1	7	7	52	463	51.2	6.52
P04104	Keratin, type II cytoskeletal 1 OS=Mus musculus GN=Krt1 PE=1 SV=4 - [K2C1_MOUSE]	98.37	3.77	1	3	3	36	637	65.6	8.15
A2A513	Keratin, type I cytoskeletal 10 OS=Mus musculus GN=Krt10 PE=4 SV=1 - [A2A513_MOUSE]	78.64	8.56	2	3	5	32	561	57	5.07
P03336	Gag polyprotein OS=AKV murine leukemia virus GN=gag PE=1 SV=3 - [GAG_MLVAV]	54.83	9.5	1	5	5	25	537	60.5	8.03
Q504P4	Heat shock cognate 71 kDa protein OS=Mus musculus GN=Hspa8 PE=2 SV=1 - [Q504P4_MOUSE]	52.97	17.54	2	11	11	24	627	68.7	5.52
Q3TTY5	Keratin, type II cytoskeletal 2 epidermal OS=Mus musculus GN=Krt2 PE=1 SV=1 - [K22E_MOUSE]	49.32	3.25	1	2	2	20	707	70.9	8.06
P60710	Actin, cytoplasmic 1 OS=Mus musculus GN=Actb PE=1 SV=1 - [ACTB_MOUSE]	41.57	14.67	2	5	5	19	375	41.7	5.48
Q9WU78	Programmed cell death 6-interacting protein OS=Mus musculus GN=Pdcd6ip PE=1 SV=3 - [PDC6I_MOUSE]	38.39	9.9	1	9	9	17	869	96	6.52
J3QQ16	Protein Col6a3 OS=Mus musculus GN=Col6a3 PE=4 SV=1 - [J3QQ16_MOUSE]	37.64	3.47	2	9	9	17	2677	288.5	8.53
P08752	Guanine nucleotide-binding protein G(i) subunit alpha-2 OS=Mus musculus GN=Gnai2 PE=1 SV=5 - [GNAI2_MOUSE]	33.33	8.73	1	3	3	13	355	40.5	5.45
Q61781	Keratin, type I cytoskeletal 14 OS=Mus musculus GN=Krt14 PE=1 SV=2 - [K1C14_MOUSE]	26.31	7.85	1	2	4	12	484	52.8	5.17
P10126	Elongation factor 1-alpha 1 OS=Mus musculus GN=Eef1a1 PE=1 SV=3 - [EF1A1_MOUSE]	25.23	8.66	1	4	4	11	462	50.1	9.01
Q922U2	Keratin, type II cytoskeletal 5 OS=Mus musculus GN=Krt5 PE=1 SV=1 - [K2C5_MOUSE]	22.11	7.24	1	3	4	9	580	61.7	7.75
B0V2N8	Annexin A2 (Fragment) OS=Mus musculus GN=Anxa2 PE=2 SV=1 - [B0V2N8_MOUSE]	21.53	22.73	3	4	4	9	176	19.6	5.96
Q9EQK5	Major vault protein OS=Mus musculus GN=Mvp PE=1 SV=4 - [MVP_MOUSE]	20.26	3.72	2	3	3	9	861	95.9	5.59
Q9WV91	Prostaglandin F2 receptor negative regulator OS=Mus musculus GN=Ptgfrn PE=1 SV=2 - [FPRP_MOUSE]	19.08	6.71	1	6	6	9	879	98.7	6.61

Q8VDN2	Sodium/potassium-transporting ATPase subunit alpha-1 OS=Mus musculus GN=Atp1a1 PE=1 SV=1 - [AT1A1_MOUSE]	18.5	6.45	1	1	5	8	1023	112.9	5.45
Q6PIC6	Sodium/potassium-transporting ATPase subunit alpha-3 OS=Mus musculus GN=Atp1a3 PE=1 SV=1 - [AT1A3_MOUSE]	17.77	7.6	2	2	6	8	1013	111.6	5.41
P11499	Heat shock protein HSP 90-beta OS=Mus musculus GN=Hsp90ab1 PE=1 SV=3 - [HS90B_MOUSE]	17.27	6.35	1	4	4	8	724	83.2	5.03
P26041	Moesin OS=Mus musculus GN=Msn PE=1 SV=3 - [MOES_MOUSE]	15.57	7.97	1	5	5	7	577	67.7	6.6
Q8C4U8	EGF-like repeat and discoidin I-like domain-containing protein 3 OS=Mus musculus GN=Edil3 PE=2 SV=1 - [Q8C4U8_MOUSE]	14.58	4.26	2	2	2	6	470	52.7	7.8
P10852	4F2 cell-surface antigen heavy chain OS=Mus musculus GN=Slc3a2 PE=1 SV=1 - [4F2_MOUSE]	12.52	10.84	2	6	6	6	526	58.3	5.91
P62806	Histone H4 OS=Mus musculus GN=Hist1h4a PE=1 SV=2 - [H4_MOUSE]	11.38	38.83	1	4	4	5	103	11.4	11.36
P99024	Tubulin beta-5 chain OS=Mus musculus GN=Tubb5 PE=1 SV=1 - [TBB5_MOUSE]	9.04	8.11	1	3	3	4	444	49.6	4.89
D3Z1M1	Guanine nucleotide-binding protein G(I)/G(S)/G(T) subunit beta-2 (Fragment) OS=Mus musculus GN=Gnb2 PE=2 SV=1 - [D3Z1M1_MOUSE]	8.92	9.69	4	2	2	4	227	25	7.34
Q62470	Integrin alpha-3 OS=Mus musculus GN=Itga3 PE=1 SV=1 - [ITA3_MOUSE]	8.6	1.8	1	2	2	4	1053	116.7	6.57
P09055	Integrin beta-1 OS=Mus musculus GN=Itgb1 PE=1 SV=1 - [ITB1_MOUSE]	8.57	4.39	1	3	3	4	798	88.2	5.94
P05214	Tubulin alpha-3 chain OS=Mus musculus GN=Tuba3a PE=1 SV=1 - [TBA3_MOUSE]	7.79	5.33	2	2	2	3	450	49.9	5.1
P03386	Envelope glycoprotein OS=AKV murine leukemia virus GN=env PE=1 SV=1 - [ENV_MLVAV]	7.72	3.59	1	2	2	3	669	73.7	8.05
P48036	Annexin A5 OS=Mus musculus GN=Anxa5 PE=1 SV=1 - [ANXA5_MOUSE]	7.01	6.58	1	2	2	3	319	35.7	4.96
P0CG49	Polyubiquitin-B OS=Mus musculus GN=Ubb PE=1 SV=1 - [UBB_MOUSE]	6.14	28.85	11	2	2	3	305	34.3	7.53
Q8VHY0	Chondroitin sulfate proteoglycan 4 OS=Mus musculus GN=Cspg4 PE=1 SV=3 - [CSPG4_MOUSE]	6.06	0.9	1	2	2	3	2327	252.2	5.44
P63101	14-3-3 protein zeta/delta OS=Mus musculus GN=Ywhaz PE=1 SV=1 - [1433Z_MOUSE]	5.58	10.61	1	2	2	2	245	27.8	4.79
Q62261	Spectrin beta chain, non-erythrocytic 1 OS=Mus musculus GN=Sptbn1 PE=1 SV=2 - [SPTB2_MOUSE]	4.8	0.97	2	2	2	2	2363	274.1	5.58

Q61753	D-3-phosphoglycerate dehydrogenase OS=Mus musculus GN=Phgdh PE=1 SV=3 - [SERA_MOUSE]	4.41	4.13	1	2	2	2	533	56.5	6.54
P60766	Cell division control protein 42 homolog OS=Mus musculus GN=Cdc42 PE=1 SV=2 - [CDC42_MOUSE]	4.38	10.99	1	2	2	2	191	21.2	6.55
P52480	Pyruvate kinase isozymes M1/M2 OS=Mus musculus GN=Pkm PE=1 SV=4 - [KPYM_MOUSE]	4.08	3.77	1	2	2	2	531	57.8	7.47
F7ANV6	Annexin (Fragment) OS=Mus musculus GN=Anxa4 PE=2 SV=1 - [F7ANV6_MOUSE]	4.03	9.3	2	2	2	2	215	24.2	7.83
E9Q6R9	Protein Stxbp3b OS=Mus musculus GN=Stxbp3b PE=4 SV=1 - [E9Q6R9_MOUSE]	3.98	7.33	2	2	2	2	273	31.2	8.18

Table 9 – MC38 Δ*Rad51* cell sEV LC-MS/MS Round 1: Identified Proteins and Peptides List

Accession	Description	Score	Coverage	Proteins (no.)	Unique Peptides (no.)	Peptides (no.)	PSMs	AAs (no.)	MW [kDa]	calc. pI
P03336	Gag polyprotein OS=AKV murine leukemia virus GN=gag PE=1 SV=3 - [GAG_MLVAV]	154.08	15.46	1	9	9	59	537	60.5	8.03
P21956	Lactadherin OS=Mus musculus GN=Mfge8 PE=1 SV=3 - [MFGM_MOUSE]	137.49	22.68	1	10	10	56	463	51.2	6.52
P63017	Heat shock cognate 71 kDa protein OS=Mus musculus GN=Hspa8 PE=1 SV=1 - [HSP7C_MOUSE]	135.62	32.2	1	16	16	50	646	70.8	5.52
P07356	Annexin A2 OS=Mus musculus GN=Anxa2 PE=1 SV=2 - [ANXA2_MOUSE]	64.77	13.86	1	5	5	26	339	38.7	7.69
P60710	Actin, cytoplasmic 1 OS=Mus musculus GN=Actb PE=1 SV=1 - [ACTB_MOUSE]	51.58	16	2	5	5	21	375	41.7	5.48
P99024	Tubulin beta-5 chain OS=Mus musculus GN=Tubb5 PE=1 SV=1 - [TBB5_MOUSE]	49.59	15.99	1	6	6	18	444	49.6	4.89
Q8VDN2	Sodium/potassium-transporting ATPase subunit alpha-1 OS=Mus musculus GN=Atp1a1 PE=1 SV=1 - [AT1A1_MOUSE]	48.68	10.36	1	8	8	18	1023	112.9	5.45
Q9WU78	Programmed cell death 6-interacting protein OS=Mus musculus GN=Pdcd6ip PE=1 SV=3 - [PDC6I_MOUSE]	46.17	13.12	1	11	11	18	869	96	6.52
P11499	Heat shock protein HSP 90-beta OS=Mus musculus GN=Hsp90ab1 PE=1 SV=3 - [HS90B_MOUSE]	46.09	14.92	1	9	9	17	724	83.2	5.03
P0CG49	Polyubiquitin-B OS=Mus musculus GN=Ubb PE=2 SV=1 - [UBB_MOUSE]	40.2	40.66	4	3	3	16	305	34.3	7.53
P10852	4F2 cell-surface antigen heavy chain OS=Mus musculus GN=Slc3a2 PE=1 SV=1 - [4F2_MOUSE]	32.27	15.59	1	8	8	12	526	58.3	5.91
P08752	Guanine nucleotide-binding protein G(i) subunit alpha-2 OS=Mus musculus GN=Gnai2 PE=1 SV=5 - [GNAI2_MOUSE]	31.08	8.45	1	3	3	12	355	40.5	5.45
P48036	Annexin A5 OS=Mus musculus GN=Anxa5 PE=1 SV=1 - [ANXA5_MOUSE]	29.34	12.23	1	4	4	12	319	35.7	4.96
P53986	Monocarboxylate transporter 1 OS=Mus musculus GN=Slc16a1 PE=1 SV=1 - [MOT1_MOUSE]	27.24	9.94	1	3	3	10	493	53.2	7.47
Q9WV91	Prostaglandin F2 receptor negative regulator OS=Mus musculus GN=Ptgfrn PE=1 SV=2 - [FPRP_MOUSE]	26.93	12.63	1	9	9	10	879	98.7	6.61
P10126	Elongation factor 1-alpha 1 OS=Mus musculus GN=Eef1a1 PE=1 SV=3 - [EF1A1_MOUSE]	25.35	6.49	1	3	3	10	462	50.1	9.01

P26041	Moesin OS=Mus musculus GN=Msn PE=1 SV=3 - [MOES_MOUSE]	22.17	7.28	1	4	4	9	577	67.7	6.6
Q04857	Collagen alpha-1(VI) chain OS=Mus musculus GN=Col6a1 PE=1 SV=1 - [CO6A1_MOUSE]	20.54	4.1	1	4	4	8	1025	108.4	5.36
P04104	Keratin, type II cytoskeletal 1 OS=Mus musculus GN=Krt1 PE=1 SV=4 - [K2C1_MOUSE]	18.77	3.77	1	3	3	6	637	65.6	8.15
P97449	Aminopeptidase N OS=Mus musculus GN=Anpep PE=1 SV=4 - [AMPN_MOUSE]	16.27	6	1	4	4	6	966	109.6	5.9
Q62470	Integrin alpha-3 OS=Mus musculus GN=Itga3 PE=1 SV=1 - [ITA3_MOUSE]	16.02	3.13	1	3	3	6	1053	116.7	6.57
P11276	Fibronectin OS=Mus musculus GN=Fn1 PE=1 SV=4 - [FINC_MOUSE]	15.44	2.95	1	6	6	6	2477	272.4	5.59
P09055	Integrin beta-1 OS=Mus musculus GN=Itgb1 PE=1 SV=1 - [ITB1_MOUSE]	15.09	9.02	1	6	6	6	798	88.2	5.94
Q9Z127	Large neutral amino acids transporter small subunit 1 OS=Mus musculus GN=Slc7a5 PE=1 SV=2 - [LAT1_MOUSE]	15.04	8.4	1	3	3	6	512	55.8	7.9
Q68FD5	Clathrin heavy chain 1 OS=Mus musculus GN=Cltc PE=1 SV=3 - [CLH1_MOUSE]	13.86	3.58	1	5	5	5	1675	191.4	5.69
P17182	Alpha-enolase OS=Mus musculus GN=Eno1 PE=1 SV=3 - [ENOA_MOUSE]	13.59	7.6	1	3	3	5	434	47.1	6.8
P63101	14-3-3 protein zeta/delta OS=Mus musculus GN=Ywhaz PE=1 SV=1 - [1433Z_MOUSE]	13.58	15.51	1	3	3	5	245	27.8	4.79
P52480	Pyruvate kinase PKM OS=Mus musculus GN=Pkm PE=1 SV=4 - [KPYM_MOUSE]	13.39	8.47	1	4	4	5	531	57.8	7.47
P15379	CD44 antigen OS=Mus musculus GN=Cd44 PE=1 SV=3 - [CD44_MOUSE]	12.34	3.08	1	2	2	7	778	85.6	4.96
P10107	Annexin A1 OS=Mus musculus GN=Anxa1 PE=1 SV=2 - [ANXA1_MOUSE]	12.26	6.65	1	3	3	5	346	38.7	7.37
Q8R422	CD109 antigen OS=Mus musculus GN=Cd109 PE=1 SV=1 - [CD109_MOUSE]	11.67	3.26	1	4	4	5	1442	161.6	5.57
P51912	Neutral amino acid transporter B(0) OS=Mus musculus GN=Slc1a5 PE=1 SV=2 - [AAAT_MOUSE]	10.85	4.88	1	2	2	4	553	58.4	7.84
Q8VHY0	Chondroitin sulfate proteoglycan 4 OS=Mus musculus GN=Cspg4 PE=1 SV=3 - [CSPG4_MOUSE]	10.68	2.28	1	4	4	4	2327	252.2	5.44
P61750	ADP-ribosylation factor 4 OS=Mus musculus GN=Arf4 PE=1 SV=2 - [ARF4_MOUSE]	10.38	11.67	1	2	2	4	180	20.4	7.14
P03386	Envelope glycoprotein OS=AKV murine leukemia virus GN=env PE=1 SV=1 - [ENV_MLVAV]	9.82	3.59	1	2	2	3	669	73.7	8.05

P06151	L-lactate dehydrogenase A chain OS=Mus musculus GN=Ldha PE=1 SV=3 - [LDHA_MOUSE]	9.7	9.94	1	3	3	4	332	36.5	7.74
Q02013	Aquaporin-1 OS=Mus musculus GN=Aqp1 PE=1 SV=3 - [AQP1_MOUSE]	9.59	7.06	1	2	2	4	269	28.8	7.43
P62806	Histone H4 OS=Mus musculus GN=Hist1h4a PE=1 SV=2 - [H4_MOUSE]	9	21.36	1	2	2	4	103	11.4	11.36
G5E829	Plasma membrane calcium-transporting ATPase 1 OS=Mus musculus GN=Atp2b1 PE=1 SV=1 - [AT2B1_MOUSE]	8.37	2.3	1	2	2	3	1220	134.7	5.91
P18572	Basigin OS=Mus musculus GN=Bsg PE=1 SV=2 - [BASI_MOUSE]	7.95	5.91	1	2	2	3	389	42.4	5.85
P58252	Elongation factor 2 OS=Mus musculus GN=Eef2 PE=1 SV=2 - [EF2_MOUSE]	7.68	4.08	1	3	3	3	858	95.3	6.83
P62071	Ras-related protein R-Ras2 OS=Mus musculus GN=Rras2 PE=1 SV=1 - [RRAS2_MOUSE]	7.32	11.27	1	2	2	3	204	23.4	6.01
Q61753	D-3-phosphoglycerate dehydrogenase OS=Mus musculus GN=Phgdh PE=1 SV=3 - [SERA_MOUSE]	7.31	7.32	1	3	3	3	533	56.5	6.54
P23242	Gap junction alpha-1 protein OS=Mus musculus GN=Gja1 PE=1 SV=2 - [CXA1_MOUSE]	6.84	6.28	1	2	2	3	382	43	8.76
P07091	Protein S100-A4 OS=Mus musculus GN=S100a4 PE=1 SV=1 - [S10A4_MOUSE]	6.82	8.91	1	2	2	3	101	11.7	5.31
F8VPU2	FERM, RhoGEF and pleckstrin domain-containing protein 1 OS=Mus musculus GN=Farp1 PE=1 SV=1 - [FARP1_MOUSE]	6.75	4.2	1	3	3	3	1048	118.8	7.88
Q02788	Collagen alpha-2(VI) chain OS=Mus musculus GN=Col6a2 PE=1 SV=3 - [CO6A2_MOUSE]	5.96	3	1	2	2	2	1034	110.3	6.42
Q9QYJ0	DnaJ homolog subfamily A member 2 OS=Mus musculus GN=Dnaja2 PE=1 SV=1 - [DNJA2_MOUSE]	5.49	5.1	1	2	2	2	412	45.7	6.48
Q9WTI7	Unconventional myosin-Ic OS=Mus musculus GN=Myo1c PE=1 SV=2 - [MYO1C_MOUSE]	5.4	2.35	1	2	2	2	1063	121.9	9.35
Q80W68	Kin of IRRE-like protein 1 OS=Mus musculus GN=Kirrel PE=1 SV=1 - [KIRR1_MOUSE]	5.02	3.93	1	2	2	2	789	87.1	5.92
P97429	Annexin A4 OS=Mus musculus GN=Anxa4 PE=1 SV=4 - [ANXA4_MOUSE]	4.9	6.9	1	2	2	4	319	35.9	5.57
Q61187	Tumor susceptibility gene 101 protein OS=Mus musculus GN=Tsg101 PE=1 SV=2 - [TS101_MOUSE]	4.8	5.63	1	2	2	2	391	44.1	6.71
Q03145	Ephrin type-A receptor 2 OS=Mus musculus GN=Epha2 PE=1 SV=3 - [EPHA2_MOUSE]	4.58	2.46	1	2	2	2	977	108.8	6.23
O35474	EGF-like repeat and discoidin I-like domain-containing protein 3 OS=Mus musculus GN=Edil3 PE=1 SV=2 - [EDIL3_MOUSE]	4.54	4.17	1	2	2	2	480	53.7	7.58

P17809	Solute carrier family 2, facilitated glucose transporter member 1 OS=Mus musculus GN=Slc2a1 PE=1 SV=4 - [GTR1_MOUSE]	4.5	3.66	1	2	2	2	492	53.9	8.87
P62880	Guanine nucleotide-binding protein G(I)/G(S)/G(T) subunit beta-2 OS=Mus musculus GN=Gnb2 PE=1 SV=3 - [GBB2_MOUSE]	4.49	6.47	1	2	2	2	340	37.3	6

Table 10 – MC38 Δ*Rad51* cell sEV LC-MS/MS Round 2: Identified Proteins and Peptides List

Accession	Description	Score	Coverage	Proteins (no.)	Unique Peptides (no.)	Peptides (no.)	PSMs	AAs (no.)	MW [kDa]	calc. pI
P04104	Keratin, type II cytoskeletal 1 OS=Mus musculus GN=Krt1 PE=1 SV=4 - [K2C1_MOUSE]	104.86	3.77	1	3	3	38	637	65.6	8.15
A2A513	Keratin, type I cytoskeletal 10 OS=Mus musculus GN=Krt10 PE=4 SV=1 - [A2A513_MOUSE]	98.28	8.56	2	3	5	40	561	57	5.07
P21956	Lactadherin OS=Mus musculus GN=Mfge8 PE=1 SV=3 - [MFGM_MOUSE]	62.66	11.88	1	5	5	28	463	51.2	6.52
Q61781	Keratin, type I cytoskeletal 14 OS=Mus musculus GN=Krt14 PE=1 SV=2 - [K1C14_MOUSE]	54.41	7.85	1	1	4	23	484	52.8	5.17
Q61414	Keratin, type I cytoskeletal 15 OS=Mus musculus GN=Krt15 PE=1 SV=2 - [K1C15_MOUSE]	52.37	7.52	2	2	5	23	452	49.1	4.86
Q3TTY5	Keratin, type II cytoskeletal 2 epidermal OS=Mus musculus GN=Krt2 PE=1 SV=1 - [K22E_MOUSE]	44.83	3.25	1	2	2	18	707	70.9	8.06
P60710	Actin, cytoplasmic 1 OS=Mus musculus GN=Actb PE=1 SV=1 - [ACTB_MOUSE]	31.4	11.2	2	4	4	14	375	41.7	5.48
P10126	Elongation factor 1-alpha 1 OS=Mus musculus GN=Eef1a1 PE=1 SV=3 - [EF1A1_MOUSE]	28.76	6.28	2	3	3	12	462	50.1	9.01
P08752	Guanine nucleotide-binding protein G(i) subunit alpha-2 OS=Mus musculus GN=Gnai2 PE=1 SV=5 - [GNAI2_MOUSE]	27.67	6.2	1	2	2	10	355	40.5	5.45
Q504P4	Heat shock cognate 71 kDa protein OS=Mus musculus GN=Hspa8 PE=2 SV=1 - [Q504P4_MOUSE]	23.95	13.24	2	7	7	10	627	68.7	5.52
J3QQ16	Protein Col6a3 OS=Mus musculus GN=Col6a3 PE=4 SV=1 - [J3QQ16_MOUSE]	18.85	2.39	2	6	6	8	2677	288.5	8.53
Q922U2	Keratin, type II cytoskeletal 5 OS=Mus musculus GN=Krt5 PE=1 SV=1 - [K2C5_MOUSE]	17.99	5.34	1	3	3	8	580	61.7	7.75
P53986	Monocarboxylate transporter 1 OS=Mus musculus GN=Slc16a1 PE=1 SV=1 - [MOT1_MOUSE]	15.62	4.46	1	2	2	6	493	53.2	7.47
P09055	Integrin beta-1 OS=Mus musculus GN=Itgb1 PE=1 SV=1 - [ITB1_MOUSE]	15.6	5.76	1	4	4	7	798	88.2	5.94
B0V2N8	Annexin A2 (Fragment) OS=Mus musculus GN=Anxa2 PE=2 SV=1 - [B0V2N8_MOUSE]	14.71	22.73	3	4	4	6	176	19.6	5.96
Q9EQK5	Major vault protein OS=Mus musculus GN=Mvp PE=1 SV=4 - [MVP_MOUSE]	14.62	2.67	2	2	2	6	861	95.9	5.59

P62806	Histone H4 OS=Mus musculus GN=Hist1h4a PE=1 SV=2 - [H4_MOUSE]	14.02	31.07	1	3	3	6	103	11.4	11.36
Q8BGZ7	Keratin, type II cytoskeletal 75 OS=Mus musculus GN=Krt75 PE=1 SV=1 - [K2C75_MOUSE]	13.7	3.63	4	2	2	6	551	59.7	8.31
P26041	Moesin OS=Mus musculus GN=Msn PE=1 SV=3 - [MOES_MOUSE]	13.22	7.63	1	5	5	6	577	67.7	6.6
P11499	Heat shock protein HSP 90-beta OS=Mus musculus GN=Hsp90ab1 PE=1 SV=3 - [HS90B_MOUSE]	12.37	5.11	1	3	3	5	724	83.2	5.03
Q8C4U8	EGF-like repeat and discoidin I-like domain-containing protein 3 OS=Mus musculus GN=Edil3 PE=2 SV=1 - [Q8C4U8_MOUSE]	10.83	6.17	2	3	3	5	470	52.7	7.8
Q6PIC6	Sodium/potassium-transporting ATPase subunit alpha-3 OS=Mus musculus GN=Atp1a3 PE=1 SV=1 - [AT1A3_MOUSE]	10.39	5.63	2	4	4	4	1013	111.6	5.41
D3Z1M1	Guanine nucleotide-binding protein G(I)/G(S)/G(T) subunit beta-2 (Fragment) OS=Mus musculus GN=Gnb2 PE=2 SV=1 - [D3Z1M1_MOUSE]	9.69	9.69	4	2	2	4	227	25	7.34
P52480	Pyruvate kinase isozymes M1/M2 OS=Mus musculus GN=Pkm PE=1 SV=4 - [KPYM_MOUSE]	9.4	8.29	1	4	4	4	531	57.8	7.47
Q9WV91	Prostaglandin F2 receptor negative regulator OS=Mus musculus GN=Ptgfrn PE=1 SV=2 - [FPRP_MOUSE]	8.32	3.53	1	3	3	4	879	98.7	6.61
F8WJL5	Glyceraldehyde-3-phosphate dehydrogenase OS=Mus musculus GN=Gapdh PE=2 SV=1 - [F8WJL5_MOUSE]	7.47	8.94	3	2	2	3	302	32.5	8.19
Q61753	D-3-phosphoglycerate dehydrogenase OS=Mus musculus GN=Phgdh PE=1 SV=3 - [SERA_MOUSE]	7.2	6.57	1	3	3	3	533	56.5	6.54
F6RWW8	Myelin basic protein (Fragment) OS=Mus musculus GN=Mbp PE=4 SV=1 - [F6RWW8_MOUSE]	7.15	14.67	7	2	2	3	150	16.5	10.84
Q9WU78	Programmed cell death 6-interacting protein OS=Mus musculus GN=Pdcd6ip PE=1 SV=3 - [PDC6I_MOUSE]	6.97	3.68	1	3	3	3	869	96	6.52
P28667	MARCKS-related protein OS=Mus musculus GN=Marcksl1 PE=1 SV=2 - [MRP_MOUSE]	6.89	14	1	2	2	3	200	20.2	4.61
Q03145	Ephrin type-A receptor 2 OS=Mus musculus GN=Epha2 PE=1 SV=3 - [EPHA2_MOUSE]	6.59	3.48	1	3	3	3	977	108.8	6.23
P48036	Annexin A5 OS=Mus musculus GN=Anxa5 PE=1 SV=1 - [ANXA5_MOUSE]	4.46	5.64	1	2	2	2	319	35.7	4.96
P17182	Alpha-enolase OS=Mus musculus GN=Eno1 PE=1 SV=3 - [ENOA_MOUSE]	4.42	4.38	1	2	2	2	434	47.1	6.8
J3QP71	Basigin (Fragment) OS=Mus musculus GN=Bsg PE=4 SV=1 - [J3QP71_MOUSE]	4.25	9.64	3	2	2	2	197	21.7	6.2

Q9Z127	Large neutral amino acids transporter small subunit 1 OS=Mus musculus GN=Slc7a5 PE=1 SV=2 - [LAT1_MOUSE]	4.21	5.27	1	2	2	2	512	55.8	7.9
P63101	14-3-3 protein zeta/delta OS=Mus musculus GN=Ywhaz PE=1 SV=1 - [1433Z_MOUSE]	4.2	10.61	1	2	2	2	245	27.8	4.79